ALKOXIDE-BASED PRECURSORS FOR DIRECT ELECTROSPINNING OF ALUMINA FIBERS

By

VASANA MANEERATANA

A DISSERTATION PRESENTED TO THE GRADUATE SCHOOL
OF THE UNIVERSITY OF FLORIDA IN PARTIAL FULFILLMENT
OF THE REQUIREMENTS FOR THE DEGREE OF
DOCTOR OF PHILOSOPHY

UNIVERSITY OF FLORIDA

2007

This dissertation is dedicated to my mom and dad because they have always given me so much love.

ACKNOWLEDGMENTS

It is with such great pleasure to first acknowledge my advisor, Professor Wolfgang M. Sigmund. He has not only been my greatest advisor, but also a teacher, mentor, and role model; I am grateful for my chance to mature and find my place in science and engineering under his guidance. Tirelessly he promotes the best well being for all, which has propelled me to find my role and contribute to the world as a scientist with integrity; also he has philosophized the importance to enjoy both facets of a balanced life and career. Each day I am grateful for his support. His enthusiasm is unmatched.

In addition I would like to thank my committee members, Dr. L. Amelia Dempere, Dr. Christopher Batich, Dr. Ronald Baney, and Dr. Charles R. Martin who have been monumental in moving this body of work into a proud place. Also my heart goes out to the Zaman family for their loss of a wonderful father, scientist, and colleague- Dr. Abbas Zaman.

Importantly I would like to acknowledge my parents for providing me with so much love and life experiences that has given me the strength to make it through each day. My parents raised me to never believe in a disability and to only work on the belief of abilities; therefore I am grateful to be their daughter with abilities.

Each day my husband, Michael, has endured my growth through college and graduate school and I love him for his infinite-sized heart and patience. His love is my daily support system. His love is inspiring. (He's just happy that I have written this thing.)

Without a doubt, there have been a myriad of people who have dedicated their hearts, minds, time, and other parts to this work and they should not go unnoticed. Dr. Georgios Pyrgiotakis is undoubtedly a gentle soul with an amazing mind. He has taught me so many things and is always a mentor and friend. In addition I would like to thank Yi-Yang Tsai, an extremely brilliant scientist with inspirations to bring so much to everything. It has been

pleasure to have a “brother” in this research group. Dr. Erik M. Mueller has provided me with so much emotional and scientific support throughout our careers in this department and he will forever be a friend. Dr. Bernd Liesenfeld has been a brilliant friend and colleague that introduced to me to my first steps into a materials science laboratory. Also to the rest of the Sigmund research group (past and present), your helpfulness and support is appreciated.

Within the department, many persons have been critical to assisting to find my way in and out of here with grace. I would like to acknowledge Dr. L. Amelia Dempere because she gave me a chance to grow as an individual and research assistant at MAIC when I was not sure of my place in our field. Dr. Cammy Abernathy was a wonderful person to gain a new prospective in MSE. Dr. Jones, Ms. Martha McDonald, Ms. Joni Nattiel, Ms. Alice Holt, Mr. Matthew Walters and Ms. Rachel Ngai are also acknowledged. Going through graduate school is more than a degree, and without these people and their staff, I would not have been able to get through the logistics smoothly.

Outside of the department there are individuals and organizations that have been monumental in providing such a wonderful and fulfilling experience in graduate school. First I would like to acknowledge the National Aeronautics and Space Agency (NASA) for their funding thereby the NASA Harriett G. Jenkins Pre-doctoral Fellowship (JPFP), which is managed by the staff at the United Negro College Fund Special Programs Corporation (UNCFSP). The UNCFSP has program staff that has been instrumental in providing the students of the JPFP program with the utmost care and vigor for our futures, especially Dr. Melissa Green, Dr. Sonya Greene, Ms. Sondra Lancaster, Mr. Ian McCommons, and Ms. Tamika Wiggins.

In addition I'd like to thank the NASA Higher Education Division for their vision to see underrepresented persons pursue higher education degrees and of course. Dr. Harriett G. Jenkins had selfless goals for equality. She is my hero because her goals in life are driven by an inherent goodness that overwhelms all things negative. I feel so fortunate to have met and been awarded a fellowship after my hero. Dr. Mabel Matthews is the sunshine of the program and works with her heart on her sleeve, and she is such a wonderful example of a true administrator and educator. I look onto her enthusiasm and integrity with awe. Both these women are highly acknowledged for giving me this opportunity to keep going and to promote science to everyone.

In addition I would like to thank those at the NASA Glenn Research Center for allowing me to pursue research endeavors that have opened my scope as a researcher in my interests and in other fields, as well. Dr. Michael Meador and Dr. Maryann Meador gave me the chance to join as a colleague to further my work and serve as an initial lead on the development of new materials for next generation spacesuits. Their enthusiasm and support was filled with so much love and care. This chance to work with them gave me opportunities to be part of new communities of science and engineering. It is my hope that other individuals experience the great joy in working with such wonderful and enthusiastic people.

The American Association for the Advancement of Science (AAAS) has given me the fantastic opportunity as a board appointed committee member to the Committee on Opportunities in Science (COOS) to assist in their goals to strengthen the sense of science in the world around us. COOS members provided me with such wonderful guidance and new prospective on things. Especially I would like to pay homage to Dr. Virginia Stearns, Ms. Laureen Summers, Ms. LaTasha Mason, and Ms. Angelique Dorazio-Sanders, these individuals have been wonderful

and have propelled me into this COOS position along with assisting with my Entrypoint! internships at NASA Goddard Space Flight Center and NASA Glenn Research Center.

In closing I would like to thank my loving friends. Friendship is something that progresses with our own personal evolution and I appreciate each person that has been part of this dynamic process of maturing.

TABLE OF CONTENTS

LIST OF TABLES

Table page

LIST OF FIGURES

LIST OF TERMS/SYMBOLS/ABBREVIATIONS

EHDA:	Electrohydrodynamic Atomization
ASB:	Aluminum tri *sec* butoxide, $Al(C_4O_7H_9)_3$
AIP	Aluminum tri *iso* propoxide, $Al(C_3O_5H_7)_3$
BA:	*sec* Butyl Alcohol or 2-Butanol
HEX	Hexyl Alcohol or 1-Hexanol
OCT	Octyl Alcohol or 1-Octanol
DOD	Dodecyl Alcohol or 1-Dodecanol
EG	Ethylene Glycol
HEG	Hexylene Glycol
DGME	Diethylene Glycol Monoethyl ether
EGM	Ethylene Glycol Monomethyl ether
AA	Acetylacetone
EAA	Ethyl Acetoacetone
mod	modified, refers to a solution in which a ligand exchange took place
PVP:	Poly(vinylpyrrolidone)
PEO:	Poly(ethylene oxide)
PVA	Poly(vinyl alcohol)
SEM:	Scanning Electron Microscope
Al_2O_3:	Alumina
EN	electronegativity
ΔH°	standard enthalphy change of formation
δ_t	Hansen Parameter (MPa)
PDF	Probability Density Function
TGA	Thermogravimetric Analysis

FTIR	Fourier Transform Infrared Spectroscopy
CO_2	Carbon Dioxide
H_2O	Water
OH	Hydroxlys
DTA	Differential Thermal Analysis
XRD	X-ray Diffraction
NMR	Nuclear Magnetic Resonance
DRIFTS	Diffuse Reflectance Infrared Transmission Spectroscopy
ρ	Density
V_{AVG}	BJH Average Pore Volume
D_{AVG}	BJH Average Pore Diameter
S.S.A.	BET Specific Surface Area

Abstract of Dissertation Presented to the Graduate School
of the University of Florida in Partial Fulfillment of the
Requirements for the Degree of Doctor of Philosophy

ALKOXIDE –BASED PRECURSORS FOR DIRECT ELECTROSPINNING OF ALUMINA FIBERS

By

Vasana Maneeratana

December 2007

Chair: Wolfgang M. Sigmund
Major: Materials Science & Engineering

The vision for space exploration in 2004 reinvigorated excitement that was engendered during the 1960's space race. Looking to assist NASA's agency wide mission to develop new technologies to enhance space travel, it is the ultimate goal of this work to support future missions with a hand-held electrospinning apparatus to instantaneously repair existing crucial ceramic fiber structures, such as spacesuits, insulative foams, and tiles.

In this research, a new type of precursor is designed based from aluminum alkoxide-based precursors, since alumina serves as a base material for a majority of high-temperature applications. The structure-processing behavior of these precursors is subsequently studied. New precursors of aluminum alkoxides were prepared by modifying solutions; as a result various types of structures were produced, ranging from continuous hollow fibers, continuous solid fibers, or hollow particles. Direct electrospinning with these alkoxide-based precursors yielded an average of 1.9 g/hr of Al_2O_3, compared to literature with the highest theoretical yield calculated to be 0.68 g/hr. Further exploration of electrospinning parameters found that flow rate directly related to exposure times; therefore fibers were produced in the atmosphere through hydrolysis/condensation with simultaneous solvent evaporation. Furthermore other processing

parameters, including the effect of the microstructure due to processing in an electric field were studied. It was found that electrospinning promotes the reaction of the alkoxide, which thereby reduces trapped solvents. As a result of firing schedules, the fibers' hollow features were preserved, and precursors with volatile species resulted in near net shaped fibers. At low firing temperatures, specific surface areas in the range of 330-345 m^2/g were found electrospun fibers. Additionally modified precursors lowered alpha transitions of fibers down to ~ 900ºC.

CHAPTER 1
INTRODUCTION

In 1962, John F. Kennedy told the Nation, "We choose to go to the moon . . . because that goal will serve to organize and measure the best of our energies and skills." Seven years later we accomplished that goal with the Apollo 11 mission and then successfully repeated the landings in Apollo missions 12, 14, 15, 16, and 17. From the period of 1969-1972, only 12 humans set foot on the moon. This leap into the unknown propelled the world into an unprecedented advance in technologies, including innovations in computers, communications, medical products and so much more. Our quest to return to the moon was revived with the President Bush's Vision for Space Exploration in 2004. This speech emphasized the importance of returning to the moon to further explore and understand the unknown. Since then, a NASA wide initiative was organized to study and develop new technologies for enhancing space travel.

Reducing payloads and sustaining missions for long periods of space travel is the ultimate goal. Spacesuits, insulative foams and tiles are materials based on ceramic fibers that provide the basis of protection from elements due to harsh thermal cycling and space radiation. Repairing such materials has not been addressed in the past due to much shorter travel times in space. However new missions that require longer stays aboard the rockets and planetary missions require a new repair system to be developed.

An ultimate goal is to provide space travelers with a modular machine that fabricates the necessary ceramic fiber materials, when repair of existing structures is needed instantaneously. Conventional methods for fabricating ceramic fibers rely on bulky fiber spinning apparatus that cannot be brought into space. An electrospinning apparatus have been explored to produce hand-held, modular repair systems for wound healing technology. Easily this technology can be transferred for ceramic fiber systems and implemented for future space exploration.

Existing ceramic electrospinning precursors are predominantly comprised of a polymer solution with the addition of sol-gel based precursors. Electrospinning of polymer-based ceramic precursors are currently used since they align well with existing electrospinning models and require little effort to prepare. Nonetheless there are many drawbacks that hinder these precursors due to the need for calcination of the polymer after spinning, structural integrity issues after calcination, slow processing times, and shrinkage.

To circumvent these issues, researchers have investigated a new method to prepare precursors to directly electrospin ceramic fibers and address the latter-mentioned issues of the predominant polymeric precursors. Initial work engendered with use of sols of appropriate rheological properties to promote electrospinning. However spinnable sols were met with challenges during preparation due to the time, temperature, environmental sensitivity, and consistency.

Goals

The goal of this dissertation is to provide the community with the preparation of a new design of aluminum alkoxide-based precursors that can be directly electrospun. The structure-property-processing relationship of these precursors will subsequently be studied. Ultimately these precursors can be prepared before spaceflight and stored for the length of the mission. This dissertation aspires to produce a new type of precursor that can serve as a template for new compositions of ceramic fibers and consistently direct electrospin ceramic fibers with increasing ceramic yield, decreasing processing times, and decreasing structural issues.

Objectives

To accomplish goals in providing and investigating new aluminum alkoxide-based precursors, the following objectives are proposed:

- Identify and prepare appropriate aluminum alkoxides and preparation methods.

- Examine electrospinning processing to fiber structure relationship for alkoxide-based precursors
- Investigate the effect of processing in an electric field on the microstructure.
- Investigate changes in the fiber structure and microstructure due to thermal processing.

Structure of Dissertation

This chapter begins discussion with an overview of chemically-derived ceramic fiber precursors, which is then followed by current precursors in the electrospinning of ceramics. This leads to the statement of the problem and the goal to prepare alkoxides-based precursors. Chapter 3 approaches material selection criteria for the aluminum alkoxide, the preparation of alkoxide-based precursors, and feasibility studies with electrospinning. Since current predictive models do not exist for alkoxide-based precursors, Chapter 4 is dedicated to investigating the various electrospinning processing parameters to optimize fiber production. Due to the chemical nature of the alkoxides, new relationships will be drawn and correlated to the flow rate, electric field, working distance, and hydrolysis conditions. Chapter 5 looks at changes in the particular chemical and physical properties due to processing in an electric field and firing the material upwards of 1300ºC. The dissertation concludes by addressing the milestones of this work and future research goals.

CHAPTER 2
CONVENTIONAL ELECTROSPINNING OF CERAMICS

Electrospinning is a buzzword these days, bringing promises of a versatile and facile bottom-up approach to fruition by being able to fabricate continuous fibrous structures of a seemingly vast array of compositions. Dzenis delivered a perspective to potentially spin continuous carbon nanotubes that otherwise would take hours or days to grow as discontinuous bundles in a chemical vapor deposition chamber meanwhile others look to combine electrospinning with microfluidics as a way to fabricate novel microelectronic [1, 2]. Whichever the application, electrospinning is a topic that is currently on the table for discussion.

The goal of this chapter is to delineate the need to redesign a new type of precursor solution for electrospinning of ceramics. This chapter will discuss the history of electrospinning and detail current types of precursors. The derivation of these precursors will be compared to those found in conventional fiber spinning, since the latter was developed due to the need to incorporate alumina for high-temperature applications. In addition, sol-gel chemistry will be discussed due to its importance in the preparation of low temperature fiber spinning precursors. Limitations plaguing current electrospinning precursors will be discussed and investigations by the Sigmund group to circumvent these limitations will be described in the latter part of this chapter. From these set of works, a new type of alumina-based precursor was derived to circumvent issues due to low yield, poor reproducibility, and shrinkage due to usage of current ceramic precursors for electrospinning.

Schematic for Electrospinning

Electrospinning can be viewed as a simple and versatile bottom-up processing technique to produce fibers and also spheres; electrospinning's notable inception can be found within

Formhals' set of patents in the late 1930's and early 1940's [3-5]. Formhals looked to revolutionize fiber spinning by utilizing an electric field to expedite textile processing.

Preceding Formhals' invention came breaking work in the field of electrostatics. This started with an observation made regarding the effect of solutions in an electric field. William Gilbert provoked his curiosity in the early 17th century, wherein his inquisitiveness in the unknown world of magnetism and electricity brought about an observation that a piece of amber could disfigure a water droplet from a sphere into a cone [6]. In the late 19th century and early 20th, there was the evolution of the Electrohydrodynamic Atomization (EHDA) theory, which came to light as an understanding that high voltage sources can transform solutions into a fine mist of charged droplets [6, 7].

Today electrospinning is defined as a processing method that relies on an electric field to draw a spinnable solution towards a collector of lower potential. Therefore any lower potential surface can be exploited for electrospinning. In the Sigmund group laboratory, a set up with a power source adjacent to a syringe pump outfitted with a syringe and metal needle at a desired distance from a grounded aluminum foil, as seen in Figure 2-1A. The development of a pendant drop at the tip of the needle or nozzle forms at 0 kV/cm. With an increase in charge, the pendant drop conically warps and finally produces a jet at the apex of the cone.

Initial precursor solutions were comprised of an organic polymer. The nature of the latter provided a backbone of long and usually entangled organic chains resulting in the ability to draw out fibers from a high viscosity solution instead of a mist of fine droplets as found with the EHDA theory with lower viscosity solutions. These polymeric-based fiber generating precursors were prepared often from high molecular weight polymers dissolved within solvents. As the jet was drawn out, it would undergo a whipping type of reaction, Figure 2-1B, due to electrostatic

repulsive forces on the surface of the fiber. The fiber can be drawn towards the collecting plate, which promoted solvent evaporation. The stretching of fibers was done solely through electrical stresses as compared to conventional fiber techniques that would require mechanical drawing [2, 8]. To add to the compositional variety, ceramic precursors or particle suspensions were combined with organic polymers to indirectly derive ceramic fibers post-calcination. The latter will be discussed in subsequent sections.

Governing Parameters in Electrospinning

The process of electrospinning is comprised of a series of parameters working in balance. EHDA relies on the principles that there is a complex blend of forces that are in play when a solution is being deformed due to electrical stresses. Referring back to the balancing act, the illustration in Figure 2-2A illustrates the different forces in the electrospinning process.

Surface tension forms the pendant drop. As the nozzle is charged from the high-voltage source, as the conduction current surpasses the surface tension threshold, a jet materializes. As the jet is accelerated downward, whipping occurs due to the electrostatic conflict between the electric field and the jet's surface charges, as seen in Figure 2-2B [8, 9]. This instability region leads to acceleration of the fluid filament and continually stretching of the fibers. The electric field (units of kV/cm) is the relationship that relates the voltage to the distance from nozzle to the lower potential surface. The flow rate is determined by the speed at which the solution is drawn out of the syringe, and the environmental factors refer to temperature and humidity settings. An important movement towards understanding the parameters of ceramic-based systems was published by the Sigmund research group, which explored the charge within solution as an additional parameter to better predict fiber diameter [10].

Precursors for Ceramics Fibers Spinning

Initially, precursors prepared for ceramic fiber spinning relied on the usage of organic polymers to assist in enhancing spinnability. [11-18]. Much like conventional fiber spinning, the preparation of precursors was the ultimate rate-determining step for producing fibers in electrospinning. Without the adequate precursor, there cannot be forward progress to produce the desired composition and structure. The goal of this subsection will be to describe the types of precursors used for mechanical and electrical ceramic fiber spinning and detail of the evolution the incorporation of sol-gel based precursors within these precursors. To do so, this subsection will initiate a discussion of precursors for conventional fiber spinning and highlight the need to develop precursors for low-temperature fiber drawing. Following, sol-gel chemistry will be discussed. The importance of sol-gel precursors for preparing precursors of alumina will be highlighted and then further elucidated for precursors utilized in electrospinning of alumina.

Conventional Alumina Fiber Spinning

Conventional spinning of fibers requires mechanical drawing. Usually an extrudate is forced through a smaller orifice and the fiber is drawn, and eventually collected. Initially ceramic materials were melted and their high-temperature melts were drawn into fiber form.

Moving into the 1900's, new solutions to circumvent limitations in melt spinning of ceramic fibers were being investigated. Initially there was a drive to lower melting temperatures down for silicates (SiO_2) based on glassy melts with the addition $CaCO_3$ [12, 16]. However the constraints due to higher temperature applications required the composition to increase in Al_2O_3 content, which lead to a new paradigm shift in ceramic fiber processing. In which case, two schools of thoughts evolved both involving chemically derived means.

Lowering of the temperature in the spinning process ensued. In the 1960's and 1970's, work was performed with chemical processing thereby slurry preparation or sol-gel based

reactions to form low temperature precursors containing a high concentration of Al_2O_3 [13, 16, 18-21]. In Figure 2-3, 3M's Nextel 610 Al_2O_3 fibers can been seen, which are conventionally spun with sol-gel based solutions.

Precursors comprised of slurries included an organic polymer additive to retain the spinnable viscosity; various types of particles were dispersed in the organic polymers, ranging from particles of Al_2O_3, hydrous alumina, or aluminum salts. The organic polymer served as the sacrificial template, which produced a composite fiber pre-form. After calcination, the sacrificial template was removed through combustion.

The other approach utilized sol-gel based materials prepared with hydrous aluminum salts, $AlX_n(OH)_{3-n}$ that forms hexa-coordinated hydroxy-bridged species. These species formed dimers, trimers, oligomers, intermediates, and Al_{13} complexes (cage of 12 octahedral coordinated aluminums surrounding a single tetrahedrally coordinated aluminum) [16, 20, 22, 23]. Anion ligands, such as Cl^-, NO_3^-, or organics can be chosen, but commercially, aluminum chlorhydrates ($Al_xCl_x(OH)_y$) were used with 0.5 to 2.0 mols of anion ligands per mole of Al to optimize ceramic yield and structural issues during pyrrolysis [16, 18-20]. Some commercial Al_2O_3 fibers were also fabricated with a precursor that also combined the aluminum chlorohydrates with a mix of Al_2O_3 particles to optimize a polycrystalline oxide fiber yield after firing [18].

The $AlX_n(OH)_{3-n}$ can also be combined with organics, such as carboxylates as ligands. As seen in Figure 2-4, organic ligands, as noted by R. This allowed for polymerization with an Al-O backbone coordinated with chelating ligands (i.e. caboxylates, acetylacetonates, etc) [13, 16, 21]. These polymerized species formed when aluminum alkoxides were partially chelated and were followed by hydrolysis with 0.5 to 1 mole of water per Al. Additional organic ligands were utilized to increase the viscosity, which optimized spinnability [16, 21].

Development in the 1980's with Sakka's work shed light on the use of spinnable sols as a new type of precursor minimizing organic content. Spinnable sols utilized the idea that before the gelation point, colloidal sols can grow in a solution with viscosities in range of 1-100 Pa·s, thus providing adequate spinnability for conventional fiber drawing [13, 15, 17]. Initially sols exhibited shear-thinning properties, which proved deleterious to fiber processing [13]. Nevertheless Sakka found acid-catalyzed alumina sols, which contained long-shaped particles, exhibited Newtonian viscosities were able to conventionally fiber spin [15].

Amazingly, chemically derived processing of conventional fiber spinning precursors opened new doors to lower energy processing of ceramics, which allowed further derivations of processing, structure, and property relationships. Utilizing these chemical means, allowed for formation of various transition phases of Al_2O_3 that were absent in melt-spinning or some of the slurry techniques. Melt-spinning still proves useful means to draw single-crystalline fibers [16].

Overview of Sol-Gel Chemistry

Previous subsections discussed leveraging sol-gel based precursors to formulate precursors for low-temperature drawing of an increased content of Al_2O_3 in ceramic fibers. This section will further explore sol-gel chemistry, which establishes the framework not just for conventional precursors for fiber spinning but for existing precursors for electrospinning, too.

Sol-gel processing is an avenue that provides the versatility that engineer and scientists require designing bottom-up experiments and fabricating materials with a myriad of possibilities. This versatility can be attributed to the metal-organic precursors that often easily react to form inorganic structures at low temperatures. Taking advantage of the versatile processing parameters, an array of shapes and compositions can be formed, including fibers, monoliths, particles, thin films, coatings, and much more. The latter options are illustrated in Figure 2-5.

Livage describes the sol-gel process as an inorganic polymerization [24, 25]. The term, sol-gel is derived from the typical two components of the reaction, *sol* and *gel.* The *sol* is identified as part of a colloidal suspension that can initially be formed and the *gel* refers to the network that forms after continual growth within the solution [23-26].

Precursors in sol-gel chemistry are typified by certain ligands bound to a central metal atom. For the aluminum-based sol-gel family, some examples of precursors are $Al(NO)_3$ (Aluminum Nitrate), $Al(OC_4H_7)_3$ (Aluminum *sec*-Butoxide), $C_{15}H_{21}AlO_6$ (Aluminum Acetylacetonate). This body of work will mainly focus on alcohol-based ligands, also known as alkoxides, since they produce products with the least amount of impurities and are miscible with a variety of alcohols.

There are a series of reactions that are can occur during the sol-gel process, they can be broken down into two divisions- hydrolysis and condensation. In Figure 2-6, generic reactions are shown. Hydrolysis is simply the cleaving of the current ligand and subsequent replacement with -OH groups through a nucleophilic addition. Initially a transition state occurs when the nucleophile (-OH) is drawn to the metal with a subsequent departure of the protonated ROH species leaves the hydrolyzed metal. Meanwhile condensation is a reaction that combines and results in an oxygen to metal to oxygen bond (-O-M-O-), which can thus further polymerize during growth. This reaction proceeds through a condensation reaction, when hydrated metal groups react to release H_2O or if a hydrated metal combines with metal alkoxides thus releasing ROH through alcoholysis.

These reactions depend on: precursor miscibility in the desired solvent, amount of water, temperature, and often-optional catalysts [23-26]. Referring to the characteristics of the central metal, electronegativity plays a role in understanding the need for catalysts. For metals such as

silicon, the alkoxide ligands often bond through covalent bonds, which leads to a stability that requires an acid or a base to catalyze the cleavage and decrease gel time. Utilizing an acid or a base in the latter-mentioned system leads to control of kinetics of either nucleation or growth, respectively [26]. In the case of titanium and aluminum based sol-gel systems it has been found that the actual pH may not be the only factor, but that type of acid being utilized can change final properties of the ceramic. The ligands or nucleophiles, such as acetates (acetic acid) that result after deprotonation may serve to complex with the alkoxide ligands and reduce hydrolysis rates, thusly controlling nucleation properties [24, 27-30].

Sol-Gel Based Processing of Alumina

Typically conventional alumina products are derived from the Bayer process. In short the Bayer process was developed to hydrothermally digest the mineral Bauxite at a high pH. It can be subsequently grinded and milled into powder form for further down-stream processing. The alumina is left with a high concentration of impurities and not advantageous for applications requiring a lack of impurities, more uniform shape/size, and decrease in particle size.

Commercial alumina fibers from 3M and other manufacturers rely on the sol-gel based chemistry to form pure fibers, $\geq$ 99% Al_2O_3, along with multi-component fibers for thermal and structural applications. In addition, the use of sol-gel for processing alumina has also been utilized for thin films, adsorbents, and sensors [23].

In the 1970's sol-gel research with alumina was due in large part to Yoldas' work to form monolithic gels that are transparent up to 900ºC [27, 28, 31]. The latter-mentioned work launched an ever-present slew of work dissecting the stages of the aluminua sol-gel process to develop and enhance transition phases, size, shape, surface properties, and other properties as well [27, 28, 31-58].

Al^{3+}

Aluminum metal is from the class IIIb section of the periodic table, wherein it is the second most abundant metal from the earth's crust. This abundance still spurs scientists and engineers to further advance alumina for next generation applications. It has an ionic radius of 0.5Å with a hydration number of 6 [22]. Species such as aluminum hydroxides and oxo-hydroxides have become of interest as precursors to transition aluminas for catalyst supports and adsorbents [23].

Organic Polymeric Aids with Sol-Gel Precursors

Previously the preparation schemes for conventional fiber spinning were discussed. Low-temperature drawing with a high-content of Al_2O_3 led to incorporation of sol-gel components. Although electrospinning initiated with fiber spinning of organic polymers, however, the incorporation of sol-gel precursors into these polymeric solutions provided a method to produce ceramic fiber pre-forms. Similarly to conventional fiber spinning, these preforms required thermal treatment to combust the large concentration of organics.

Notably this sort of system experienced little issues during electrospinning, when concentrations were left to a minimum. However at higher concentrations of these ceramic precursors, Li and Xia found defects leading to beading along the fiber structure [2, 59, 60]. These beads were an example of fiber deformities that can typically be found in electrospinning. However maintaining low concentrations of ceramic precursors allowed for ceramic fiber diameters to be kept at a minimum after calcination [59].

These assumptions relied on the idea that decreasing the concentration of ceramic precursor decreases the concentration of ceramic that can be formed into a fiber, resulting in diameters as low as 20 nm[2, 59-63]. A titanium-based system was studied and a relationship was derived to better describe variations between polymer concentrations and polymer/ceramic

precursor concentrations. The latter served as just one example of research that heavily relies on a polymer matrix to smooth the electrospinning transition into ceramic systems.

A predominantly utilized organic polymer system is poly (vinylpyrrolidone) (PVP). The structure of the monomer is shown in Figure 2-7. The pyrrolidone functional group lends to the polarity of the molecule in both an alcohol and aqueous environment. In working with the latter, this polar group facilitates the electrospinnability of the material, since the possession of small charges aids the flow and production of sub-micron and/or nanometer features [64-66]. Typically works utilize molecular weights of polymers from hundred of thousands to millions. [65-68].

Ceramic precursors, such as metal-alkoxides and metal-salts have been mixed with polymers, owing to the solubility in an alcohol and/or aqueous system. Nonetheless, there were issues that ensued with certain precursors due to the inability to form stable mixtures within PVP and other organic polymeric blends.

Current Type Of Precursors In The Electrospinning Of Alumina Fibers

The previous sections provided the reader with an understanding of precursors used in both conventional and electrical fiber spinning techniques. Comparisons of sol-gel based solutions that were incorporated into predominantly polymer-based precursors were described for both spinning systems. The goal of this subsection is to describe to the reader of the types of precursors currently published for Al_2O_3 fibers. In doing so, limitations due to yield, production rate, and precursor preparation consistency will be highlighted. Research to augment current alumina-based electrospinning precursors in the Sigmund group will be discussed. Within these findings, the basis for a new type of precursors will be derived. Further chapters will discuss preparation of these new precursors and characterization of the products produced through electrospinning.

Precursors With Polymer And Metal-Organic Components

The low yield of ceramic fibers from typical sol-gel precursors dispersed in organic polymers is the obvious advantage to yielding fiber diameters in the range of 10's of nanometers and up after calcination. For example, examining Azad's work, it was found that precursors were prepared with aluminum (2,4 pentadionate) dissolved in acetone at 6.85 $x10^{-2}$mol/L with an equal volume of 15 weight percent PVP in ethanol. This was electrospun at 0.03 mL/hr [69]. Calculation for the spinning time is 166.6 hours for a 5mL syringe. Furthermore in a 5mL syringe, the calcined fibers were ~350nm (however reported at ~150nm) but the maximum amount of Al_2O_3, that can be fabricated is 0.0175g. Thus, in about 167 hours or ~ 7days, this precursor can produce 0.0175 g of Al_2O_3. The hourly rate for electrospinning is 0.000104g of Al_2O_3/hr.

Panda and Ramakrishna explored the use of other sol-gel aluminum precursors, such as $Al(NO)_3$ and Aluminum Acetate $(AlAc)_3$ in polymers, PVA and Poly(ethylene oxide) (PEO) [70]. Salt to polymer concentrations were set at 10, 50 and 100 %. These researchers reported issues with beading and structural deformities with all three loadings. Beading was found in the 10 wt% and roughness in the 100 wt%. In this work, the fastest production rate calculated from the six recipes is 0.69g of Al_2O_3/hr.

Nonetheless since fiber diameters values were not completely provided, the implementation of the Carnoy 2.1 software, an image analysis software, was used to measure fiber diameters, by averaging 10 fibers that were within the plane of focus of Figure 9 in Panda's article. The mean diameter was found to be 0.298 μm (298 nm) with a standard deviation of 0.026 μm (0.026 nm). Unfortunately this figure was improperly labeled and the aluminum precursor or polymer being were not identified. However, it is believed to be 100 wt% solids

loading, since it was noted that the 100 wt% would yield roughly appearing fibers, as observed. The textured fibers weres comprised of interesting attributes, such that its grains were relatively large in comparison to the fiber diameter; after 5 grains were measured, the mean grain diameter is 0.109 μm (109nm) with a standard deviation of 0.020 μm (20 nm). In addition the above-mentioned analysis, both Panda and Azad demonstrated that calcined fibers exhibit a wavy-like and somewhat broken appearance.

The use of precursors, as described by Panda, yielded relatively the same fiber diameters in a shorter amount of time than Azad's work. Smaller grain sizes are optimal for high-strength applications, but disadvantageous by increasing the rate of high-temperature creep properties. In the commercially available > 99% Al_2O_3 fibers such as DuPonts FiberFP, 3M's Nextel 610, and Mitsui Mining's Almax, grain sizes are kept at ~0.02 ratio of grain size to fiber diameter to maintain strengths for reinforcement applications.

Limitations with electrospinning precursors derived from polymers as sacrificial template can result in the structural issues due to the extent of shrinkage after calcination. The higher the concentration of organic polymer, there will be a larger degree of shrinkage.

Direct Electrospinning With Aged Sols

Larsen's work responds to the issue of sacrificial templating of Al_2O_3 fibers by electrospinning aged colloidal sols fabricated by hydrolyzing acid catalyzed aluminum alkoxides complexed with chelates producing diameters of ~ 200μm, similiarly to Sakka's work with Al_2O_3 precursors for conventional fiber spinning [71]. There were no recipes or processing parameters published. However a similar article that utilized aged sols of TiO_2 with an acid catalyzed titanium alkoxide demonstrated that fibers with green state diameters of 2.28 μm could be electrospun at a faster rate of 0.023 g of Al_2O_3/hr.

Reproducibility of aged sol precursors for electrospinning

Previously in the Sigmund group, there was desire to reproduce Larsen's work to understand the reproducibility of the aged sol precursors. Initially it was found that it was difficult to control the aging of sols for complete electrospinning to occur. Aging of the sols required a delicate balance between hydrolysis and gelation. Controlling conditions such as component concentrations, hydrolysis rate, and aging time resulted in precursors that remained stable only up to one hour. Nevertheless gelation would result during the electrospinning process at the fastest optimal flow rate values, resulting in cessation of the fiber fabrication.

Increasing Al_2O_3 Yield in Electrospinning

Current sets of work rely on a low ceramic yield which thereby helps to produce sub-micron fiber diameters after calcinations. Since the concentration of precursor has been shown to linearly relate to the fiber diameter, a necessary balance should be investigated to still maintain submicron features [59, 62].

Metal salts have been incorporated with polymers to help increase yield of the ceramic fibers. These metal salts, such as Aluminum Chloride ($AlCl_3$) have lower molecular masses than other type of sol-gel precursors, such as alkoxides. $Al(NO)_3$ is commonly found in the form of $Al(NO)_3 \bullet 9H_2O$ and as a salt its hydrolysis products are comprised of a range of species [22]. These hydrolyzed species actually proceed through a condensation reaction that can produce a variety of poly-nuclear species. This is a result of the interactions of hydroxide ligands (bound to aluminum) that thermodynamically favors maximization of the hydrogen bonding [23]. Various types of polynuclear species can be formed, in addition to the Al_{13} ion [22, 23].

Initially it was necessary to understand the miscibility of the salts in both water and alcohol systems. Assessing these limits allowed for an initial understanding of solids loading. After this sort of understanding, the respective polymers can be added to form spinnable precursors.

In this set of work, a set of solutions: A. 100 v/v % H_2O, B. 25v/v%Ethanol (ETOH) in H_2O, C. 50v/v% ETOH in H_2O and D. 100 v/v % ETOH were utilized and various amounts of salts were dissolved into the solutions at 70ºC. This subsection explores the solubility of the salt in various water and ethanol mixtures. At 55 wt% solids loadings all salts dissolved, and further experimentation (loading in increments of 5 wt%) was stopped due to the high percentage of solubility of the salt in water. However gelling was noticed in the 100 v/v% ethanol system at 20 wt% and higher. The appearance of gelling was transitory and since moderate heat of 70ºC was being applied, the gel disappeared through constant stirring. However upon cooling down to room temperature, solutions of various loadings all exhibited some form of gelling behavior. With the addition of polymer, it was found that the minimum threshold which did not gel was a equal volume 10wt% $Al(NO)_3 \bullet 9H_2O$ in ETOH mixed with a 7.5 wt% PVP (1.3×10^6 g/mol) in ETOH, which resulted in a 1.33 wt% ratio of salt to polymer.

Solutions that gelled inhibited polymer addition and thus further electrospinning processing. Limitations existed with high solids loadings of aluminum salts, >10 wt%, due to hydrolyzed species forming immiscible gelatinous products, leading to strong species that dominate and do not allow for even dispersion of the polymer or proper spinning Newtonian behavior.

Experimental Trends in Metal Alkoxide Incorporation into Polymers

Salt solubility was the limiting factor after 10 wt% solids loading. The use of sol-gel alkoxides can allow for increased miscibility into organic solvents and polymers. The mixture of an alkoxide-based solution into the desired electrospinning polymer backbone is another avenue

that has not been explored with sol-gel aluminum compounds. Alkoxides, such as Aluminum *tri* sec butoxide (ASB) and seen in Figure 2-8, have been previously utilized in other applications due to their miscible nature with alcohols and other polar and non-polar solvents.

Aluminum alkoxides are rather unique, since they can form various coordinated alkoxide species [47]. This results in a heterogeneous mixture of the neat, dimeric, tetrameric, and other oligomers. In the case of ASB, this tendency to form various coordinated structures leads to the viscous behavior of the solution [47].

Five solutions were investigated by combining PVP with ASB and *sec* butyl alcohol (BA). In Figure 2-9A, there is a list of the compositions ranging from 1 weight (wt) % polymer up to 15 wt%. Each sample was made three times. The corresponding ternary diagram for the 5 chosen mixtures are illustrated in Figure 2-9B.

It was demonstrated in previous experiments that directly mixing ASB with PVP resulted in precipitates due to the highly reactive ASB combining with the hygroscopic PVP. Therefore it was necessary to dilute ASB in BA before the addition of subsequent polymer. ASB was diluted in a 1:1 molar ratio with BA. The addition of 4 wt% PVP, the solutions barely formed a homogenous phase, requiring additional time and mixing avenues to assist.

For example, the 10wt% solution was magnetically stirred at 40ºC and afterwards sonicated for 4 hours for complete miscibility. However, the 5wt% solution took the whole day to solubilize, nonetheless there was an apparent difference in the difficulty to dissolve the unmixed regions. Before the sonication, there seemed to be a phase separation within the solution, a transparent ball of gel formed within the solution. After sonication and some mechanical stirring, the solution became homogenous and the solutions were kept for further testing with electrospinning.

The solutions chosen for electrospinning were the 1wt%, 2wt%, 4 wt%, and 10wt% due to the homogeneity of the mixed solutions. In regards to the 1 wt% solution, the pump rate was set at 0.762cc/hr and with a 5mL syringe, the maximum yield was calculated at 0.075g of Al_2O_3 /hr. In comparison with Panda's work, the yield was 0.69g of Al_2O_3 /hr, resulting in nearly a one hundred times difference in the magnitude of production produced.

The 10 wt% solution produced fibers that exhibited some beading, therefore resulting in calcined fibers that had some bulb shaped regions amongst the fiber as seen in Figure 2-10A. In Figure 2-10B, different type of structures contrast those found in Figure 2-10A. It can be observed, there was a presence of fiber beading, particles, and small fibers. After implementing the imaging software, Carnoy 2.1, to measure the diameters of the respective structures, particles had an average diameter of 3.2 μm with a standard deviation of 0.4 μm; meanwhile the fiber regions averaged diameters of 1.2 μm with a standard deviation of 0.06 μm.

These structures formed from the 5 wt% were analyzed on the Scanning Electron Microscope (SEM). There seems to be two types of structures appearing: one that was indicative of polydisperse spherical structures that range size from 3.5 μm to 15 μm.

It is believed that electrospinning a low concentration of polymer within the precursor, $\leq$ 5 wt%, resulted in the production of various type of structures. The Energy Dispersive Spectroscopy (EDS) X-Ray map was consulted to investigate the compositional homogeneity of these structures, as seen in Figure 2-11. Sample preparation was done with a carbon stub, copper tape, and gold-palladium coatings. The EDS X-ray map was taken to illustrate the regions that promoted Al K_α x-rays. It was found that some regions were distinctly aluminum rich as indicated by the strength of the Al K_α x-rays appearing in red. Meanwhile other portions did not

appear due to a poor or lack of Al K_α x-rays, which indicated that some regions did not contain Al.

This work sheds new light on the usage of aluminum alkoxides. The electrospinning of high concentration alkoxides in precursors reacted outside the presence of polymer to form respective electrospun structures.

Discussion on Modification of Existing Precursors Designs

The main concerns that were found with current precursors for ceramic electrospinning are with precursor reproducibility (as seen with spinnable sol preparation), low yield, and slow production times. Further work within the Sigmund group looked to investigate the reproducibility of spinnable sols. The latter was met with challenges during the preparation and also during the electrospinning stages. Although spinnable sols provided adequate means to direct electrospin and eliminate excessive organics due to polymers, the difficulty during preparation and gelation during the electrospinning process was the biggest deterrent for further use.

To increase the ceramic yield, the solubility of $Al(NO_3)_3$ was examined in both alcohol and water media. Since the salt can be dissolved in both water and alcohol, its solubility was initially analyzed. A gelatinous precipitate was avoided below the concentration limit of solids loadings of 10wt% solids in water or water/alcohol mixtures. When mixed with the polymer system, Panda's work was surpassed with a salt to polymer ratio of 1.33, conversely this only increased the production rate from 0.69 g Al_2O_3/hr to 0.71 g Al_2O_3/hr.

The use of aluminum alkoxides provided the basis to be more miscible in various organic media. Since there was a lack of published works in the field of aluminum alkoxides incorporated into polymer systems for electrospinning, miscibility ranges were thus investigated.

Studies to incorporate PVP with 1:1 ASB:BA solutions were tracked. Values were noted in the ternary diagram in Figure 2-9. Incorporating PVP into ASB/BA solutions showed that 10 wt% PVP loadings into the ASB/BA solution provided fibers in the single micro range with bulb like features along the diameter, as seen in Figure 2-10A. Nonetheless, when the solutions approached the outer limits of the solubility regime, such as with the 5wt%, heterogeneous structures appeared, Figure 2-10B, with a wide distribution of fibers, particles, and varicose fibers. These structures may be indicative that the electrospinning process resulted in polymer-less structures. In Figure 2-11, an x-ray map was performed to track the regions of aluminum to differentiate the polymer regions. It was found that heterogenous electrospun structures were formed due to the alkoxides' reaction to undergo hydrolysis and condensation. Electrospinning of alkoxide solutions with a minimum concentration of polymer assisted in the goal to attempt to increase ceramic yield. However, it was found that the yield and production rate still remained miniscule compared to published works. Nevertheless, the production of polymer-less structures with high concentration alkoxide precursors should be leveraged to increase yields and to also decrease the extent of post-calcination shrinkage.

Design Considerations for Future Aluminum-based Precursors for Electrospinning

This chapter explored the evolution of both conventional and electrospinning ceramic fiber processing methodologies and transitioned into explaining the role of sol-gel chemistry. This chapter focused on altering current ceramic electrospinning precursor designs to increase yield, assist in reproducibility, and possibly increase production times.

As a corollary, direct electrospinning seemed to be an indication of an improved method to circumvent the issues found with polymer incorporation, but the tedious nature of preparing and aging sols actually hindered processing times. Nonetheless, further works found extreme phase separation below 5 wt% PVP in the ASB/BA system which formed heterogeneous polymer-less

structures. The sol-gel chemistry of ASB dominated in such a way to allow for the metal alkoxide reacting forming and depositing structures, independent of the polymer backbone. Therefore, new design iterations for precursors can arise by exploring metal alkoxides to produce spinnable solutions, by stripping the precursors of other multi-component counterparts and additional organics.

When alkoxides were incorporated into polymers, precursors were reproduced in a facile manner. In addition, solutions remained consistent and did not undergo any time-dependent gelation. In addition, direct electrospinning of polymer-less structures with alkoxide-based precursors will be chosen to for further study to form the basis for a new type of precursor solution that can thereby increase ceramic yield, decrease issues due to reproducibility during preparation, and increase structural integrity due to a lower concentration of organics.

.

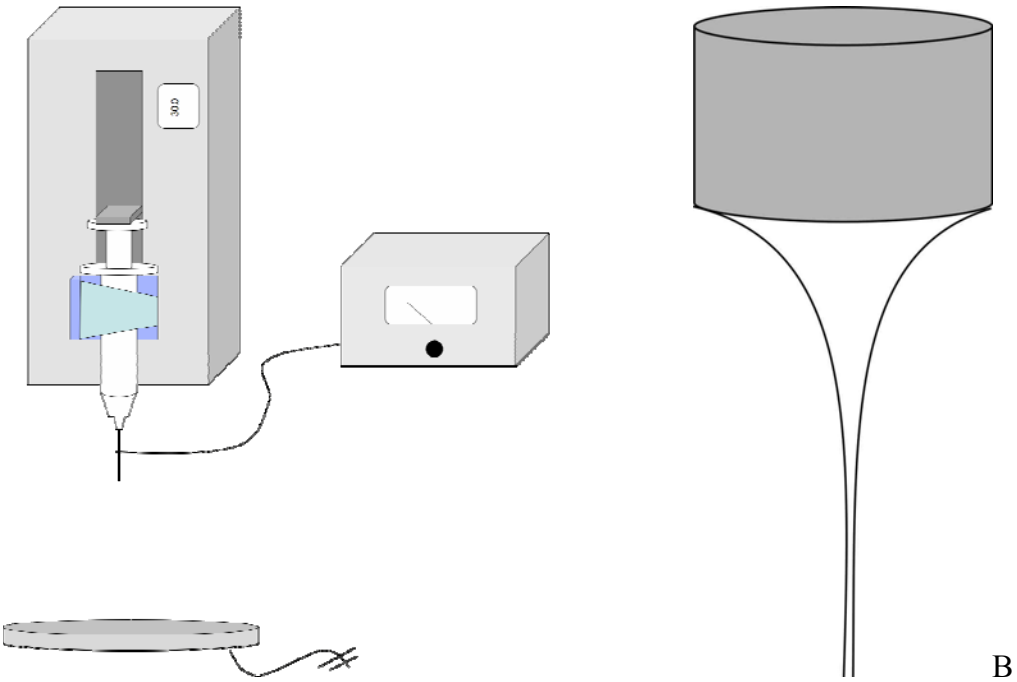

Figure 2-1. General Electrospinning Schematics: A) Typical Components In An Electrospinning Set-Up. (Adapted from R. P. A. Hartman, D. J. Brunner, D. M. A. Camelot, J. C. M. Marijnissen, B. Scarlett, Journal of Aerosol Science 30 (1999) 823-849.) B) Illustration Of Nozzle Tip.

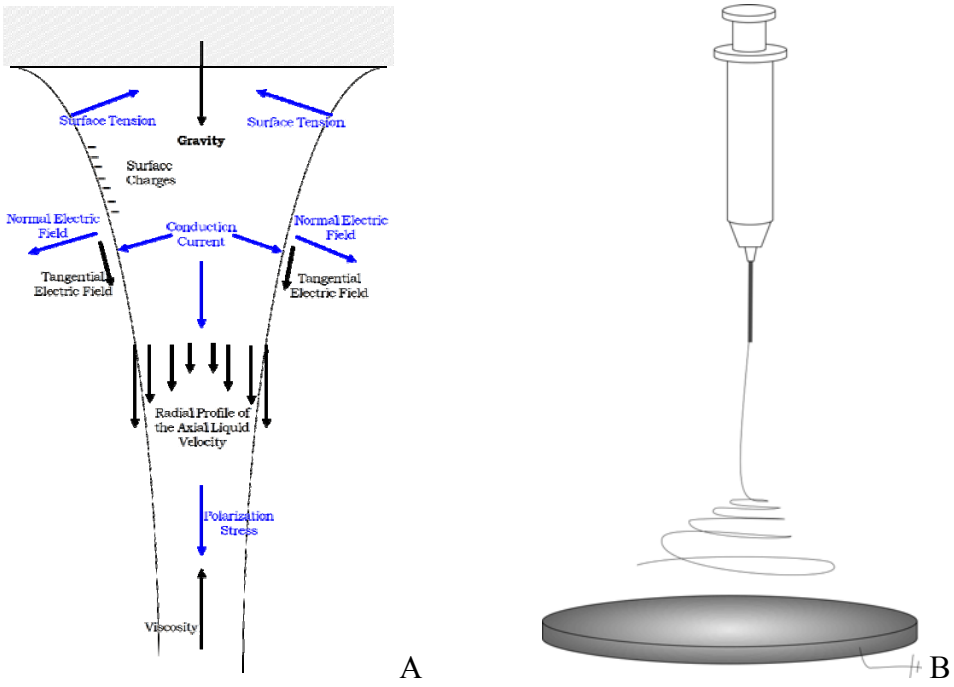

Figure 2-2. Close-Up Of Electrospinning Schematics: A) Summary Of Electrostatic Stresses Experienced By The Jet At The Tip Of The Nozzle. (Adapted R. P. A. Hartman, D. J. Brunner, D. M. A. Camelot, J. C. M. Marijnissen, B. Scarlett, Journal Of Aerosol Science 31 (2000) 65-95.) B) Example Of Whipping Action Experienced By The Jet (Figure Not Drawn To Scale).

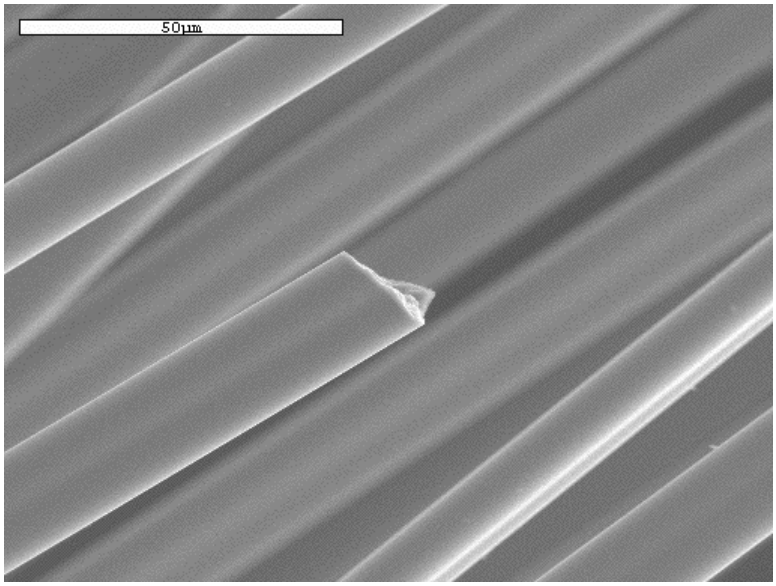

Figure 2-3. SEM Of 3M's Nextel 610 Fibers. >99% Al_2O_3 As Received From 3M With Fiber Diameters Averaging At 14µM Along With Noted Grain Sizes Of 0.1 µM.

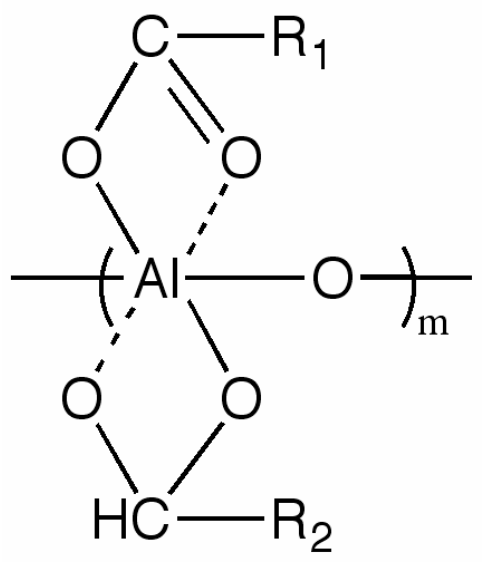

Figure 2-4. Example of Generic Aluminoxane Polymer. (Note: R_1 And R_2 Are Organic Ligands, While m Is The Degree Of Polymerization)..

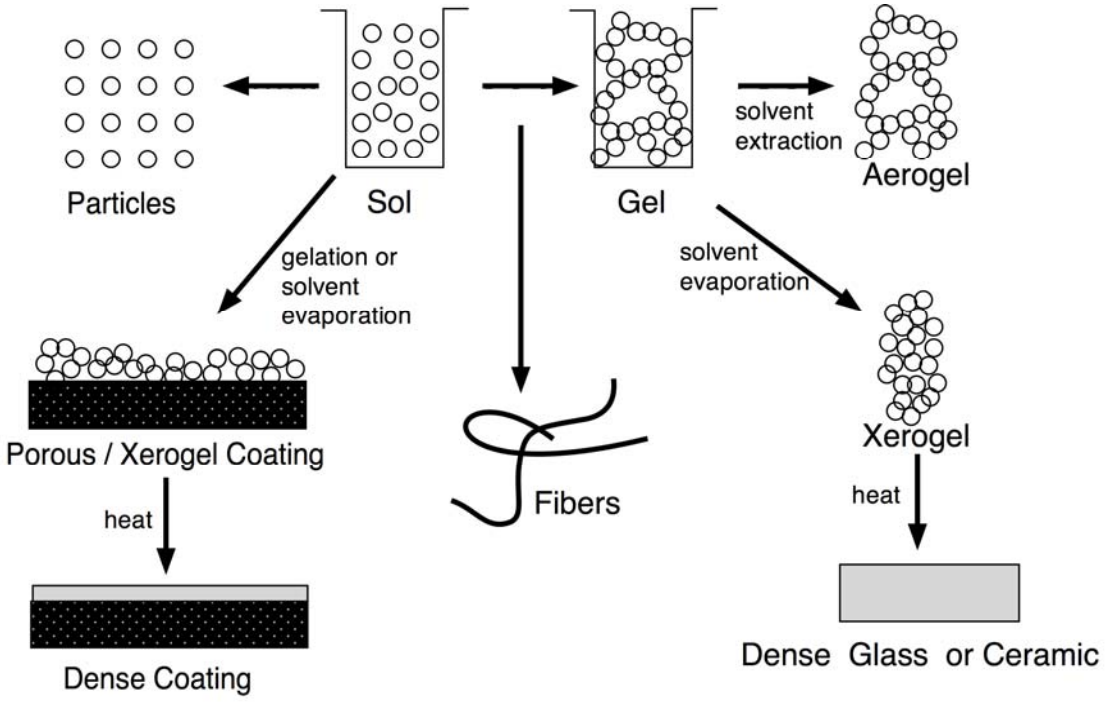

Figure 2-5. Schematic for Potential Processing Routes Of Sol-Gel Based Materials. (Adapted From C. J. Brinker, G. W. Scherer, Sol-Gel Science: The Physics And Chemistry Of Sol-Gel Processing, Academic Press, Boston, 1990.)

Hydrolysis

i. $M(OR)_x + xH_2O \longrightarrow M(OH)_x + xROH$

Condensation

ii. $(OR)_{x-1}M\text{-}OH + OH\text{-}M\text{-}(OR)_{x-1} \longrightarrow (OR)_{x-1}M\text{-}O\text{-}M(OR)_{x-1} + H_2O$

or

iii. $(OR)_{x-1}M\text{-}OR + OH\text{-}M\text{-}(OR)_{x-1} \longrightarrow (OR)_{x-1}M\text{-}O\text{-}M(OR)_{x-1} + ROH$

Figure 2-6. General Set Of Reactions For Hydrolysis And Condensation. (Note: The M Denotes A Metal With A Given Charge Of x, The -OR Are Respective Ligands. Condensation Can Proceed With Two Types Of Reactions Until Respective Completion: ii.) Partially Hydrolyzed Molecules Link Together; iii.) Partially Hydrolyzed Molecule Links With An Alkoxide Ligand.)

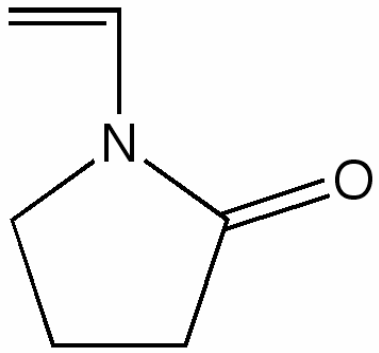

Figure 2-7. Unit of n-Vinyl Pyrrolidone.

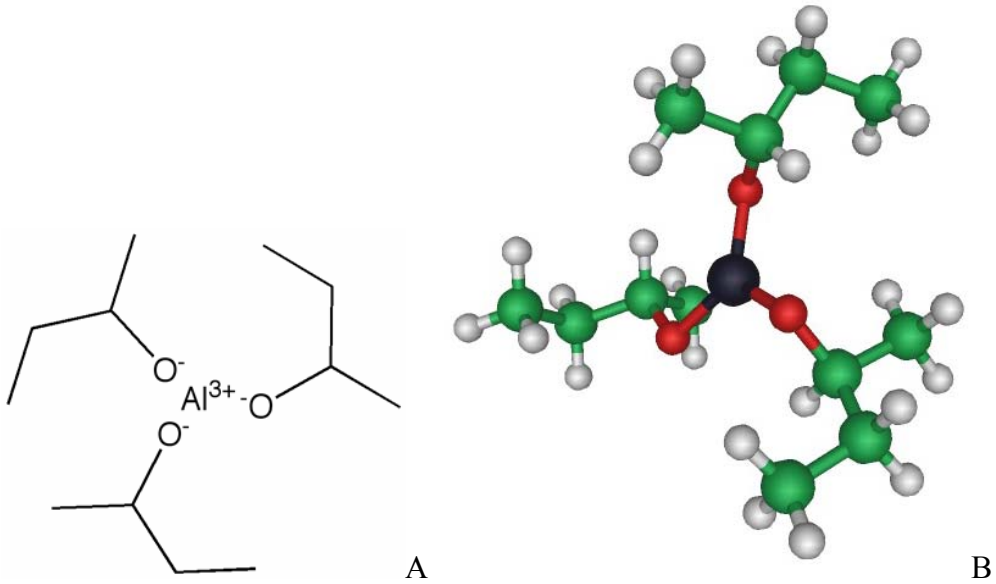

A B

Figure 2-8. Molecule Of Aluminum Tri *Sec* Butoxide (ASB), $Al(OC_4H_9^S)_3$: A) Chemical Structure Drawing. B) Ball And Stick Model, Key: Black = Aluminum, Red = Oxygen, Green = Carbon, And Grey = Hydrogen.

Proportion in weight (%)		
PVP	ASB	BA
1	47.5	51.5
2	45	53
4	40	56
10	25	65
15	12.5	72.5

A

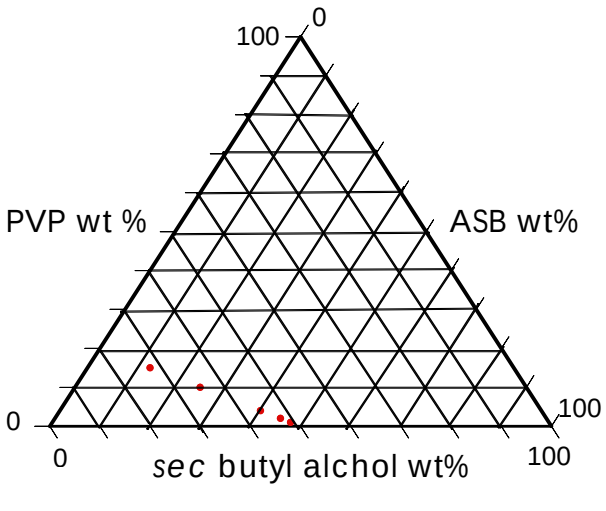

B

Figure 2-9. Data For Metal Alkoxide Incorporation Into PVP: A) Composition Of Precursor Mixtures Of PVP, ASB, And *Sec* Butyl Alcohol In Weight Percentages. B) Ternary Diagram Of Compositions.

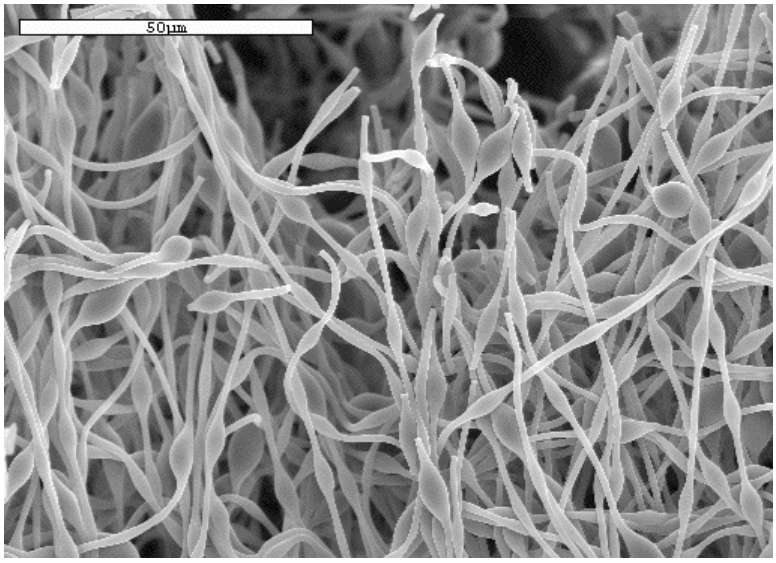

A

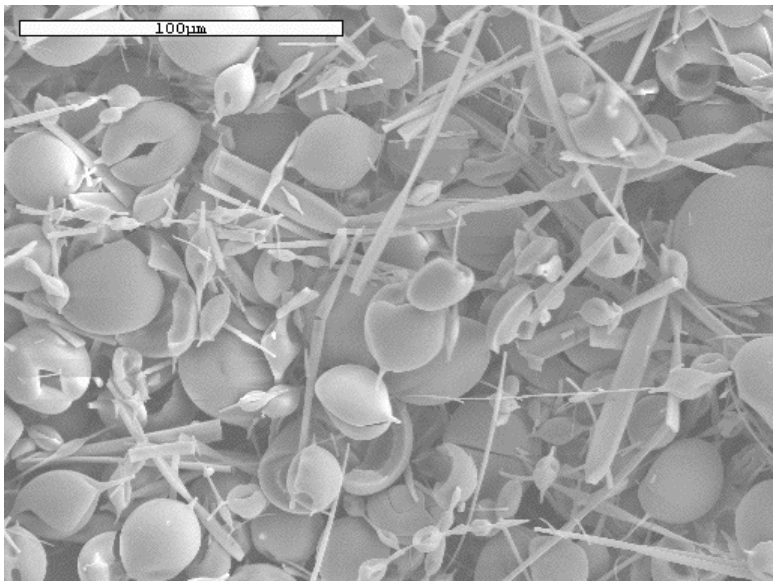

B

Figure 2-10. SEM Of Electrospun PVP With ASB/BA: A) 10 Wt% PVP With ASB/BA, Scale Bar At 50 µM. B) 5 Wt% PVP With ASB/BA, Scale Bar At 100 µM.

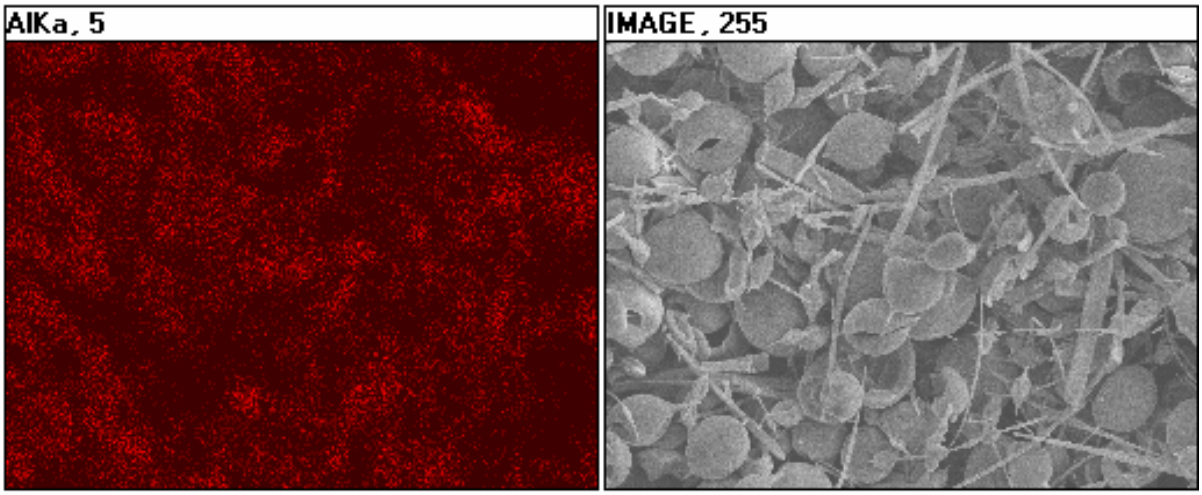

Figure 2-11. X-Ray Map Of Aluminum K_a From SEM Of 5 Wt% PVP With ASB:BA

CHAPTER 3
ALKOXIDE-BASED PRECURSOR DEVELOPMENT

Alkoxide-based precursors are used to form the basis for a new class of electrospinning precursors to circumvent previously mentioned issues with the reproducibility of precursors, low ceramic yield, and structural integrity issues due to calcinations. Electrospinning of alkoxide-based precursors will rely on atmospheric moisture to promote solvent evaporation in parallel with hydrolysis and condensation of the extrudate. Although the schematic for this new precursor design was simply stated, the concept relies on an inherent understanding of aluminum alkoxides, selection of the ideal metal alkoxide, and interaction with various types of solvents and ligands.

In following the reader will be guided through the selection, processing methodologies and findings made when preparing precursor solutions. Proof of concept electrospinning tests performed on the solutions for further assessment will be presented in the end of the chapter to report on structures and stimulate further investigative parameters.

Selection of Aluminum Alkoxides

Material selection is an integral part of the processing, structure and property relationship. Inherently metal alkoxides have physical properties largely influenced by the size and shape of the alkyl groups (R) as well as the valency (x), atomic radius, stereochemistry, and metal's coordination number [72]. The M-OR bonding characteristics of the compounds can be seen to posses a significant ionic character due to the high electronegativity of oxygen (Pauling scale = 3.5) [72, 73]. Furthermore the metal to oxygen to carbon bonds ($M^{\delta+}$ - $O^{\delta-}$ - C), as seen with aluminum, possesses an ionic character of 65% for metals with electronegativity (EN) values around 1.5 [72, 73]. An interesting trait of metal alkoxides is their tendency to exhibit solubility

in organic compounds along with volatile behavior, which is a result of the covalently bonded nature of the compound.

Aggregation, also known as oligomerization, is commonly found in metal-alkoxides systems and extensively studied in the aluminum-based alkoxides. Bradley explains that the extent of aggregation (*n*) for an alkoxide with a stoichiometry $[M(OR)_x]_n$ depends on the following: 1.) As the metal atom becomes more electron deficient, oligomerization increases; 2.) The tendency to increase the degree of association (*n*) with alkoxo bridged systems is due to the larger size of the metal atom; 3.) Increasing steric effects due to alkyl substituents demands inhibit aggregation and is found to be more important than the electronic nature of the substituents, while determining extent of aggregation [72-74]. Another simplistic reasoning provided by Guglielmi is that oligomerization is driven by its tendency of the metal to maximize its coordination number, even through bonding of nearby alkoxide molecules, which in some cases is also codependent on the nature of the solvent and concentration [43]. Volatility of the alkoxide derivative is another property that must be taken into account during material selection. Volatility is a dynamic property of some alkoxides, wherein the bond changes of the $M^{\delta+} - O^{\delta-} - C$ can increase or decrease in polarity due to inductive effects with changes with volatility [43, 72]. The general acceptance is that the volatility of the alkoxide is inversely related to the degree of oligomerization [43, 72].

Aggregation is a one of the characteristics that is believed to assist in choosing alkoxides for electrospinning precursors, since it increases the viscosity and hence spinnability of the compound. The viscosity of the precursors varies due to chain length and branching of alkyl groups, in addition to the degree of molecular association. However there are no derivatives that ascribe a rule to account for the range of viscosity values for oligomerization [43].

The steric crowding properties differ for the alkoxide ligands exhibiting (-O - CH_2) bonding to metal, as seen with (R= *n*-C_4H_9, *i*-C_4H_9, *n*-C_5H_{11}, etc), resulting in symmetric aggregated molecules. Meanwhile sterically bulky groups, such as secondary or tertiary, (*s*-C_4H_9, *t*-C_4H_9, etc) promotes tetra-coordinated Al atoms into penta-coordinated or hexa-coordinated Al atoms- wherein dimers and trimers are formed as less constrained species with the impediment.

The most commonly studied and utilized aluminum alkoxide in ceramic applications is aluminum tri *iso*propoxide (AIP) and aluminum tri *sec*butoxide (ASB) as seen in Figure 3-1 and Figure 2-8, respectively. Both encompass sterically bulky OR groups and have been shown to form tetra-, penta- and hexa-coordinated compounds, as opposed to solely a trivalent based $Al(OR)_3$ [47, 75]. An example of a large oligomer formed is the tricyclic structure for a hexa-coordinated aluminum alkoxide in Figure 3-2. This is the most bulky oligomer found in freshly prepared aluminm alkoxides [47].

The commonly found alkoxides, ASB and AIP, are often found in different physical states. ASB is found in its neat state as a viscous liquid. Meanwhile AIP is found in powder form and has to be solubilized in appropriate solvent(s) at elevated temperatures [72, 73, 76]. AIP is the most abundantly produced aluminum alkoxide, since its formed by reaction of aluminum metal and isopropanol in the presence of catalysts; ASB is synthesized from alcoholysis of AIP with *sec* butyl alcohol thereby fractional distillation [72, 76].

Since AIP comes in powder form, its high specific surface area has a tendency to undergo hydrolytic attack - it then becomes difficult to differentiate between either the hydrolyzed and alkoxide white powder. However, freshly distilled AIP is initially found in a trimeric state; a tetramer oligomer forms upon aging soon after preparation [43, 47, 72]. This tetrameric form

increases difficulty in solubility, as studied in aliphatic solvents for ink and painting applications [77, 78].

Choosing a lower weight OR ligands, such as methoxides, would be a disadvantage since there is an unusually low solubility of this metal alkoxide in organic solvents. This is due to the factors that affect aggregation and the idea that small sized groups such as the methyl groups do not tend to form oligomeric forms [72, 74].

Therefore the availability and selection of ASB as the primary alkoxide, as a new class of precursor for electrospinning, would simplify further mixing due to its liquid state, presence of large oligomeric species, ability to dissolve in a variety of organic solvents and a multitude of modification studies performed. In addition, the complex alkoxide has been extensively studied as a precursor to prepare transition phases of alumina for catalytic and sensing applications [27, 28, 31, 35, 36, 40, 48, 50-52, 54, 58, 79-87].

Establishing Processing Parameters for Determining Precursor Spinnability

The concept of aluminum alkoxide-based precursors without organic polymer additives is currently nonexistent in all fiber spinning research realms. However, from previously mentioned works described in Chapter 2, there were polymer-less structures formed during electrospinning of ASB and PVP precursors.

Spinnability is a generic term to qualify solutions that are able to produce fibers through electrospinning. Previously these parameters were reviewed for each genre of precursor in both conventional and electrospinning methodologies. Spinnability with the chosen alkoxide will thusly depend on more factors due the dynamic chemistry. The pendant dropping of the alkoxide solution in the atmosphere will result in hydrolysis and condensation. This inorganic polymerization increases the localized viscosity. Additional solvents may deter or accelerate hydrolysis *via* an alcoholysis, complexing, and/or inability to evaporate during drawing. In fact

it is believed that the hydrolysis and condensation of the metal alkoxide should assist in stabilizing the fibers during electrospinning, thusly stabilizing the fiber backbone.

Previous Rheological and Hydrolysis Studies of Aluminum Alkoxides

There have been no reported works done in the field of rheology and hydrolysis studies to understand the neat ASB. There is a propensity to hydrolyze and undergo condensation, that makes the precursor difficult to prepare for analysis.

A hydrolyzed atmosphere is apparent in all but the strongest of vacuum chambers. Performing rheology studies has proven difficult, due to the lack of available glove boxes that incorporate a rheometer. In regards to hydrolysis studies, kinetic studies are not well documented, according to Brinker and Scherrer, because aluminum alkoxides undergo such facile kinetic pathways towards nucleophilic addition [23].

Preparing Precursors

In this section, there will be a discussion about the various precursors that were prepared. Before the precursors were prepared, it is vital to understand the role that various solvents and methodologies have with ASB. The goal of this chapter will be discuss the preparation of various alkoxide-based precursors and subsequent proof of concept electrospinning studies. The latter will provide an initial structure to processing relationship from the freshly derived precursors.

There have been numerous discussions regarding the use of solvents, such as alcohols, glycols, β-diketones, and more. Key works studied the delaying the kinetics of ASB by modifying the ligands through complexing or transesterification reactions [30, 33, 35-37, 42, 45, 46, 55, 72, 77, 78, 82, 88-91]. However, these previous-mentioned generalizations only skim the surface of works that have been explored with ASB and its similar counterparts. This subsection will present precursor preparation strategies.

ASB and Alcohols

Earlier it was mentioned that ASB is a product of alcoholysis and fractional distillation from AIP. This process can also be referred to as an alcohol exchange or transesterification. The $-OR_1$ groups are subsequently replaced with a different $-OR_2$ group. Most metal alkoxides, except for silicon, can react with a variety of alcohols- primary, secondary, tertiary.

The neat body of ASB is a very viscous liquid. This noticeable viscous solution is due to a large part of the aggregation of the alkoxides. The solution in ambient atmosphere tends to also display some surface textures due to localized solidification of the solution as a result of volatility.

Obviously there are associated reasons that contribute to the ability to exchange: 1.) Solubility of reactants and products, 2.) Steric demands, 3.) Relative standard enthalpy change of formation, ΔH°, of ionization of reactants and products, 4.) Relative bond strengths of ligands to metal, 5.) Any presence of strongly bridged and/or more replaceable terminal alkoxo groups, and 6.) Presence of oxygen attached electron-donating and withdrawing groups [72].

Shifting the equilibrium to the desired direction requires fractional distillation of the lower boiling point alcohol (usually as an azeotrope with benzene). BA was previously explained to be the acronym to *sec* butyl alcohol or 2-butanol and can form an azeotrope with benzene with in a 13/87 azeotrope fraction mixture with an azeotrope boiling temperature of 78.9ºC. BA has a Hansen parameter (δ_t) of 22.2 MPa [92].

The Hansen parameter is a parameter defined as the square root of the cohesive energy density [93]. In short, it is calculated as a parameter, based on the thermodynamics of the solution, to assist in predicting solubility of solvents and other compounds.

In addition to the readily used benzene, BA forms azeotropes with cyclohexane, diisobutylene, toluene, and water. Regarding water, the azeotrope is 34/66 (BA:H_2O) with a temperature of 88.7ºC. Interestingly enough, it has been demonstrated that high-boiling alcohols may be used; however, repeated treatment will be required to complete evacuation of the solvent [76].

Native alcohol

The initial preparation was the dilution of neat ASB within its' own alcoholic species. Solutions of ASB were weighed in jars and stoichiometric amounts of BA were added. The molar ratios of ASB:BA that were prepared were: 1:3, 1:2, 1:1, 2:1, and 3:1. The upper and lower limits of dilution were prepared based on the general compound structure. For example the 3:1 is a three molar ratio of ASB and one of the BA; for every nine alkoxide ligand there was one solvent being added.

At least three repeated solutions were made in three different batches for each set of experiments. Solutions were sealed in the jars by preventively using Teflon tape wrapped threads and paraffin film sealing the outside.

Higher ordered alcohols

Higher ordered alcohol exchange was created with hexyl alcohol (1-hexanol), octyl alcohol (1-octanol), and dodecyl alcohol (1-dodecanol). The respective δ_t for these solvents are 21.9, 21.1, and 20.4 MPa; meanwhile the value for cyclohexane and hexane are 16.8 and 14.9 MPa [92].

Method 1 for higher ordered alcohols

ASB was measured into screw-top vials and the appropriate alcohols were dispensed. The molar ratios of ASB:alcohol were 3:1, 2:1, 1:1, 1:2, and 1:3. Solutions that were adequately

mixed were all the alcohols in the molar ratio ranges to create solutions: with hexanol (ASB:HEX), octanol (ASB:OCT), and (ASB:DOD)

Method 2 for higher ordered alcohols

ASB was measured into cyclohexane (later repeated with hexane) and then the appropriate amount of desired higher ordered alcohol was added. The reaction was set up with a refluxor attached with to a vacuum line for a vacuum distillation. Once the internal temperature of the solution reached the temperature of the azeotrope boiling point, the vacuum was turned on. The vacuum assured residual removal of volatile species and expedited the distillation process. The thermometer inserted into the refluxor was used to monitor the start and end points of fractional distillation. The experiments were later repeated by substituting cyclohexane with hexane to allow removal of the solvent without volatilization of the alcohols or BA alkoxide. The molar ratio of ASB:alcohol of interests in this exchange were 1:1, 1:2, and 1:3.

Analysis of prepared with higher ordered alcohols

Once the solutions were cooled, they were collected into amber screw-top jars. The cooled solutions exhibited a physical appearance that was not apparent in any of the lower alcohol species. The appearance of the resulting precursors was an opaque greasy feeling semi-solid. This appearance may be related to the higher length of straight alkyl chains and formation of subsequent symmetric groups with subsequent polymerization.

The extent of the semi-solidification was more pronounced for increasing alkyl length of the respective alcohols. Therefore further experiments were not repeated for secondary and tertiary groups of those respective alcohols. Although there were no investigations with any isomers of pentyl alcohol, it was clear that the solubility of the alcohol exchange should result in a similar trend.

Additional, the inability to form solutions after exchange in high-ordered alcohol modification, it may be an advantage to steer clear of usage of the higher-ordered alcohols due to their immiscibility in water and even higher boiling points. This may lead to increased difficulty during hydrolysis during the fiber electrospinning with an additional difficulty in solvent evaporation.

ASB and Glycols and Glycol Ethers

The use of various types of glycols with aluminum alkoxides has been a subject of study [36, 56, 88, 90, 91, 94]. The basic glycol is comprised of dihydroxy functionality such as ethylene glycol; in contrast, an alcohol has one hydroxy ligand. Essentially chemists find that glycols can be highly reactive towards metal alkoxides, thusly forming homoleptic and/or mixed alkoxide-glycolates of metals [32, 33, 36, 43, 72, 77, 78, 88, 94, 95]. Another derivative of a glycol is the glycol ether; the latter is a product of a reaction of a glycol and an alcohol, which results in one hydroxyl functionality and an oxygen in the main alkyl chain. Both the glycol and glycol ether are have demonstrated the reduction of steric demands- the increase in coordination numbers and oligomerization in the native alkoxide; in addition chelating and center bridging is also possible [72-74, 77, 78, 88, 90, 95]. Two types of preparation methods were used: 1.) Mixing the glycolates with ASB or a diluted ASB and 2.) Performing a vacuum distillation in non-reactive solvent.

Incoporating glycolates takes in regards general selection trends: 1.) Central metal properties and its oxidation state, 2.) Type of glycolate and structure, and 3.) The stoichiometry and concentration. This work will study the addition of various solvents: ethylene glycol (EG), 1,6-hexylene glycol (HEG), ethylene glycol monobutyl ether (EBE), and diethylene glycol monethyl ether (DGME).

Glycols

Selection of the glycols was based on previous works and solubility. Since EG is the most common glycol, it was chosen. Both the EG and HEG were chosen based on their solubility in the native BA alcohol and also in water. Meanwhile the length of HEG also approaches the limit of solubility in BA.

Method 1 for glycols

Anhydrous EG and HEG were immediately stored with zeolite molecular sieves to deter water adsorption and used immediately. Measured amounts of EG or HEG was added, respectively, to the neat ASB in screw-top vials. The experiments were repeated with two new batches of chemicals. A total of three repeats were preformed. Molar ratios of ASB:glycol were 3:1, 2:1, 1:1, 1:2, and 1:3.

Method 2 for glycols

A known amount of ASB was added to cyclohexane. In following, EG or HEG were added to the solution and the heat was increased to right under the azeotrope temperature and then the vacuum was turned on. Once the temperature in the refluxor decreased to its starting temperature, the vacuum was turned off and cooling began. In following the experiment was repeated with hexane to allow further removal of the non-reacting solvent. Molar ratios for ASB:glycol in this ligand exhange were: 1:1, 1:2, and 1:3.

Analysis of prepared solutions with glycols

Both type of methods resulted in the production of the presence of insoluble materials. During the initial experiments, it was thought that the first method simply precipitated aluminum hydroxide species. After subsequent meticulous preparations, the insoluble material was still present in both method 1 and method 2. Works by McMahon discovered the presence of Alucones, preceramic polymers of aluminum alkoxides made through reaction with ethylene

glycol [88]. Essentially these substances have proposed functionalities that vary in degree of coordination, depending on the synthesis method. The main difference between alucones and previous studied aluminoxanes (Figure 2-8) is the fact that the former does not undergo any hydrolytic reaction. These alucone substances can be fired, thus leading it to subsequent phase transformations of an intermediate phase, the gamma phase. Thermal treatment of the regularly repeating polymeric penta-coordinated structures can actually create micropores that are in periodic arrays that may be useful for catalysis applications in the gamma phase [88].

Nonetheless this insoluble preceramic polymer doesn't comply with the design specifications to produce homogenous solutions that can be electrospun. These alucones have characteristics of opaque dense precipitates. Nonetheless exploration of this method explains the use of dihydroxy functionalize ligands that resulted in polymerization of the metal alkoxides into further oligomeric and polymeric forms and the inability to be used for alkoxide-based precursors.

Glycol Ethers

Glycol ethers have been utilized towards paints, coatings, and other family of applications requiring both an alcohol and water aliphatic compound. This versatile behavior of glycol ethers is essentially an interesting component to investigate the effects on the structure of ASB. Researchers have worked with these solvent as modifying ligands and also as complexes, assisting with delaying hydrolysis, creating porous materials, and changing phase transition temperatures [32-34, 36, 72-74, 77, 78, 90, 91, 94, 95]. When glycol ethers are reacted with the metal of interest for direct attachment, it has low steric repulsion and thus is able to maximize coordination. These solvents have been used to promote hexa-coordinated compounds as seen in Figure 3-2.

The same reaction methodologies, as seen with glycols, were employed with glycol ethers. Solvents utilized in this set of works were ethylene glycol monomethyl ether (or 2-methoxy ethanol) and diethyelene glycol monoethyl ether (or 2-(ethoxyethoxy) ethanol). Both solvents have δ_t values of 23.5 and 22.3 MPa. Figure 3-3 displays the general chemical structure for the two solvents. The molar ratios that were mixed are the same as in the previous subsections.

Method 1 for glycol ethers:

Solutions of ASB were initially weighed into screw-top vials. The desired volume of solvent was added to ASB and thoroughly mixed with a magnetic stir-bar with a closed lid. An exothermic reaction was observed, through a heating of the vial. The temperature of the heating was not measured. The solutions were stored with Teflon tape sealing the threads and paraffin film on the outside. In this sample batch, three repeats were made total. Also for each new batch of metal alkoxide and/or solvent, replicates were also mixed. Molar ratios of ASB:EG and ASB:DG mixed were 3:1, 2:1, 1:1, 1:2, and 1:3

Method 2 for gycol ethers

Solutions of ASB were initially weighed into cyclohexane and then the appropriate amount of EGM or DGME was dispensed. The same set-up found in the previous solvent experiments was utilized. Also for repeated experiments, the solvent was changed over to hexane. Repeats followed the same schematic as note in Method 1. These solutions were titled mod-ASB:DG. Molar ratios of mod-ASB:DG solutions were 1:1, 1:2, and 1:3. The main goal is to be able to undergo a transesterification to replace a *sec* butoxy group with EGM or DGME.

Analysis of prepared solutions with glycol ethers

Both methods produced homogenous solutions with no observations of precipitation or immiscibility. There was an obvious difference in viscosity between the two methods. Obviously this related to the the advantage that Method 2, thereby fractioning out volatile BA

species. Nonetheless through observations the precursor produced in Method 2 did not display the same physical behavior as seen with the neat ASB. The solution ebbed and flowed more fluid than observed for the neat ASB. This flow is indicative of the change in both the volatility and hydrolytic susceptibility.

ASB and β-Diketones

β-Diketones generated equal enthusiasm as with glycols because they have the comparable ability to promote a unique type of bonding. There were many striking similarities between alcohols and the various glycolates, however β-diketones drastically differ in the fact that they can take on an enolic form with side groups comprising of alkyl or aryl groups. β-diketonate ligands are known for their much less reactivity to volatility and hydrolysis and have the unique ability to undergo tautomerization and promote bidentate ligands to the metal of interest [37, 72]. Many researchers have studied and applied the use of aluminum-based β-diketonate compounds due to a better control over hydrolysis to controlling the kinetics and transforming properties of sols, gels, and much more [30, 35, 37, 42, 45, 46, 49, 56, 74, 76, 89].

Two common compounds studied in this category are acetylacetone (2,4-pentanedionate) and ethyl acetoacetate (Ethyl 3-oxobutanoate). In Figure 3-4, ethyl acetoacetate is shown with its respective tautomerization. The type of modification that takes place can range from replacing one alkoxide ligand up to all three respective ligands. Typically the trichelated aluminum of AA is often available in powder form.

The coordination of the metal - β-diketonate and subsequent oligomerization is an important factor that relates its ability to remain transparent thereby controlling hydrolysis. Bonhomme-Coury published a very detailed study of an aluminum di sec butoxide functionalized with one EAA molecule; essentially their group discussed the idea that EAA

ligands are not as labile as the alkoxide groups- preventing rapid hydrolysis and growth of the oxide network [37]. The solution synthesis for above-described methods was modified for this set of work. This subset of work only examined EAA, since works with EAA and AA should provide similar results due to chemical similiarity. Since tri functionalized aluminum β-diketones are available in solid form, it would be unnecessary to thusly study that form.

Method 1 for β-diketones

ASB was weighed out into screw top vials. Subsequently EAA was added and stirred. The samples were stored in the same fashion as previously described. Molar rations of ASB:EAA explored in this set of work were 3:1, 2:1, 1:1, 1:2, and 1:3.

Method 2 for β-diketones

ASB was weighed and mixed with cyclohexane and in further experiments, hexane. Then EAA was added and vacuum distillation was performed. The solutions were collected and samples were repeated at least 3 times for each batch or newly opened ASB or EAA precursor. Molar ratios of mod-ASB:EAA that were synthesized were 1:2 and 1:1. Ligand exchange, once again, was the main goal.

Analysis of prepared solutions with β-diketones

Both methods produced homogenous samples that seemed fitting for the next set of work to analyze its feasibility during electrospinning and also the corresponding chemical properties. Method 1 produced solutions that seemed diluted. However in method 2, the samples appeared much more viscous than that produced in Method 2.

Use of β-diketones has its advantages and disadvantages. Initially β-diketones, as ligands, can be used to increase spinnability, however there is concern over its delay in the hydrolysis..

Electrospinning Feasibility Study

This section serves as an exciting advancement to promote the study the processing of the prepared precursors. The electrospinning feasibility of the precursor essentially forms a sort of metrics for these precursors. This study, although simple in its own right, served as the catalysts for further studies of processing and material properties. In this section, the objective is to explore the electrospinnability of the precursors through the control of certain processing parameters. Various electrospinning parameters were implemented to attempt the fabrication of fibers. The goal awaiting the end of the chapter will be a discussion of the precursor solutions' performance and plans for future evaluations. Chapter 4 will be a more detailed study of relationship of electrospinning processing parameters and the structure of the fibers formed.

Electrospinning Parameters

Although models exist for current electrospinning research, these are limited to the type of and particular precursors being studied. Since alkoxide-based precursors are firstly being introduced in this dissertation, it was necessary to perform feasibility studies to obtain a general understanding of the processing to structure relationship. Therefore an initial set of processing parameters were implemented and observed to generate an understanding of the precursor behavior and hence electrospinnability. Although it was previously mentioned that rheological properties seem to be the most dominant feature in other electrospinning studies, this feasibility study concentrated its efforts on feasibility of forming structures through changes in flow rate and the electric field since the alkoxides also depend on kinetics of hydroloysis.

Looking back at the basis of sol-gel chemistry- hydrolysis and condensation reactions are fundamental. Wherein the flow rate becomes, strikingly, the most important parameter for this line of work. This field of utilizing precursors depends on the drawing of the solution out of the needle tip to then undergo hydrolysis and condensation thereby maintaining a stable fiber

backbone. This fiber stabilization occurrence can be due to the degree of oligomerization of the precursor solution also predominantly the kinetics of hydrolysis and condensation to form the inorganically polymerized oxide network.

All samples were drawn into 5cc Becton-Dickinson syringes attached to a 16-gauge needle (inner diameter of 1.65mm). Experiments were performed in the same laboratory hood at ~ 25ºC $\pm$ 3ºC with a relative humidity of R_h = 45% $\pm$ 5%. Briefly relative humidity can be defined as the amount of water calculated in the atmosphere at a desired temperature by taking the ratio of the partial pressure of water in the atmosphere and the partial pressure of the saturated water vapor [96, 97]. Laboratory hoods maintain a consistent range of relative humidity and temperature; also the values were noted for each experiment.

Solutions that were under study included:

- ASB:BA- Solutions that were directly mixed ASB and BA with ratios of 1:3, 1:2, 1:1, 2:1, and 3:1
- ASB:HEX- Solutions that were directly mixed ASB and HEX with ratios of 1:3, 1:2, 1:1, 2:1, and 3:1
- ASB:OCT- Solutions that were directly mixed ASB and OCT with ratios of 1:3, 1:2, 1:1, 2:1, and 3:1
- ASB:DOC- Solutions that were directly mixed ASB and DOD with ratios of 1:3, 1:2, 1:1, 2:1, and 3:1
- ASB:EG- Solutions that were directly mixed with ASB and EGM in ratios of 1:3, 1:2, 1:1, 2:1, and 3:1
- ASB:DG- Solutions that were directly mixed with ASB and DGME in ratios of 1:3, 1:2, 1:1, 2:1, and 3:1
- mod-ASB:DG- Solutions that underwent vacuum distillation with ASB and EGM or DGME in ratios of 1:1, 1:2, and 1:3
- ASB:EAA- Solutions that were directly mixed with ASB and EAA in ratios of 1:3, 1:2, 1:1, 2:1, and 3:1
- mod-ASB:EAA- Solutions that were underwent vacuum distillation with ASB and EAA in ratios of 1:1 and 1:2.

Feasibility flow rate studies

There were four different flow rates investigated (cc/hr): 0.254, 1.27, 3.81, and 7.62. On a side note, the time it would take to completely electrospin a 5 cc syringe would respectively be (hrs): 19.69, 3.93, 1.31, and 0.66. This study was performed at a set voltage and working distance of 10kV and 15cm (an electric field of 0.66 kV/cm).

Solutions that performed in terms of success produced some form of fibrous structures as seen in Figure 3-5A. Nonetheless other forms of solidified structures were produced. Fibrous structures included continuous fibers along with broken fibrous-like structures. Alternative structures were powders, sheets, or flakes. Precursors that were deemed unsuccessful did not produce identifiable products, since they just prematurely dried at the nozzle- leaving a solidified gel. Some other solutions did not dry- leaving puddles of unreacted precursors gathered on the collection plate.

Solutions of ASB:BA (2:1, 3:1), ASB:HEX (2:1, 3:1), ASB:EG (2:1, 3:1), and ASB:DG (2:1, 3:1), mod-ASB-DG (1:1) produced continuous fibers. These displayed features of a white cotton-like bundle as seen in Figure 3-5A. On the contrary, typical electrospun fibers with organic polymer-based precursors deposited fine fibers that appear as flat, often difficult to collect, opaque sheets well adhered to the foil. These alkoxide-based precursor fibers were easily collected without any adherence issues. Figure 3-5B is an SEM of a group of fibers collected from the ASB:BA 3:1 mixture processed at a flow rate of 3.81 cc/hr. Defected structures presented in this figure were analogous to the other precursors producing continuous fibers. Observations include some ill-formed fibers or amorphous globular structures. Besides continuous fibers, discontinuous fibers were seen with ASB:EAA 1:1, and powders with 1:1 ratios from ASB:BA, ASB:HEX, ASB:EG, and ASB:DG, as seen in Figure 3-6. There were at

least three imaging regions per sample and also a number of repeated samples; therefore these images are adequate representations.

The remainder of the solutions can be divided up into precursor solutions that- 1. Impeded the electrospinning process due to solidification or 2. Did not solidify at all into any sort of morphology. In the case of the former case, mod-ASB:EAA 1:2 and 1:3, and mod-ASB:DG 1:2, 1:3 can be classified. For the latter a myriad of solutions qualified, such as all 1:2 and 1:3 solutions of ASB:BA, ASB:HEX, ASB:OCT, ASB:DOD, ASB:EG, and ASB:DG.

Feasibility studies with other electrospinning parameters

Although the last subsection conveyed a general idea of the type of precursor solutions that can be investigated for further processing-property relationships, it was imperative to further analyze the changes in other electrospinning parameters to possibly augment any structural development. For the precursors that induced pre-mature solidification, both the flow rate and the electric field were increased, respectively. Although flow rates greater than 12.70 cc/hr eventually produced flow, but did not result in any solidified morphologies, such as fibers or particles. Additionally, increasing the electric field at the various flow rates did not assist in producing any impressive structures, either. For the solutions that resulted without any solidification, the flow rates were reduced below 0.25 cc/hr and electric field increased and decreased, respectively. Once again no other structural features could be produced as a result of changes made in this range of electrospinning parameters.

The solidification may be a result of the viscosity and volatility of the some components within the precursors, such as BA. Since the addition of ligands, such as glycol ethers and β-diketones have been found to delay hydrolysis, these extrudates are unable to completely be drawn out into fibers thereby electrospinning with ratios of 1:2 or even 1:3.

The process of electrospinning is a dynamic process with charge flow, as seen in Figure 2-2A; a solidified extrudate may not retain the ability to conduct and promote continual drawing. There may not have been apparent oxide network forming in these precursors, since the extrudates were, in fact, transparent and glassy. The latter coincides with delay in hydrolysis and condensation with these types of ligands.

The precursors that were prone to wetting and no structural formation lacked the ability to dynamically promote solvent evaporation while undergoing hydrolysis and condensation during the period of fiber drawing. An increase in solvent ratio drastically increases the amount of wetting species present, which deters drying during drawing.

Solvents with low solubility with water, may not be able to assist in the fiber forming process during electrospinning. It is believed that the miscibility with water, promoted hydrolytic attack and thus evolution of the present alcohols and other ligands. Therefore the solvent addition of EAA impeded the ability to hydrolyze adequately since it has a low water solubility of 3 wt% and low volatility and boiling point [98]. Thus it was found that some of the precursors' shortcomings were due to solvent volatilization, hydrolysis-condensation kinetics, and also water miscibility.

Discussion of Prepared Precursors

The production of alkoxide-based precursors was developed from limitations that existed with current electrospinning precursors designs. Fiber production, in this chapter, initiated further investigation of the electrospinning process and structure behaviors of alkoxide-based electrospun alumina fibers. The next chapter moves out of its precursor preparatory phase into a down-stream production, resetting the frame of mind thereby allowing thorough study of the electrospinning parameters that relate to structure along with chemical and physical properties of the chosen precursors.

Material selection of the metal-alkoxide, ASB, resulted from a more detailed understanding of the native aluminum alkoxide behavior, physical properties, and interaction with various types of solvents. Hence solvent interaction took place thereby a simple addition into ASB or through ligand modification. The addition of solvents resulted in a myriad of results, ranging from total miscibility to polymerizations, nonetheless it was found that some precursors prepared from alcohols, higher-ordered alcohols, glycol ethers, and β-diketones have produced both continuous and discontinuous fibers along with particles and globules. This chapter concludes in a positive light by bringing forth a new set of precursors for electrospinning and a curiosity to understand what's in store in the realm of electrospinning.

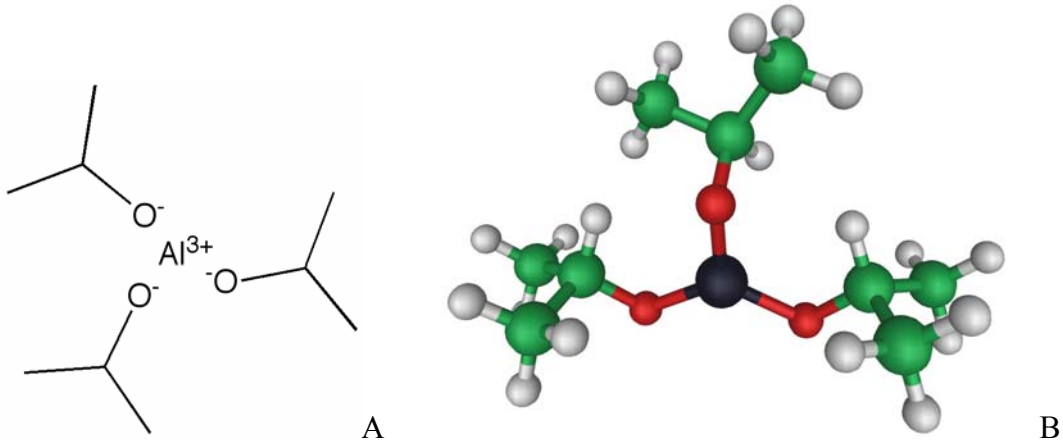

Figure 3-1. Structure Of Aluminum Tri Isopropoxide, $Al(OC_3H_7^{i})_3$: A) Chemical Structure Drawing. B) Ball And Stick Model, Key: Black = Aluminum, Red = Oxygen, Green = Carbon, And Grey = Hydrogen.

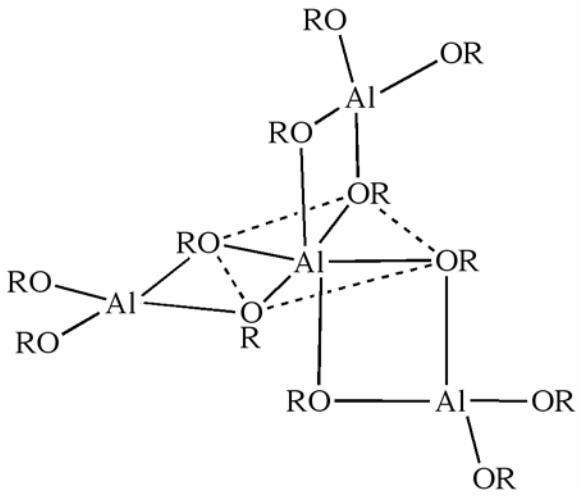

Figure 3-2. Hexacoordinated Tricyclic Structure For Tetrameric Aluminum Alkoxide Structures, R=Alkyl Groups. (Adapted from O. Kriz, B. Casensky, A. Lycka, J. Fusek, S. Hermanek, Journal Of Magnetic Resonance 60 (1984) 375-381.)

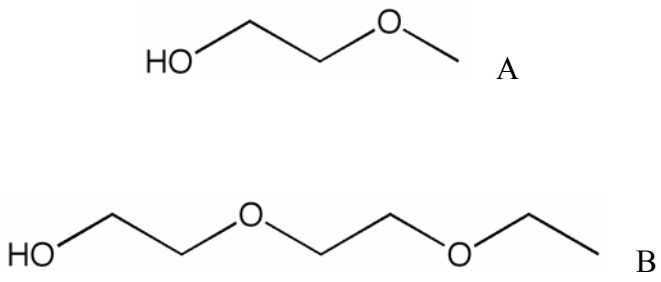

Figure 3-3. General Chemical Structures For Glycol Ethers: A) Ethylene Glycol Monomethylether (EGM). B) Diethylene Glycol Monethylether (DGME).

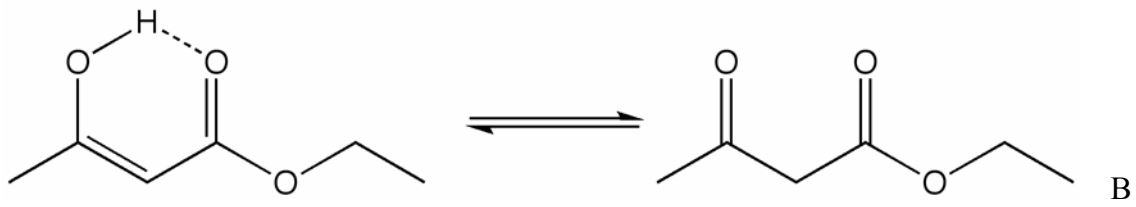

Figure 3-4. General Structures During Tautomerization Of Ethyl Acetoacetate (EAA).


A

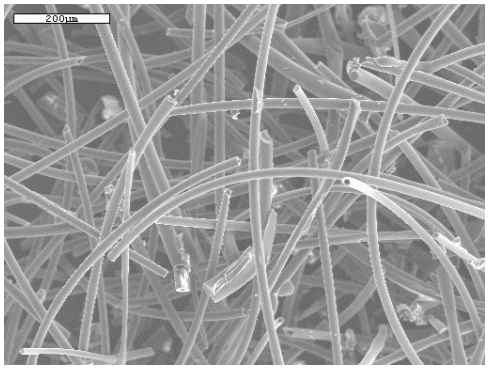

B

Figure 3-5. Observed Fiber Bundles From Electrospinning Feasiblity Study Of 3:1 ASBBA Solution 3.97cc/hr And 0.667kV/cm: A) Photograph Of Fibrous Bundle Formed. B) SEM Of Elecrospun Fibers From ASB:BA 3:1 Precursor In Feasibility Study, Scale Bar = 200 µm.

A

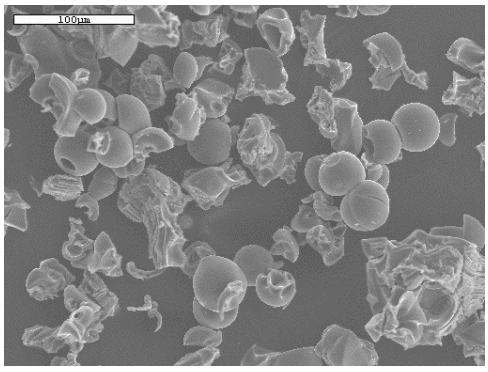

B

Figure 3-6. Alternative Morphologies Formed At 3.81 cc/hr And 0.667 kV/cm: A) Discontinuous Fibers Of Mod-ASB:EAA 1:1 Solution, Scale Bar = 100 µm, B) Particles And Globules From ASB:BA 1:1 Solution, Scale Bar = 100 µm.

CHAPTER 4
ELECTROSPINNING PARAMETERS GOVERNING ALUMINUM-BASED CERAMIC FIBER FORMATION FROM ALKOXIDE-BASED PRECURSORS

The main goal of this chapter is to derive an understanding of the relationship that electrospinning parameters have on the alkoxide-based solutions. Previous models were derived to explain the fiber diameter relationships fabricated through electrospinning, but limited to the particular chosen precursors [2, 7-10, 64, 65, 67, 68, 99-104]. Nonetheless these models ultimately delineated factors that may be studied to control electrospinning feasibility and ultimately fiber diameter. Parameters include solution charge, electric field, surface tension, and flow rate. Since this work is established with alkoxide-based precursors to circumvent some of the inherent issues in previously made precursors, it is necessary to understand the relationship that the latter mentioned processing parameters have on these new solutions. This chapter will begin with the selection of precursors to further study and follow with analysis from flow rate studies, voltage, working distance, the electric field, and needle gauge. This chapter will conclude with analysis with changes in the hydrolysis conditions. Although at the time, it is too premature to derive a model, this chapter will provide the necessary cognizance to pursue further down-stream processing of the alumina-based fibers.

Precursor Selection

It was first necessary to select precursors that would represent the group they are derived from. Importantly precursors that were identified to produce continuous fibers and particles will be analyzed in this chapter for its potential uses in a variety of applications.

To best represent the various groups of feasible solutions, the ratios of 3:1, 2:1, and 1:1 of ASB:BA and ASB:DG were selected to represent the alcohol and glycol ether addition-based solutions. Furthermore, the 1:1 mod-ASB:DG served as a representative of the ligand exchanged glycol ether group. Regarding the alcohol-added precursors, the native alcohol, BA, was

preferred as the alcohol medium, since it did not interfere with the current coordination state of the alkoxide. Although the addition of a glycol ether will slightly contrast the alcohol-added reactions, the larger molecule of DGME was chosen. Hydrolysis and condensation rates should differ, which should indicate a change in the electrospinning parameters. The use of DGME, or a glycol ether for that matter, changes the bonding state to a dominant hexacoordinated state, along with the tetra-coordinated state, as well [90]. Moreover the mod-ASB:DG will also be investigated, since the ligand modified solvent assures removal of free solvents and thusly can change the nature of the hydrolysis/condensation reaction nature. Therefore the amount of precursors being studied is reduced down to seven total solutions. Nonetheless the use of repeated solutions were assured throughout the course of this work.

Flow Rate

Flow rate was chosen as the initial variable to test because the flow rate directly determines the time of exposure of the precursor to the atmosphere. Exposure results in hydrolysis, condensation and solvent evaporation. Although the test resembles the parameters in the previous sections on electrospinning feasibility, this work provides a more detailed analysis of the optimal processing ranges of flow rate to its respective structures.

Flow Rate Methodology

The flow rate conditions were studied with a 5cc syringe and a 1.651mm diameter disposable blunt-tip needle. The electric field was set at 10kV and working distance of 15cm. The flow rates that were studied ranged from 1.27cc/hr up to 17.8 cc/hr. These tests were repeated to account for variability. The experiments were done in the laboratory hood's electrospinning set-up with the temperature at 25ºC $\pm$ 3ºC at a R_h = 45% $\pm$ 5%.

Precursors of ASB:BA

At the largest solvent concentration of 1:1, there were no fibers produced with any of the flow rate conditions. Nonetheless particles, particularly hollow particles, were formed that ranged in size dispersity depending on the flow rate as shown in Figure 4-1A. At 3-1 for ASB:BA, it is hypothesized that the hydrolysis and condensation still yields solid structures, wherein the large concentration of the solvent leads to discontinuous stabilization of the jet walls, better known as varicose instability as described by the EHDA theory. This break up of the jet thus can drive particles to form as the most thermodynamically stable shape. In addition, the smaller concentration of oligomers results in destabilization of the inorganic oxide polymer.

Meanwhile the 3:1 solutions demonstrated that continuous hollow fibers could be formed above 6.35 cc/hr. However, at flow rate values above 12.70 cc/hr, continuous fibers were ill formed due to a lack of adequate solvent evaporation, which resulted in the bundles fusing together with a wet appearance on the collection plate. At low flow rate values, less than 2.57 cc/hr, dried hydrous alumina globules were collected, as seen in Figure 4-1B. These conditions produced solidification of the precursor at the needle tip. These low flow rate structures differ from those found with the higher concentration of solvent, possibly due to the rapid drying. This rapid drying may form skins that dry before the rest of the body can react, resulting in incongruent drying. Earlier it was noted that the nature of the neat ASB alkoxide has a semi-solid liquid property, which may be a result of the BA volatility and extent of oligomerization. Since these ASB:BA 3:1 solutions have little concentration of solvent, it is expected that the facile drying of the surface resembles the neat alkoxide solutions. However between 2.54 and 6.35 cc/hr, partial hollow structures were formed, characterized by some rods, malformed fibers, particles, and globules, as seen in Figure 4-1C. The latter is an indication that the rate of drawing the alkoxide can increase the possibility of forming stabilized fibrous walls that leads to

continuous fiber formation. There is still some varicose instability that can factor into this relationship, which produces the discontinuous and distorted fibers. Above 6.35cc/hr continuous bundles of tubular fibers formed, but the optimum range for fabrication of fibrous bundles with few deformed structures, such as particles or rods were found between 7.62 cc/hr and 11.43 cc/hr for this particular ASB:BA system, as seen in Figure 4-1D.

The morphological difference between the 1:1 and 3:1 solutions may be a result of a critical concentration of hydrolyzed species necessary to form the stable jets and overcome varicose instability from the electric field's interaction with the precursor. Above this critical concentration of the ceramic precursor, the extrudate can undergo the necessary hydrolysis and condensation reactions that maintain the structural integrity of the jet for subsequent continual fiber drawing. The optimum flow rate values for 2:1 were similar as the 3:1 solution. Above and below this optimum flow rate resulted in the similar types of deformed structures. As a result of using a lower concentration precursor of 2:1 at optimal flow rates, there was a higher density of deformed or discontinuous structures found within the bundles. These continuous bundles were comprised of a presence of shorter fiber lengths overall when compared to the 3:1 batch. The latter reiterates the idea that at this threshold concentration of ASB, such as 3:1, a consistent distribution of continuous hydrolyzed fibers can be produced.

Flow Rate and Precursors of ASB:DG

In following with the flow rate study of ASB:BA, it was found that the ASB:DGME with a 2:1 molar ratio proved to provide more consistent fibrous bundles with an optimum flow-rate range of 6.35 cc/hr to 10.16 cc/hr. The fibrous bundles were similar in appearance-predominantly tubular.

Results for the 3:1 ratio in this flow rate study showed that it was more difficult to consistently form fibers due to the excess solidification at the nozzle tip at the lower limits of

6.35cc/hr. This produced defected structures, such as amorphous globules. Nonetheless fibrous bundles were formed in faster flow rate ranges of 7.62 cc/hr up to 12.70 cc/hr.

Wherein at the 1:1 ratio, particles were also formed that resembled the structures found with the ASB:BA 1:1 system. This latter mentioned inconsistency relates back to the alkoxide precursor to solvent concentration. As the alkoxide flows, there must be enough solvent to allow flow and simultaneous hydrolysis for the stabilization of the jet. With the 1:1, there was too much solvent that prevents continual inorganic polymerization of the jet. Similarly the ASB:DGME 3:1 system lacked enough solvent to allow consistent flow and formation. Ratios of 2:1 produced more consistent fiber bundles, as seen in Figure 4-2, which had more solvent concentration.

Flow Rate and Precursor of mod-ASB:DG

The modified precursor was observed to perform much differently than the precursors derived from solvent addition. At the previously determined flow rates, the lower limits were unable to produce fibers. The lower limit for this system was found to be 10.160 cc/hr. Also the fibers appeared slightly different, such that there was a slight transparency associated with the fibers, the overall bundle was much like the cotton balls observed in previous precursors. Right below lower limits, the flow rate 7.62 cc/hr produced some discontinuous fibers with some broken and defected pieces, as shown in 4-3A. However within the range of 10.160 cc/hr and 14.478 cc/hr, continuous structures were better formed. These continuous bundles had more of a presence defects amongst the fibers, seen as particles, globular structures, and fused fibers. In addition the presence of hollow fibers were not as pronounced as those formed in the solvent-addition precursors

Discussion of Flow Rate Analysis and Hollow Tube Formation

Most strikingly, it was found that hollow tubes were formed amongst most of the fibrous bundles. The tubes were consistent for the continuous fibers formed in the solvent-addition based precursors, meanwhile not as common-placed with the modified solution. Electrospinning fibers previously has stemmed from precursors made with organic polymer incorporation or aged sols. The fabrication of tubes have only been a result of mechanically designed nozzle devices and/or heterogeneously chemicals mixing to thereby selective etch or dissolve to form the cavity [62, 105-108]. Therefore the fabrication of tubules is a novel finding in this research.

It is believed that as the jet is being drawn to the collection plate, there is dynamic interplay between the solvent volatilizing and also the hydrolysis and condensation taking place. As a solvent volatilizes, essentially it cools the surface down and draws additional hydrolyzed species to the surface. During this time, the oligomers present are hydrolyzing and forming enlarged polymerized species that form the stable backbone to form the fiber. Since the reaction must take place at the exposed surface of the fiber, the hydrolysis and condensation takes place from outside towards the inside. The driving force for these alkoxides, once exposed to a hydrolyzed atmosphere, is to undergo nucleophilic addition. As the outside inorganically polymerizes, there is a continual polymerization of the alkoxides to form the complete oxide network. The hollow center may be left with the remnant solvent that is immiscible with the newly formed oxide network. A consistent inner diameter dimension was not found in our continuous samples, however it remains a potential aspect for further study.

The contrast that stems from the mod-ASB:DG is that the hydrolysis and condensation tendencies are modified due to the glycol ether ligand. One obvious difference is the scarcity of "free" solvent available in the system. The ligand is designed to produce a precursor, less prone to hydrolytic attack than its neat precursor, ASB, and also to increase its coordination state. As

this precursor is being extruded out of the nozzle, the atmospheric moisture definitely promotes hydrolysis and condensation. The increase in coordination state implies larger aggregates should be found within the precursor. Therefore the polymerization process may proceed thereby outside in, but without the competition of the added solvent. In some micrographs, we have found a predominance of solid fibers, however semi hollow fibers and also hollow fibers can be seen, too in Figure 4-4. Examining the solid fiber in Figures 4-4A and B, it can be seen the mark in the center of the fiber serves as a sort of weld-line, wherein the polymerization join together radially inward, as opposed to leaving a hollow center, in Figure 4-4C.

Nonetheless there were no noticeable trends with flow rate and inner-wall diameter. This shouldn't deter attention that future work opportunities may exist to probe the ratio of the inner and outer wall diameter due to correlating processing parameters. Flow rate represents such a fantastic factor that allows us to indirectly relate the sol-gel kinetics of our precursor solutions to the process of electrospinning. In turn we are able to derive differences from precursors with distinct chemistries. ASB:DG solutions electrospun bundles more optimally with a 2:1 ratio as compared to the BA system with an optimal ratio of 3:1. Since the hydrolysis of the DGME system is slower than the sBA system, slightly slower flow rates ranges provides an adequate amount of time for the stable jet to form, along with the use of a solution with more solvent concentration.

The addition of DGME promotes the formation of hexa-coordinated bonds, meanwhile the BA system is mainly comprised of tetra-coordinated bonds [50, 63]. The increased coordination state results in a larger state of aggregation within the solution. This aggregation manifests itself by drying prematurely in solutions of ASB:DG 3:1 compared to the same relative flow rates as

ASB:DG 2:1. Since the 2:1 promotes further flow with additional solvent, it was found to produce the more consistent final product.

In this subsection, various solvents and processing methods outlined optimal flow rates to produce fibers on a larger scale. In the next chapter use of these parameters to produce fibers for further chemical and physical property analysis. In the proceeding sections of this chapter, there will be an investigation to understand fiber diameters relating to simple electrospinning processing parameters.

Other Electrospinning Parameters

In this section, we make light of the processing and structure relationship by studying whether the electric field, voltage, working distance, and needle gauge are believed to have an effect on the fiber diameters electrospun from the alkoxide-based precursors. Looking back at Fridrikh and Sigmund's equation to model electrospinning process parameters and fiber diameters [10, 109], we find the electric field has an inverse relationship with fiber diameter. Increasing creates more of an electrical force to draw the fiber, which then decreases the diameters. These models were drawn with polymers in mind that undergo both an elastic response while being drawn. In our system, an inorganic polymerization is taking place with a hydrolytic nucleophillic-addition driven reaction, in contrary the organic system is a large molecular polymer entangled with its own counterparts in solution, awaiting deformation.

In the alkoxide-based system, we find that the reaction is taking place upon drawing into the atmosphere. It is necessary to dissect the electric field to understand the difference between the electric field and working distance. Although the electric field (kV/cm) relies on the relationship of the voltage and distance, the alkoxide-based system may rely on the factor working distance to allow adequate solvent evaporation along with hydrolysis/condensation reaction time.

It has been postulated that the orifice size of the nozzle relates to the final diameter of the fiber, therefore this matter also compelled this work to relate this condition to the alkoxide-based systems [102]. This subsection might present an opportunity to explore whether the orifice shapes the extrudate in such a way to derive a fiber diameter relationship.

Therefore this subsection starts by exploring the relationship of the electric field to then understand the difference due to the working distance and end with a recount of the needle gauge relationship.

Methodology

In light of the SEM micrographs taken of the fiber diameters, a statistical methodology needed to be derived describing the fiber diameter size distribution. Previous works publish fiber diameters as scatter plots by either eliminating the distribution or utilizing error bars to account for some form of statistical variance. However with error bars, there is ignorance in the number based distribution of the fibers. The number based distribution, histogram, actually paints a more accurate picture of the distribution being produced.

In this work we chose only to explore one solvent-addition based precursor to streamline the number of experiments. Upon deriving of relationships, further precursors can be explored for optimal processing parameter relationships, further down the line. Solutions of the ASB:DGME system with a 2:1 molar ratio were electrospun at 10kV at working distances of 10cm, 15cm, and 20cm with a 7.62 cc/hr flow rate. In addition samples were electrospun at 20kV at 20cm also with the same flow rate. Each of the parameters was tested with needle diameters of 1.245 mm, 0.889 mm, 0.711 mm, and 0.556 mm.

The Carnoy 2.1 software was used to measure fibers captured in the SEM. Carnoy establishes a pixel to distance ratio, in which case, the cursor measures the scale bar at a particular distance and thus computes a ratio of micrometer (μm) per pixel. SEM images at

200X were analyzed, at least 3 images were taken per given condition, and fibers within the same depth of focus were measured. The limitations of the distance per pixel measured with 200X micrographs is within 1 μm, therefore measurements were recorded in μm to the corresponding whole number.

The data set comprised of recorded diameters, which was utilized to create a histogram to confirm single or multi-modal means and standard deviations per measured condition. In following, means and standard deviations were calculated per data set distribution. Afterwards the data was plotted and fit with both a Levenberg-Marquardt and Robust fitting to a Gaussian peak fit using the pro Fit 6.0.4 software. Chi-squared values were accepted for fittings of values less than 11, due to the wide range of possible fiber diameters. Once fitted means and standard deviations were computed, a probability density function (PDF) was graphed about the computed mean(s). The gaussian PDF was calculated with the expected value to be the same as the mean and standard deviation calculated per data set distribution. A fitted curve is thus graphed with the calculated PDF. The corresponding graphs are a delineation of the probability of finding a certain fiber diameter with graphical axes of probability versus fiber diameter.

The probability density function was implemented since it is a continuous function that describes the distribution more accurately. Essentially the function delineates a curve, in which case, the probability is ascribed in the y-axis and fiber diameter in the x-axis. The area underneath the curve is 1, and each point along the curve is the probability of finding that fiber diameter. Utilizing the PDF gives us a better idea of the fiber diameter distribution, as compared to the scatter plots and error bars that ignore distributions and even other relevant parameters during the analysis.

Fiber Diameter Relationship and the Voltage, Working Distance, and Electric Field

Within the same needle gauge, 1.245 mm, there were no apparent trends in the mean fiber diameters that were calculated with the electric fields of 0.5kv/cm, 0.667kV/cm, and 1.0kV/cm. Figures 4-5A-B, illustrates the probability distribution functions with needle diameters of 1.245 mm and 0.712 mm respectively. The distribution at 0.5kV/cm illustrates different behaviors for the different needle gauges and it will be further discussed in the next section.

There is an independent nature of the fiber diameter relative to the electric field, which lends itself to the dynamic set of hydrolysis and condensation reactions taking place. This opposes previous studies that relate the inverse relationship of the electric field to ceramic fiber diameters [10]. Additionally the working distance is necessary for solvent evaporation together with hydrolysis. Therefore the second part of this study compares the same electric field, 1.0kV/cm, but set different working distances as seen in Figure 4-5 C and D. Figure 4-5C is the PDF for various needle gauges at 1.0kV/cm at 10cm and Figure 4-5D shows 1.0kV/cm at 20cm.

The PDF for the same electric field values show a very different trend, as seen in Figure 4-5 C-D. The distance at 20 cm demonstrated that fibers with smaller mean diameters could be produced with a high probability than those found at 10cm. It was observed that the samples electrospun in the 10cm working distance deposited smaller bundle sizes overall. Some fusing or collapse of the tubular structures was found in some bundles, which lead to fibers that could not be adequately measured as seen of fiber bundles in Figure 4-6A.

The 20 cm bundles produced fibers with low concentration of defected structures within the fibrous bundle. These fibers were extremely long and had no apparent signs of wetting from poor solvent evaporation. However, the fiber distribution is vast and this may be related to some of the jet splitting that is observed during the electrospinning process. At these higher working distances, there may be more destabilizing elements, as due to the electric field. Other research

groups are still making continual improvements and this aspect is currently not the focus of this work [7, 65, 100, 110-112]. As observed, before the whipping occurs, there is some splitting of the jet; this may be attributed to jet hydrolysis and condensation, which may solidify during the deposition and also induce some fiber division. Consequently the electric field is not a parameter that can dutifully predict the mean fiber diameters of our system, but can be used to decipher a range of fibers being fabricated as seen in the PDF's. In addition it is found that the electric field is also not independent of the working distance due to the factors related to the hydrolysis and solvent evaporation in the stabilization of the jet. A larger working distance can yield a range of fiber diameters that include much smaller fiber diameters, even less than 6μm.

Fiber Diameter and the Needle Gauge

At first glance at Figures 4-5 A and B, the 0.5 kV/cm setting shows a decrease in mean of the PDF with decreasing needle gauges. Therefore the effect of the needle gauge was studied to elucidate trends in fiber diameter and production. Although previous studies have shown no relationship of the needle gauge in the polymer electrospinning condition, this sol-gel based system is dependent on exposure to atmospheric hydrolysis [102]. Therefore the needle gauge may relate to the exposed reaction surface.

In parallel to the investigation performed with various needle gauges at the same electric field, as seen in Figures 4-5C-D, there were also studies performed at the 0.5kV/cm and 0.667kV/cm, respectively, that wholly demonstrate no apparent trend of the mean fiber diameter or distribution relative to the needle gauge. The range of nozzle sizes studied does not have a profound effect on the feasibility of electrospinning nor relate a general trend in fiber diameter distributions. This certainly is in line with previous works performed on polymer systems [102]. It is believed that the fibers produced from the electrospinning are independent of the needle gauge and more independent on the reaction rate of the hydrolysis/condensation.

Discussion of Other Electrospinning Processing Parameters

The findings that were presented earlier demonstrated that fiber diameter studies had to be refined to be able to delineate trends in the fiber diameter distribution. These were polished from previous uses of scatter plots and errors bars with the use of probability distribution functions, which to continuously graph distribution of fiber diameters. This set of work utilizes PDF functions in determining fiber distributions to delineate trends in processing conditions.

The electric field has been determined to correlate to the electrical stresses drawing down the fiber jet, thereby increasing it can thus decrease fiber diameters. Upon further examination, it was found that no trends were exhibited with the electrical field stress increase. Nonetheless this may relate to the nature of the precursors that were developed, as opposed to the polymeric ones that used in the previous models. Dependence on the hydrolysis and condensation for fiber formation may be independent on changes in the electric field, pass a certain threshold. Typically the electric field drives down the jet and through the whipping, the fiber diameter shrinks. The reactive tendencies of the alkoxide-based precursor doesn't allow for the continual shrinking of the fiber, since the formed oxide network can not undergo further shrinkage due to electrical stresses. The inorganic network differs from the organic counterpart due in part to its lack of free volume and inelastic behavior.

The components of the electric field depend on the working distance, which thusly may effect the alkoxide reactions. Suspended and drawn in the atmosphere, these fibers demonstrated that a change in the working distance with the same electric field value of 1.0 kV/cm also lead to different fiber deposition behaviors. Values of 10 cm and 20 cm were compared and found that agglomeration and fiber wetting occurred with the former and smaller diameter distributions were located in the latter. Evaporation relates to the distance and the smaller working distances decreases evaporation times and thus result in ill-formed fibers. The longer suspension allowed

for fibers to be split during the jet whipping. Nonetheless effortlessly these hollow and continuous strands were drawn and fiber diameter distributions concentrated between the range of 15-20 μm.

In the needle gauge relationship study, it is noted that there were no relationships established between the different needle gauges. Even the smallest gauges still allowed jet production with no significant issues regarding stunted flow or other known associated issues with alkoxide solutions and their instantaneous reactivity.

All in all there were no distinct trends other than exploitation of longer working distance to provide adequate solvent evaporation and an array of smaller fiber distributions. In conclusion a model to relate structure and electrospinning parameters for alkoxide-based precursor cannot be derived from these set of experiments.

Hydrolysis Studies

In this part of the chapter, the hydrolysis conditions are studied in the electrospinning process. Hydrolysis is the main driving force for deriving the ceramic material from the sol-gel precursor. The hydrolysis/condensation assists with forming the stable fiber backbone during the spinning of the precursor. In this subsection, the discussion will focus on experiments performed by directly electrospinning into water and also at different relative humidity settings.

Electrospinning into Water

Serving as a grounded collector, water placed in a beaker is utilized as the collection device. Fibers directly electrospun into the water ensures complete hydrolysis of the formed fibers and allows for comparison regarding dimensions.

Methodology

The typical electrospinning set-up, as seen in Figure 2-1A, is modified to include a reservoir for water at the collection plate. Aluminum foil was fashioned around a large plastic

weighing boat and 25mL of deionized water was poured, a grounded wire was then connected to the foil. A 5cc syringe was filled with the 2:1 solution of ASB:BA. Processing parameters were set with a flow rate of 10.16 cc/hr, working distance of 15cm, voltage of 10kV (electric field 0.667 kV/cm), and needle gauge of 0.889 mm. The relative humidity is determined to be 42%.

Analysis of electrospinning into water

Fibers, both continuous and hollow, were identified in the SEM micrographs within Figure 4-7. After performing fiber diameter analysis and plotting the PDF of the function, the mean diameter of this distribution was 24.5 μm, as shown in Figure 4-8. There is a single mode distribution of fiber sizes produced. Electrospinning into water also slightly deforms the fibers by creating some oblong fibers, however the shape and morphology is comparable to the fibers produced onto the aluminum foil. Therefore it can be identified that the size distribution of the fibers are comparable to the fibers spun into the atmosphere, therefore an increase in hydrolysis during collection doesn't change drastically alter the size or hollow nature of the fibers. The size should therefore be determined at the tip. This study confirms that electrospinning into both the atmosphere or into water, assures complete hydrolysis of the fibers and thusly forms hollow features with solvent-addition based precursors.

Humidity Study

Following the latter work, it can be deduced that fiber morphology and diameters are determined independent of collecting fibers onto an aluminum foil or into water. Hollow fibers and continuous fibers can still be formed. Nonetheless, since alkoxide solutions are dependent on the moisture content in the atmosphere and forms as a result of the reaction, it was necessary to further understand the changes associated with increasing the relative humidity.

Methodology

This electrospinning was performed in a glove box with a R_h of 65% with a precursor solution of ASB:DG 2-1. The electrospinning parameters were set at 0.667 kV/cm (10kV at 15cm) electric field with needle diameter of 0.712 mm and 7.62 cc/hr flow rate.

Analysis of humidity study

Essentially it was necessary to understand the effects of an increasing relative humidity setting, since alkoxide precursors are extremely sensitive to hydrolysis. It has been found over the course of this work, that humidity conditions are usually found to be ~ 40% in the glove boxes and in the hoods. Therefore an increase in the humidity rate should allow for comparison of the baseline found in these sectors. In the SEM micrographs of these fibers, it is found that there are interesting changes in morphology. The fibers seem a bit shorter and also deformed, displaying a varicose structure. Since varicose structures are comprised of variable widths, the previously used fiber diameter measurement technique was modified. Equal measurements of the thinnest portion and the widest portions were measured and analyzed with a total of 20 measurements each. Then they were graphed separately indicating separate probability density functions. The overall mean of the fibers are measured to be 15.46 μm with a standard deviation of 5.12. The mean for the widest portion is measured at 19.92 μm with a standard deviation of 2.55 and the narrowest portion is measured at 11.00 μm with a standard deviation of 2.31.

Varicose instability relates to issues with the electric field, in which case there is complex break-up from the rheologic conditions of the fluid and the electrical stresses [100]. These two factors work in opposing directions. An increase in humidity conditions, increases the probability of hydrolysis and thusly condensation. The latter increases the localized viscosity,

therefore inhibiting a uniform stretching of the fiber in an electric field. When the electric field and the viscosity are at odds, the varicose structure appears.

This contrasts the latter subsection of electrospinning into water. The water collection case had an initial relative humidity of 42%, therefore that condition dictated the fiber morphologies that were comparable to fibers studied earlier in the chapter. At the increased humidity conditions, the fibers appeared more disfigured due to rapid inorganic polymerization inhibiting uniform stretching of the fibers. Even so, these fibers appear to have the hollow morphology and form continual fibers at these processed conditions. Therefore it is concluded that increasing the relative humidity rate, also increases the chance for forming overall a smaller mean of fibers with varicose morphologies.

Conclusions of Electrospinning Parameters Governing Fiber Formation with Alkoxide-Based Precursors

This chapter highlights key factors in electrospinning that relate processing parameters to the fiber structure derived from alkoxide-based precursors. A definitive finding in most of this work is the presence of hollow and continuous fibers produced by electrospinning. The production of these fibers was independent of mechanically derived electrospinning set-ups or chemically derived etching. Furthermore solid fibers and hollow particles can also be produced.

These precursors are dominated by the hydrolysis/condensation chemistry and therefore found to directly relate to the flow rate of the syringe pump. Precursors that are dominated by tetra-coordinated species, such as ASB:BA, require less solvent to be optimally electrospun. However flow rates for these precursors were higher relative to the ASB:DG system. The solvent in the former precursor is volatilized quicker; meanwhile the latter has larger aggregates due to the hexa-coordinated species requiring an increase in solvent concentration and slower flow rates.

The modified precursor, mod-ASB:DG demonstrated a difference from the solvent-addition precursors, in which case, the fibers were mostly solid structures and required the fastest range of flow rates. Owing to the larger concentration of hexa-coordinated and aggregated molecules, these fibers were able to set into fiber form even at higher flow rates and slower hydrolysis/condensation rates.

Seeking trends in the nozzle diameter, electric field, and working distance required a new approach utilizing statistics to compare fiber distributions. Utilizing a pixel-measurement software equipped with probability distributions functions, graphical relationships were able to be plotted for the various parameters. PDF graphs were used to describe trends in fiber distributions. This statistical methodology contrasts previous works with scatter plots and error bars that do not adequately define the diameter distribution. With PDF's there no defined relationships were derived for the nozzle diameter, electric field, or even working distance. However working with a longer working distance provided a PDF demonstrating small diameter fiber production, below 10 μm.

Works with polymer models relate fiber diameters to be inversely related to electric field strengths [9, 10, 65, 109]. Polymers can be elastically deformed by the electric field and hence change in diameter with changes in strengths. On the other hand, the inorganic oxide material does not undergo such elastic deformations to adhere to the same models. The latter should describe the independence of fiber diameter and the electric field for alkoxide-based precursors.

There were no model derived as a result of the change in needle gauges in one particular study in the polymer-based systems [102]. Opposing works believe that nozzle diameters can be related, however works with alkoxide-based precursors show a lack of trend [9, 10, 65, 109].

Due to the sensitivity of alkoxide-derived precursors, it was necessary to also explore the role that water plays with the fiber formation. Initially a study performed thereby electrospinning into water, illustrated that hollow and continuous fibers can still be formed. The resemblance of these fibers to ones previously fabricated indicates that the electrospinning process should allow thorough hydrolysis and condensation of the alkoxide.

In addition to the latter, an increase in the relative humidity conditions showed that varicose instability appears. These fibers exhibited an overall smaller mean, compared to counterparts electrospun in relative humidity values of ~ 45%, however measurements required two separate diameter measurements to accurately detail the variability due to the varicose behavior. The increase in humidity rate thusly increases localized inorganic polymerization, resulting in incongruous stretching of the jet. Nonetheless the hollow nature of the fibers was preserved with the change in the humidity.

Varicose instability was studied in both the EHDA and electrospinning realms. In polymer-dominated ceramic precursors, beading is apparent in the fiber backbone. This beading creates a defected structure by creating large bulb-like structures along the backbone of the fiber. Beading is decreased with an increase in conductivity of the solutions [10].

Overall this work sought out to further understand processing parameters to electrospin alkoxide-based precursors. Although a model was not derived, the importance of the chemistry of these sol-gel based precursors is the key factor to further understanding the process to structure relationships.

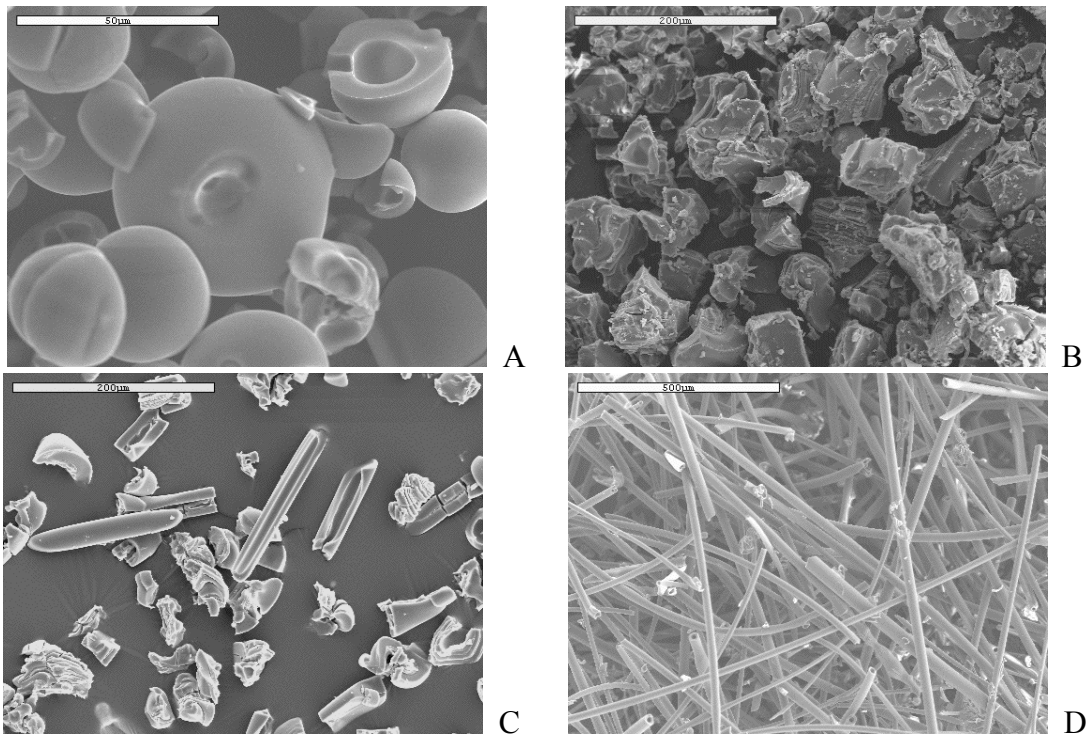

Figure 4-1. Flow Rate Relationship For Electrospun ASB:BA Solutions At 10kV, 15cm, and 0.712mm Needle Gauge: A) Hollow Particles Produced With A 1:1 Solution At 5.09 cc/hr With Scale-Bar = 50 µm. B) Globules Produced From A 3:1 Solution At A Low Flow Rate Of 2.57 cc/hr With Scale-Bar = 200 µm. C) Partial Fibers And Other Deformed Structures Produced From A 3:1 Solution At A Moderate Paced Flow Rate Of 5.05 cc/hr, 10kV With Scale-Bar = 200 µm. D) Bundle Of Fibers Produced From A 3:1 Solution At A Flow Rate Of 5.05 cc/hr With Scale-Bar = 200 µm (V. Maneeratana, W. M. Sigmund, Chemical Engineering Journal In Press (2008).)

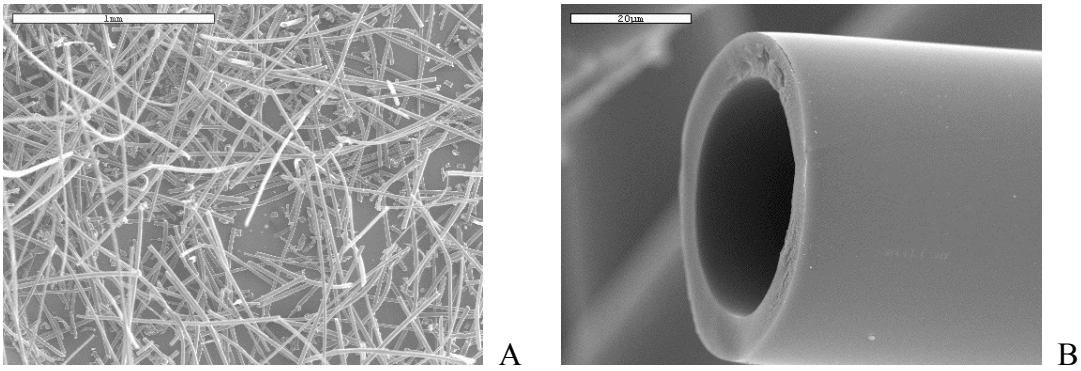

A B

Figure 4-2. Fibers Formed With The 2:1 ASB:DGME Solutions With Parameters Of 6.35 cc/hr, 10kV, 15cm, And 0.712 Mm Needle Gauge: A) Fibrous Bundle With Scale-Bar = 1mm. B) End Of Hollow Fiber With Scale-Bar = 20 µm (V. Maneeratana, W. M. Sigmund, Chemical Engineering Journal In Press (2008)).

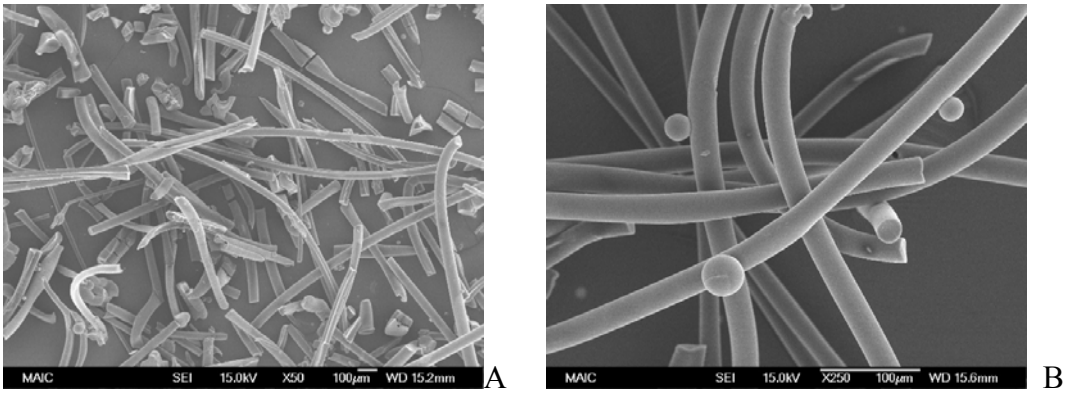

A B

Figure 4-3. SEM Of 1-1 Mod ASB:DG At 10kV, 15cm, and 0.712 mm Needle Gauge: A) Discontinuous Fibers Found At Flow Rate Of 7.62 cc/hr, Scale Bar = 100µm. B) Continuous Fibers With The Presence Of Some Defects At Flow Rate Of 10.61 cc/hr, Scale Bar = 100µm.

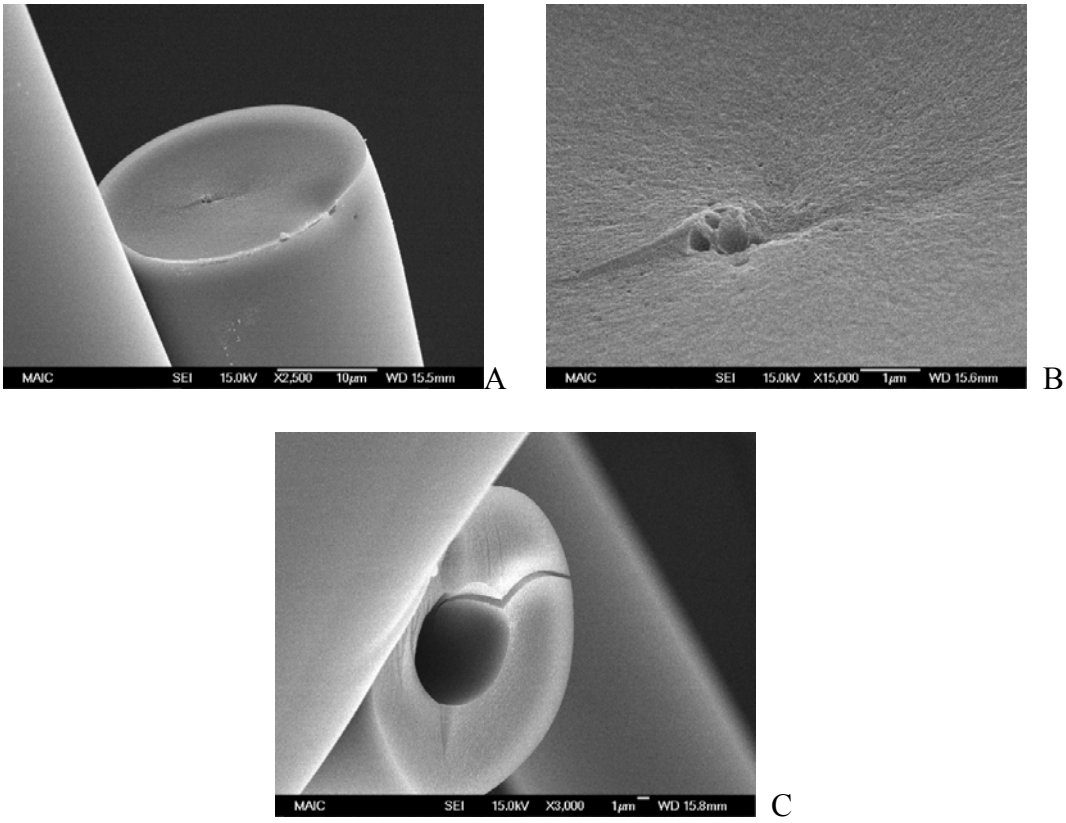

Figure 4-4. Solid And Hollow Fibers From 1:1 mod-ASB:DG Processed At 10.61 cc/hr, 10kv, 15cm, And 0.712 mm Needle Gauge: A) Solid Fiber, Scale Bar = 10 µm. B) Center Of Solid Fiber, Denoting Oxide Polymerization From Outside In, Scale Bar = 1µm, C. Hollow Tube, Scale Bar = 1µm.

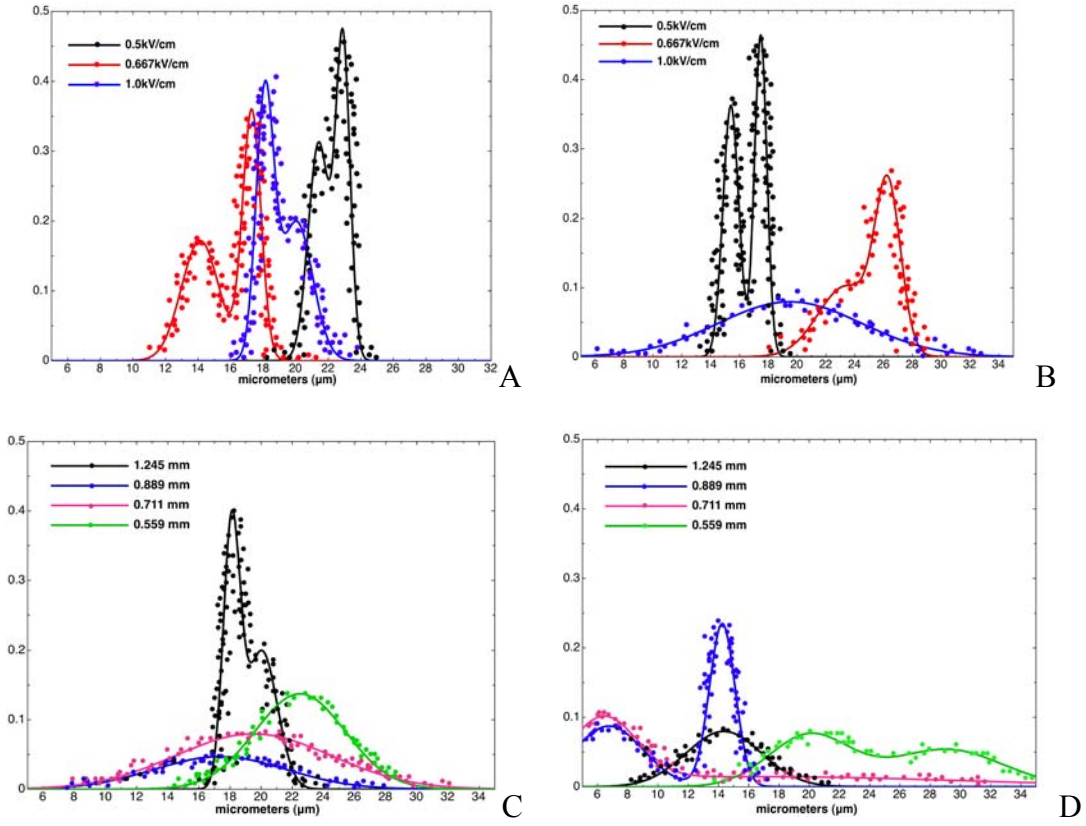

Figure 4-5. Comparative Probability Density Functions for Various Electrospinning Parameters: A) Setting At Various Electric Fields With Needle Diameter Of 1.245 mm And 7.62 cc/hr Flow Rate. B) Comparison At Various Electric Fields With Needle Diameter Of 0.712 mm And 7.62 cc/hr Flow Rate. C) PDF Of 1.0kV/cm at 10cm And 7.62 cc/hr Flow Rate. D) PDF Of 1.0kV/cm At 20cm And 7.62 cc/hr Flow Rate (V. Maneeratana, W. M. Sigmund, Chemical Engineering Journal In press (2008)).

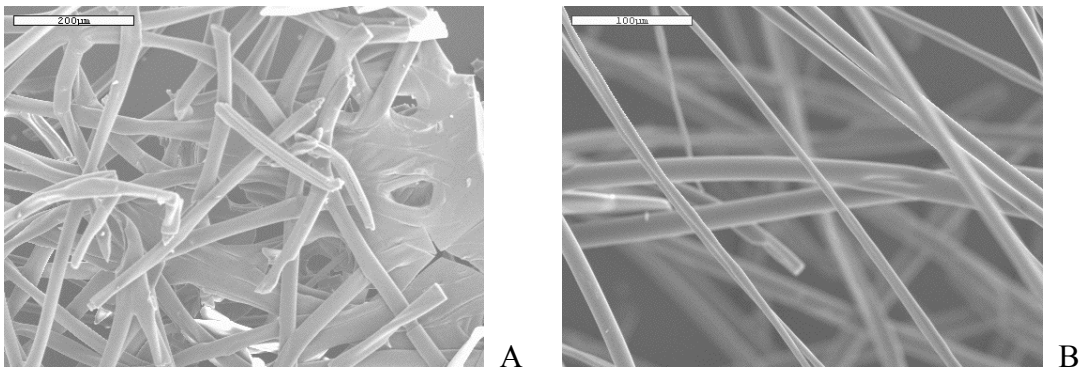

A B

Figure 4-6. Fiber Bundles Produced At 1.0kV/cm But With Different Working Distances Set at A Flow Rate Of 7.62cc/hr and Needle Diameter Of 0.711mm: A) Working Distance Set At 10cm, Scale Bar = 200 µm. B) Working Distance Set At 20cm, Scale Bar = 100µm.

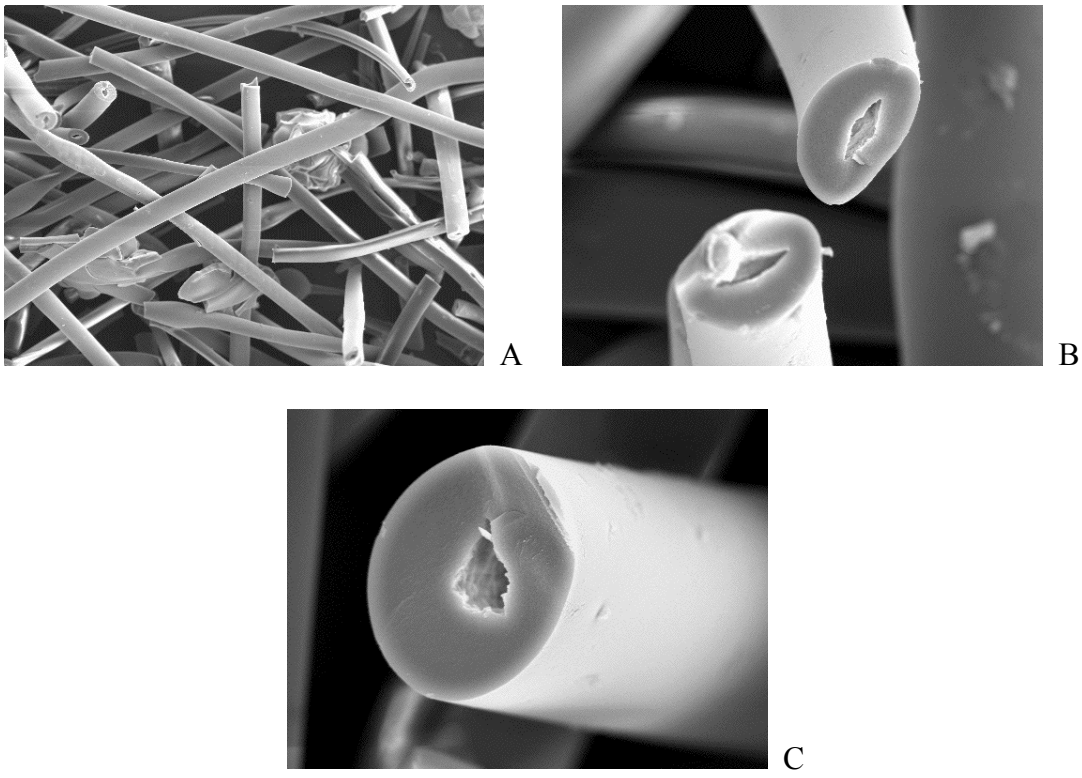

A B C

Figure 4-7. SEM Of Fibers Processed From Electrospinning Into Water Reservoir for 2:1 ASB:BA Precursor: A) 200X. B) 1500X. C) 2500X.

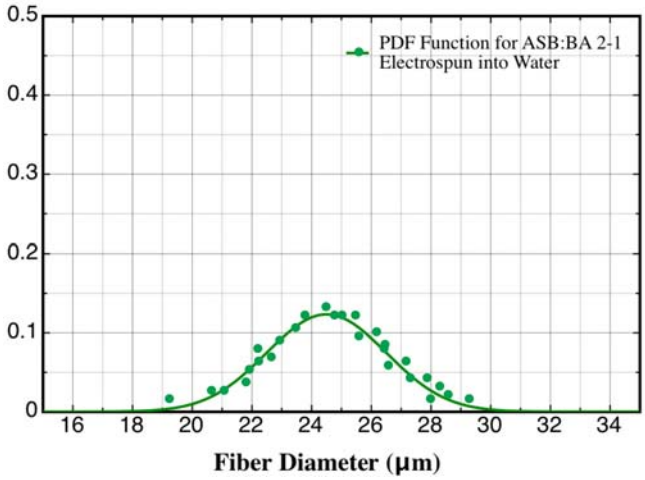

Figure 4-8. Probability Density Function for Fibers Processed From Electrospinning Into Water Reservoir with 1:2 ASB:BA Precursor Solution.

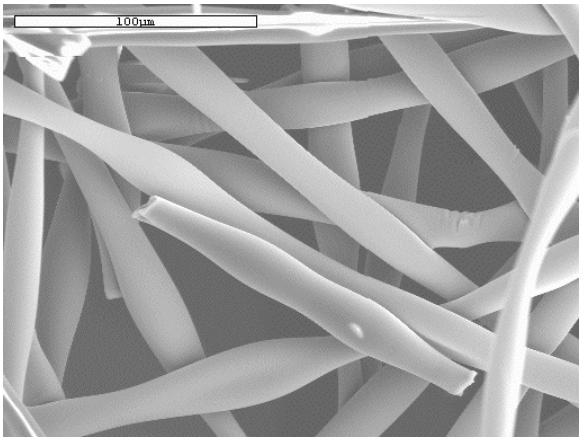

Figure 4-9. SEM Micrographs Of Electrospun Fibers From ASB:DG 2-1 In R_h 65%.

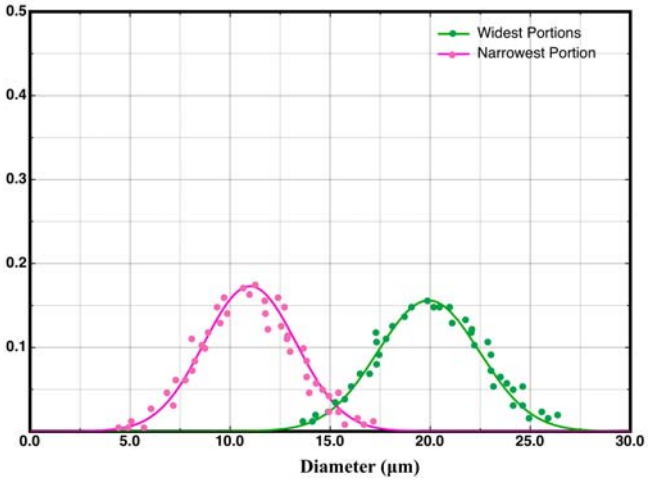

Figure 4-10. Probability Density Function for Electrospun Fibers from ASB:DG 2-1 in R_h 65%. Means Measured from the Widest and Narrowest Portions of the Fibers.

CHAPTER 5
PROPERTY COMPARISONS OF THERMAL PROCESSING IN AN ELECTRIC FIELD

This chapter presents an exciting progression by investigating properties exhibited by fibers electrospun from alkoxide-based precursors. Previously the design, preparation, and processing parameters were detailed. From those aspects, ideal precursors and optimal processing parameters were selected.

This chapter looks to investigate structural changes as a result of thermal processing electrospun alkoxide-based fibers. Typically in sol-gel processing, the presence of organics is higher than in other ceramic processing schematics. Since the fired form is oftentimes the most used state, it is imperative to explore issues related to shrinkage and mass loss. Thermal processing of ceramics also yields inherent chemical changes in addition to phase transitions. The goal of this section is to elucidate the physical and chemical changes that are a result of thermal treatment and explore possible changes.

Within this chapter, any effects the electric field may have on these structures will also be explored. Processing in an electric field presents many advantages, one that allows us to draw these ceramic fibers without any mechanical force. Therefore a further look into the field's effect on phases and chemical groups will also be investigated.

Specifically addressing the issues of mass loss and chemical changes, electrospun materials are contrasted with their respective controls. Thermogravimetric analysis (TGA) will probe the organic removal rate; and additionally coupling Fourier Transform Infrared Spectroscopy (FTIR) to the TGA allows tracking of the evolution of organics during the heating process. Furthermore FTIR and X-ray Diffraction (XRD) will investigate bulk materials undergoing bonding rearrangements. SEM micrographs will be analyzed for dimensional

changes and finally the surface area and pore size will be investigated to elucidate changes in the porous nature.

Thermogravimetric Analysis

Analysis in this section explores the weight loss of organics during thermal treatment. The electric field is believed to draw the alkoxide precursor. During the drawing, the precursor can adequately react with the atmospheric hydrolysis and subsequently remove the other organics by evaporation. TGA should provide analysis of a comparison between the electrospun material compared to control (air dried powders).

Coupling FTIR to the TGA allows for analysis of the gas that is being burned off from the material. It should provide adequate identification of species evolved during the firing cycle.

Methodology for TGA Analysis

TGA was employed at a heating rate of 10ºC/min with electrospun samples of ASB:DG, ASB:BA, mod-ASB:DG, and the respective controls. Controls of the alkoxide-based precursors were fabricated by drying solutions on aluminum foil in similar atmospheric conditions. Samples were weighed in Al_2O_3 -lined platinum crucibles and loaded in the Netzsch STA 449-C Jupiter. Samples were run in breathing air at 50cc/min with protective argon gas at the same setting.

TGA Analysis

The graphs in Figure 5-1 illustrate the trend that the electrospun materials exhibit relatively less percent mass loss than the control. The proposed mechanism for fiber formation from alkoxide-based precursors requires drawing of the aggregated precursor allowing exposure to the atmosphere thereby undergoing simultaneous solvent evaporation and hydrolysis/condensation. In contrast controls are based on the respective precursor solutions dried on an aluminum foil. As a result there may be possible agglomerates with trapped solvent residue or incomplete

hydrolysis/condensation. The difference in mass loss for the ASB:BA and ASB:DG is ~ 10 %. Since the mod-ASB:DG system exhibited a different trend in fiber formation and drying, it retained more solvent within the fiber and only exhibited a difference of ~ 4%.

Various heating rates of 1ºC/min and 5ºC/min were studied but exhibited no notable contrasts. Also there were insignificant differences in the mass loss rates between ASB:DG, ASB:BA and mod-ASB:DG. This TGA study supports the claim that electrospun materials contain less mass due to solvents. Further chemical analysis will assist in detailing the changes in the chemical groups and phase transformations that occur during firing.

Methodology for TGA-FTIR Analysis

A TA Instruments TGA was coupled with a Thermo Nicolet FTIR. A heating rate of 10ºC/min was utilized with a platinum weigh boat. In addition, a liquid nitrogen cooled MCT/A detector was employed within the FTIR. Intensity of the gas evolution was graphed in a Gram-Schmidt reconstruction and respective FTIR spectra were analyzed at chosen intervals along the Gram-Schmidt reconstruction. To maintain comparable values in the Gram-Schmidt reconstruction, the amount of samples were maintained for each run at 60mg $\pm$ 3mg.

TGA-FTIR Analysis

Simultaneous TGA-FTIR allowed us to track chemical changes in the gas phase with respective electrospun and control samples during heating. As the TGA undergoes the heating cycle and records the mass loss, the gas being evolved is drawn into an adjacent FTIR unit through a heated transfer line. The transfer line functions by directing the gas to the FTIR's gas cell.

For an FTIR resolution of 4 cm^{-1}, interferogram collection times are less than one second. This reconstruction is a result of total IR response versus time or temperature obtained through an algorithm plotting the intensity of gas at the detector during absorption as a function of time

[113]. This algorithm allows real time integration of absorbance measurements for gas and liquid. The Gram-Schmidt reconstruction is used to contrast the amount of evolved gas burned off to support conclusions made from the TGA data.

The reconstruction process initially forms a basis set or background set of interferograms before the eluted species are directed into the gas cell [114]. The Gram-Schmidt vector orthogonalization is an algorithm that removes background information and thus measures the differences between the background and all infrared active species that have been eluted [114]. Background information includes the light-burst at zero optical path difference, collection conditions, and low signal to noise ratios. To apply the orthogonalization, each interferogram must be considered as an n-dimensional vector [114]. Interferograms from the TGA-FTIR can be individually and sequentially orthogonalized to form a reconstruction of the total infrared absorbance of any infrared active chemical component in the light path of the collection cell over time/temperature [114].

When comparing Gram-Schmidt reconstructions, it was found that the intensity of the absorbate was lower for electrospun samples, which supports conclusions from the TGA section that lesser organics are trapped within the electrospun fibers. A combined graph of the Gram-Schmidt reconstruction and TGA data is shown for the ASB:BA system in Figure 5-2A and the corresponding stacked FTIR spectra for the electrospun ASB:BA in Figure 5-2B. The Gram-Schmidt for the control exhibits a broad band between room temperature and a maximum at 90ºC. Meanwhile the electrospun reconstruction is a smaller sinusoidal-like band that is ~11 times less in intensity than the control.

Although the Gram-Schmidt for electrospun and control samples is different, the actual FTIR spectra are relatively the same. FTIR is measured in relative intensities and did not show

any considerable differences in the identification of compounds. Therefore the stacked FTIR spectra in Figure 5-2B can be referenced for both the electrospun and control samples to identify the groups at each firing temperature. In the stacked FTIR, each spectrum can be matched to a specified firing temperature.

At 90ºC, the FTIR spectrum identifies mainly groups due to carbon dioxide (CO_2), hydroxy (OH) groups from water. CO_2 is located as a distinct split peak at 2400-2350 cm^{-1}. OH groups can be identified at 4000-3400 cm^{-1} and 2000-1250 cm^{-1}. The former set of peaks is due to loosely adsorbed water stretching. Bending of the adsorbed OH is found at 2000-1250 cm^{-1}. Wwater is expected, since the hydrated aluminum and any trapped solvents are hydrophilic at this temperature point.

At 160ºC, the FTIR stacked spectrum shows peaks for CO_2, BA, and water. It is expected that at this temperature point, most trapped solvents should be burned off. In the presence of air and heat, hydrocarbons react with oxygen through combustion. Typical byproducts are water and CO_2. However during the combustion reaction, byproducts can be comprised of derivatives of carbon-carbon and/or carbon-oxygen bonds. Although there is still the presence of OH groups, there is a decrease in the OH stretching and bending intensities at 4000-3400 and 2000-1250 cm^{-1}. A split broad peak appears from 3000-2800 cm^{-1}, corresponding to the stretching of -CH_3 and -CH_2-. Also a shoulder appears at 2800-2700 cm^{-1} and it is assigned to the HO-CH_2- hydroxy stretch in the BA. The broad peak at 1750 cm^{-1} is assigned to carbonyl (C=O) stretching that is a possible byproduct during hydrocarbon combustion; another broad peak at 1525 cm^{-1} is assigned to C=C, another byproduct during combustion. The split peak 1125-1085 cm^{-1} is assigned to the stretching of the carbon in the C-OH of the saturated secondary alcohol

group. A minor peak appears at 875 cm^{-1} and is assigned to the skeletal vibration of the chiral carbon in BA.

CO_2 is also found at 2400-2350 cm^{-1}.. After 250ºC and 350ºC, CO_2 is still present, but noticeably reduces in intensity compared to the spectrum at 160ºC.

The respective differences exhibited by the Gram-Schmidt reconstruction between electrospun and control samples are much the same for the ASB:DG and mod-ASB:DG systems, respectively. Therefore these reconstructions were not included. However a contrast will be drawn between the selections of DG versus BA as a solvent in the next part. The difference between the Gram-Schmidt reconstruction absorption intensities of BA and DG is contrasted to reveal differences between precursors with a high vapor pressure solvent, BA, and a lower one, DG. Flow rate analysis in Chapter 4, found that precursors containing only BA required faster flow rates than those found with the DG system. The latter was believed to be due to volatility of BA species. As previously noted in the TGA analysis section, electrospun samples with DG exhibited ~ 42% mass loss compared to electrospun samples with BA ~58%.

As seen in Figure 5-3A, the Gram-Schmidt reconstruction is compared for the control samples of the BA and DG system. Since control samples have higher intensities displayed in the Gram-Schmidt reconstruction, the comparison of control samples better demonstrates the differences elicited by DG and BA based precursors. It is expected that DG samples retain a larger amount of trapped solvents due to the low volatility of DG.

In the reconstruction of control DG, the majority of absorption takes place between 140ºC and 240ºC. The reconstruction for DG shows the highest intensity at 0.37 compared to the 0.11 for the BA system. DG has a lower vapor pressure of 0.0219 torr at 25ºC compared to BA's 13

torr at 25ºC. Figure 5-3B is a stacked FTIR spectra comparing temperatures for the control DG at 100ºC, 145ºC, 160ºC, 175ºC, 250ºC, and 770ºC.

At 100ºC, the presence of stretching and deformation of water (OH) can be identified at 4000-3400 and 2000-1250 cm^{-1}. The stretching of $-CH_3$ and $-CH_2-$ starts to appear at 3000-2800 cm^{-1}. CO_2 appears at 2400-2350 cm^{-1}. Stretching of C-OH from the secondary alcohol appears at 1205-1125 cm^{-1}. Combustion byproducts start to appear at 1525 cm^{-1} as C=C and 1750cm^{-1} C=O. A peak at 700 cm^{-1} and can be assigned to twisting and rocking of $-CH_2-$.

At 145ºC, peaks maximize for the $-CH_3$ and $-CH_2-$ stretching, CO_2, C=O, C=C, and C-OH. Additionally there is a shoulder appearing at 2800-2700 cm^{-1} and it is assigned to the $HO-CH_2-$ and $-O-CH_2-$ stretch in the BA and DG. The small peak appearing at 875 cm^{-1} is assigned to the skeletal vibration of the chiral carbon in BA.

At 160ºC, most of the above-mentioned peaks start decreasing. However peaks at 2200-2100 cm^{-1} become slightly more defined and can be assigned to conjugated alkenes and alkynes. These double and triple bonds may also be combustion byproducts.

At 175ºC, the intensity of the various peaks reduces. After 250ºC and 770ºC, there is a lack of presence of any hydrocarbon group, except for CO_2.

These FTIR spectra provide this research with an understanding of the type of chemical groups being evolved during the firing schedule. This proves helpful in deciphering optimal firing times to rid the system of hydrocarbon species. Analysis of the bulk material should assist in further supporting the chemical changes occurring in the respective electrospun or control materials during the firing. Moreover Gram-Schmidt reconstructions adequately supported TGA data confirming that a lesser amount of burned off organics in electrospun materials relative to the dried controls.

Methodology for Bulk FTIR Analysis

To analyze the fired bulk material in the FTIR, the Diffuse Reflectance Infrared Transform Spectrocopy (DRIFTS) mode was employed. DRIFTS required that electrospun and control samples be ball-milled with dried Potassium Bromide (KBr), respectively, with a Wig-L-Bug. A liquid nitrogen cooled MCT/A detector was used and the set-up was set at a 4 cm^{-1} resolution, 64 scans, and autogain. In this study, the DRIFTS spectra are reported in diffuse absorbance, "absorbance" rather than Kubelka-Munk units, since quantitative analysis was not performed. Samples were fired at the respective settings. After firing, samples were stored and analyzed in the FTIR under ambient conditions.

Bulk FTIR Analysis

Previous work investigated changes to the electrospun and control materials during firing. Organic groups were burned off and electrospun samples elicited less mass loss than their control counterparts. Additionally FTIR was coupled to the TGA to analyze the gas that was released from the samples during firing. The work in this bulk FTIR section supports further chemical analysis of the electrospun or control samples to correlate changes due to processing in an electric field and also firing.

In Figure 5-4, stacked DRIFTS spectra of ASB:DG illustrate the changes in the electrospun fibers after firing at: room temperature, 100ºC, and 300ºC. The rather broad band in the range of 3650 cm^{-1} - 2900 cm^{-1} is due to the presence of a combination of stretching of adsorbed hydroxyls, due to water, and hydrated aluminum [115-117]. The sharpness of the band decreases, as the sample is fired, which shifts the band slightly towards lower wavenumbers.

The set of defined peaks from 3000 cm^{-1} - 2850 cm^{-1} is a result of the stretching of $-CH_3$ and $-CH_2-$. In addition it has been noted that the latter may also include hydroxyls coordinated to aluminum cations [116, 118, 119]. As the material is fired, thermolysis of the solvent molecules

occurs along with evaporation of water, the broad band between 3000 cm^{-1}-2850 cm^{1} decreases at 100ºC and 300ºC. At 300ºC the residual peak found at 2975 cm^{-1} denotes the decreased presence of solvent and stretching of hydroxyls adsorbed or coordinated in the material [119].

At room temperature and 100ºC, there is a broad peak at 1650 cm^{-1}, this can be assigned to bending of absorbed water on Al-OH. In the TGA-FTIR data, a peak at 1525 cm^{-1} was assigned to C=C. Since the experimental conditions are different for this bulk analysis, combustion byproducts should be rare. 1525 cm^{-1} is assigned to bending of OH group in hydrated aluminum [40, 115, 119]. Peaks at 1650 and 1525 cm^{-1} disappear after the material is fired at 300ºC. A large peak at 1600 cm^{-1} grows at the expense of those peaks and is assigned to the adsorbed water on the Al-O-Al polymer [40, 115, 119].

At room temperature there is a small peak at 1450ºC and becomes more defined at 100ºC. This is assigned to the deformation of the water adsorbed to Al-OH [116, 120]. As the temperature of firing increases to 300ºC, there is an increased growth of Al-O-Al and shifts the peak of the OH deformation peak adsorbed to Al-O-Al to 1465 cm^{-1}. The increased presence of loosely adsorbed water, as seen with peaks at 1600 and 1465 cm^{-1}, is due to the growth of the inorganic oxide network [115]. Alkoxides react to form hydrolyzed species, which are extremely hydrophilic. As the firing schedule increases, the Al-OH further undergoes condensation and forms the Al-O-Al network. Instead of OH groups being primarily bonded, they become loosely adsorbed with the higher firing temperatures [115].

The group of peaks at 1400-1300 cm^{-1} is generally assigned to the hydrocarbon groups found associated with DG and BA. The peak at 1380 cm^{-1} is assigned to the deformation of C-H. At room temperature it starts as a broad peak and decreases in the sample fired at 300ºC. In addition, peaks at 1350 and 1300 cm^{-1} appear at room temperature and in the fired sample at

100ºC, but completely disappear after 300ºC. This is assigned to the deformations of the C-OH. Along the same line, a doublet at 1125-1085 cm^{-1} is assigned to the chiral carbon stretching in BA. Similarly it appears in the first two spectra and disappears after 300ºC.

The peaks at 1250, 945, and 850 cm^{-1} are assigned to the deformation of the Al-OH bond. Initially these peak are noticeable for the room temperature and material fired at 100ºC, but the Al-OH bond evidently disappears at 300ºC at the expense of the Al-O-Al inorganic polymer towards lower wavenumbers [116, 120].

After comparison of an FTIR spectra for an electrospun and a control sample of ASB:BA in Figure 5-5, there are no noticeable changes that can be found to differentiate the two samples.

In summary FTIR analysis provides the perspective that during thermal transitions, adsorbed and bonded water compounds change due to a decrease in hydrophilicity. Additionally the growth of the inorganic polymerization of Al-O-Al appears as Al-OH disappears. To further elucidate the FTIR analysis of chemical bonds and respective changes in phase transitions, XRD is utilized in the next section.

Phase Transitions

Intriguing research has been explored in the field of exploiting certain phases of alumina for catalysis purposes; meanwhile the alpha phase is typically used for structural applications. As previously discussed in Chapter 2, the work of Yoldas opened doors to the bottom-up approach to study crystallinity in sol-gel alumina systems. This presented the opportunity to design and produce catalytically active transition phases which exist before the alpha phase is formed in excess of 1000ºC [27, 28, 31, 58]. This system requires hot water hydrolysis to transform tetrahedral to octahedral spaced Al species in the presence of certain acids. This results in the nucleation of the boehmite phase (δ-$AlO(OH)_3$), which then leads to a γ-Al_2O_3 ($\leq$

475ºC), θ-Al_2O_3 (≤1100ºC), and α-Al_2O_3(≤1300ºC) [40]. Yoldas believed that solely tetrahedral coordination undergoes a singular transition into α-Al_2O_3 [23, 27, 28, 31, 40, 58, 117]. The latter produces an amorphous structure called bayerite with hydrolysis at ≤ 70ºC. However others have found phase transitions in the cold-water hydrolysis systems with the presence of eta, theta, and/or gamma.[23, 27, 28, 31, 40, 53, 58, 75, 115, 117, 119, 120].

This alkoxide-based electrospinning process relies on atmospheric hydrolysis of the drawn precursor. The resultant phase compositions will be explored and compared to cold and hot water hydrolysis phase formation trends. Our precursors both have tetra-coordinated and hexa-coordinated species, therefore the latter is expected to exhibit transition phases on its way to the high temperature stable alpha phase. The purpose of this subsection is to delineate trends in phase transformations of these precursors and the effect the electric field may have on these phases. In this subsection, Differential Thermometric Analysis (DTA) along with XRD were performed on samples that were both electrospun and control dried to compare the firing for ASB:BA, ASB:DG, and mod-ASB:DG.

Methodology

Along with the TGA analysis, simultaneous DTA was performed to analyze the electrospun and control samples. Experimental conditions can be referred back to the TGA section. X-ray Diffraction (XRD) was performed on a Philips APD3720 with a step size of 0.02º in the range of 20ºC-70ºC and a time per step of 1.25 sec/step. The following JCPDS cards utilized were:

- Boehmite, JCPDS: 21-1307
- Gamma Al_2O_3, JCPDS: 10-0425
- Theta Al_2O_3, JCPDS: 11-0517
- Alpha Al_2O_3, JCPDS: 46-1212
- Delta Al_2O_3, JCPDS: 46-1131
- Beta Al_2O_3, JCPDS:10-0414

- Gibbsite, JCPDS: 33-0018
- Nordstrandite, JCPDS: 24-0006
- Doyleite, JCPDS: 38-0376
- Bayerite, JCPDS: 20-0011
- Diaspore, JCPDS: 05-0355

Results and Analysis from Phase Transition Studies

Differential Thermal Analysis (DTA) was performed on three precursors to map the energy changes due to thermal treatment. XRD serves to support the DTA by identifying particular phases or lack of phases in the thermal schedule.

As seen in Figure 5-6A of the ASB:BA system, there are a series of bands: endotherm between 25ºC-250ºC, exotherm ~ 250ºC, exotherm between 850ºC-900ºC, and 1150ºC-1225ºC. The first two bands can be supported by the FTIR analysis; this band is rather broad and includes the removal of adsorbed water, BA, and dehydroxylation of the alumina gel [115]. The exotherm ~250ºC includes residual carbon combustion along with possible reorganizing of the oxide network. The corresponding stacked XRD spectra can be found in Figure 5-6B for the electrospun fibers comparing room temperature, 300ºC, and 900ºC. In addition Figure 5-6C compares spectra at 300ºC for electrospun and control samples.

The XRD spectra at 900ºC cannot be used to distinguish a particular phase, but there are some bands formed that may be an indication that a low concentration small crystallites may have formed. This supports the claim by O'Dell and colleagues in the field of ^{27}Al-NMR; an increase of hexa-coordinated Al appears with increasing firing temperature- resulting in possible transition phases within the material that remain undetectable by XRD [75]. When comparing the DTA for the electrospun material and the control, the noticeable differences are in the relative intensities of the initial endotherm and exotherms. However the exotherm ~875ºC for

the electrospun is more broad than the control. The last exotherm shifts for the electrospun material to 1160ºC compared to the control at 1210ºC.

Looking at effects due to the electric field, a spectrum at 300ºC was compared for the ASB:BA system. The exotherm at 250ºC is much more larger than the control. However the spectra seen in Figure 5-5C shows no apparent changes between the electrospun and control. Unfortunately the changes in the DTA spectra between the electrospun and control cannot be accounted for by XRD.

However when various batches of electrospun fibers in the ASB:BA system are rerun in the DTA, the alpha phase seems to shift slightly. In Figure 5-6D, the apex of the alpha transition occurs ~1210ºC. Additionally the exotherm ~875ºC increases in sharpness in contrast to Figure 5-6A. Therefore it can be presumed that the electrospinning process does not produce additional nucleation of crystallites or lower transition temperatures for the alpha phase. However this set of analysis does illustrate that the change in the conditions of these materials may be a result of some aging. Aging has been known to shift the transitions slightly over a small range of temperatures in the processing of ASB [75, 118]. Nonetheless the inherent changes in phase transitions are not effected by these slight shifts nor do they show a discernible difference due to the electric field.

In Figure 5-7 and Figure 5-8, the ASB:DG system is studied. In Figure 5-7 A the DTA spectra for ASB:DG illustrates a series of peaks: an endotherm ~ 100-150ºC, exotherm ~ 250ºC, small endotherm ~ 400ºC, exotherm ~ 875ºC, and exotherm > 1100ºC. Figure 5-7B is a stacked XRD demonstrating the trends of the control bulk material fired at room temperature, 300ºC, and 900ºC. The control displays a more prominent exotherm at 875ºC. The trend in the DTA spectra is similar to that of the ASB:BA system, but the differences are found with the exothermic band

between 250ºC-400ºC. The broader exotherm may relate to two types of reactions taking place. The first case being the hydrocarbon combustion and hydroxyl evolution; meanwhile the second case may be structuring of the oxide network with the increased presence of hexa-coordinated aluminum cation sites [75]. These hexa-coordinated Al sites promote the growth of transition phases [28, 64, 94, 96, 98, 100]. The ratio of ASB:DG is 2-1, therefore for every two ASB molecules there is one that should have reacted by a transesterification of the glycol ether leading to hexa-coordinated aluminum alkoxides [90]. These should therefore undergo formations to form transition phases [75, 90].

The stacked XRD of Figure 5-7B shows the change of rather broad bands for samples fired at 300ºC into more defined peaks at 900ºC. O'Dell's work relating the low concentration of hexa-coordinated Al explains that the three main bands can be matched to both the boehmite and gamma phases [75]. Boehmite is formed from hexa-coordinated Al as an orthorhombic structure; the gamma phase forms from both the tetra-coordinated and hexa-coordinated Al as a cubic structure [27, 28, 31, 40, 46, 52-54, 79, 86].

Interpretation of the spectrum at 300ºC may be a combination of both the boehmite and gamma phases. The first band should correspond to the boehmite [120] at 28.18º and gamma [220] at 21.96º. The second band is more difficult to decipher, but can represent a set of peaks in the boehmite [031] at 38.37º and gamma [222] at 39.52º, and gamma [400] at 45.90º. The third band can represent the boehmite [231] at 64.03º, boehmite [002] at 64.98º, and gamma [440] at 67.09º. These respective diffracting planes [hkl] are chosen based on the highest respective intensities within the measurement range.

However the peaks found in the 900ºC spectrum for both the electrospun and control ASB:DG can be matched to the gamma phase. The main components of the spectra can be

matched to [311] at 37.63º, [222] at 39.52º, [400] at 45.90º, [511] at 60.95º, and [440] at 67.09º. These peaks and bands exhibit broadening that can indicate the presence of nanometer scaled crystals [121]. The [440] peaks were chosen to contrast spectra of electrospun and control materials, as seen in Figure 5-8 A and B. Peak fitting and calculation with the Scherrer equation determined the crystal size. The calculated crystal width is normal to the diffracting plane and the constant, 0.94 was chosen for approximate unity [121]. Firstly peak fitting was performed for both control and electrospun as seen in Figure 5-8C. The peak fitting and Scherrer equation results are included in Figure 5-9 showing a calculated crystal size of 8.4 nm for the control and 8.3 nm for the electrospun case. During the peak fitting, there was a slight shift in the peak position, however due to such broadening, these effects are within the error of the measurement [121].

There are no notable contrasts can be drawn for the electrospun and control samples. However it is interesting to find the formation of nanocrystalline gamma phases that were more defined in the ASB-DG system than the ASB:BA system. These materials contain both the tetra-coordinated and hexa-coordinated species, however the DG species increases the presence of the hexa-coordinated species, thereby increasing the possibility of forming transition phases [53, 75, 90]. The hexa-coordinated species can nucleate into boehmite phases in small concentrations undetectable by XRD [75, 122]. It is believed that the small quantity of boehmite phase can assist in nucleating the cubic gamma phase, by serving as heterogeneous nucleation sites. As seen in Figure 5-10 the presence of the hexa-coordinated is located in the MAS-NMR spectra for Al at - 70 ppm. This coordination state increases the possibility of forming detectable gamma phases with the ASB:DG system. In part due to the larger concentration of tetra-coordinated Al,

the other phase transition do not occur and the alpha phase then occurs at lower temperatures than Yolda's methods [27, 28, 31, 40, 52, 53, 58, 75, 79, 123].

To contrast the solvent addition systems, Figure 5-11 includes the DTA spectra for the modified precursor, mod-ASB:DG and a stacked XRD spectra. This precursor varies from the previous system in the inherent bonding nature of the precursor and also the electrospinning behavior. In the DTA, similar peaks are located in the ASB:DG system. There is a more prominent exotherm at the 450ºC for the electrospun compared to its control. The latter exotherms are ill-defined in the ~900º and between 1100-1200º. These ill-defined exotherms may be further investigated in the stacked XRD spectra showing that there is a combination of broad alpha peaks and intermixed with the gamma phase. The spectrum at 1200ºC can be compared to the 900ºC to identify the budding phase. Within the 900ºC spectrum, the gamma is still apparent for the [400] ~ 45.90º within the band ~ 67.09º for the [440]. The intriguing nature is that the alpha formation is appearing at a lower temperature, which is an appeal to researchers avoiding high-temperature coarsening of the alpha phase [57].

The 300ºC spectrum demonstrates the formation of rather broad bands that are a combination of both the gamma and boehmite phases better defined than the ASB:DG system at 300ºC. There are four major bands that can be identified as a combination of both the gamma and boehmite phases. The first band can be attributed to the boehmite [120] at 28.18º. The second band is less defined in the region from 35º- 47º that includes the boehmite [031] at 38.34º, gamma [220] at 36.96º, gamma [222] at 39.52º, and gamma [400] at 45.90º. The third encompasses a broadening from boehmite [051] at 48.93º and boehmite [200] at 39.21º. The last band may incorporate boehmite [231] at 64.03º, boehmite [002] at 64.98º and gamma [440] at 67.09º. The increased presence in the boehmite phases relates to an increase in hexa-coordinated

Al. The precursor is prepared with a 1:1 ratio of alkoxide and DG thereby vacuum distillation. This increase in hexa-coordination of Al may lead to increase boehmite nuclei promoting the gamma phase growth in the presence of tetra-coordinated Al [53, 122].

To conclude from this set of studies, there are no apparent differences with respect to phase transformations due to processing in an electric field for the BA, DG or mod-DG system. The hexa-coordination manifests into phases fired at 300ºC, such as boehmite, that are often a minority in the predominant tetra-coordinated Al system. This minority, although often difficult to be distinguished, were more discernible in the ASB:DG and mod-ASB:DG systems than in the ASB:BA system. The former two systems produced distinct phase resolution fired at 900ºC. At those temperatures, the ASB:DG system contained nanocrystalline gamma phase, meanwhile the mod-ASB:DG system incorporated a combination of the gamma and alpha phases. This set of work increases the understanding transition phases by "cold-water" hydrolysis of the precursors through electrospinning, without the use of acids, aging treatments, and high-pressure systems. Essentially this study also explores the phase transition and production of transition phases in fibers produced through the fabrication of alkoxide-based electrospinning owing the possibility for usage as catalysts or materials that can decrease high-temperature coarsening of the alpha phase.

Dimensional Changes

This section relates the change in the fiber diameter after firing at 1200ºC for electrospun fibers in contrast to the green state. These changes occur as a result of organic mass loss and structuring of the oxide network. Changes in dimensions can be deleterious by changing the structure of the fibers, resulting in cracks and breakage. Since electrospinning is a highly sought after technique to fabricate various coatings and/or multi-component devices (i.e. layered filters) drastic shrinkage due to firing may reduce its viability. The drawing of the alkoxide-based

precursor drives the hydrolysis and condensation reaction, resulting in a less relative amount of organic species being burned off. Since the fibers are formed as a result during the drawing and atmospheric exposure, small dimensional changes are not expected to alter the structure or the integrity of the fibers.

Methodology

Samples were fired to 1200ºC at 10ºC/min in air. Precursors, ASB:BA, ASB:DG, and mod-ASB:DG were utilized. SEM micrographs were utilized and analyzed utilizing the Carnoy Software 2.1. Measurement and PDF's were calculated in the same methodology as previously stated in Chapter 4. The ASB:DG system was electrospun at 0.667 kV/cm, 0.711mm inner needle diameter, 7.62 cc/hr, and 43% R_h. Meanwhile the ASB:BA system was electrospun at 1.0kV/cm (20cm), 0.711 mm inner needle diameter, 8.98 cc/hr, and 45% R_h. The mod-ASB:DG system was electrospun at 0.667 kV/cm, 0.711mm inner diameter needle, 10.10 cc/hr, and 43% R_h.

Results and Analysis of Dimensional Changes

The PDF for ASB:BA and ASB:DG systems depicts a definite shrinkage in the fiber diameter distribution as shown in Figure 5-12A and B. In the ASB:DG system, the change that occurs goes from a bimodal distribution with a mean ~23.5 μm to a single distribution with a mean ~ 18.5 μm. The ASB:BA system observes a smaller change from ~ 25 μm down to ~24 μm. Nonetheless the average error of Carnoy's pixel measurement is ~ 1μm. Therefore the changes in the ASB:BA can be construed as negligible. The apparent change in the ASB:DG system and the lack of change in the ASB:BA may still be difficult to analyze due to the distribution of fibers. The little or lack of change may be due to the hydrolysis and condensation reactions that occur upon electrospinning. Previously discussed in the TGA section, the

ASB:DG system is comprised of more trapped organics due to the low-vapor pressure nature of solvent that can remained trapped within the network.

In Figure 5-15A noticeable distortions can be found along the walls of the tubular structures. The outside walls of the tubular structures show some cracking. The cracking does not lead to any apparent breakage of the fiber and does not permeate through the structure. The cracking may be due to the heating rate, in which case, cracking may ensue due to drying stresses from trapped solvents. For down-stream usage of these fibers, heating schedules can be scrutinized to provide a more consistent structure along the fiber walls through drying, aging or a lower heating rate.

Figure 5-14 illustrates the morphological difference between mod-ASB:DG due to firing. Previously the observations made regarding the fibers were due to the propensity to form solid continuous fibers with a minute few hollow tubules. The green state of these fibers had a bimodal distribution of fibers. The bimodal distribution had peaks in the range of 27 μm and 32 μm, respectively. After firing the samples exhibited a single modal distribution at 17 μm. There is an obvious larger shrinkage resulting from the mod-ASB:DG due to the larger presence of organics and the slower hydrolysis/condensation rate.

Surface Area and Pore Analysis

Potential usages of such fibers are in the realm of filtration, insulation and acoustic dampening. Additionally these electrospun fibers can be used for biological scaffolds and reinforcing materials for structural applications. These bundles of electrospun fibers from alkoxide-based precursors form interconnected structures with an innate porous nature. The porous nature of these fibers can be related to a myriad of factors due to: fiber stacking, hollow

centers, and drying of the alkoxide. The nature of these pores and exposed surface area is then assessed and compared for various electrospun fibers before and after firing at 1200ºC.

Methodology

Fibers were electrospun from ASB:BA 3-1, ASB:DG 2-1, and mod-ASB:DG. All fibers were electrospun at $R_h = 42\% \pm 3\%$ with needle gauge of 0.712 mm, electric field of 0.667 kV/cm (10kV/15cm), and respective flow rates of 8.89, 7.61, and 10.10 cc/hr. First set of samples outgassed at 150ºC for 6 hours as a Quantachrome mandatory protocol before each measurement. The second set were then fired at 1200ºC and then outgassed at 150ºC for 1 hour before measurement.

Density (ρ) experiments were performed in a Quantachrome Ultrapycnometer 1000 and an average of 3 runs was recorded. Specific surface area (S.S.A.), pore volume (V_{AVG}), and pore diameter (D_{AVG}) were performed on a Quantachrome Nova 2200. The Brauner-Emmett-Teller (BET) analysis was used for S.S.A. analysis. The Barrett–Joyner–Halenda (BJH) analysis was used for pore analysis. Average pore values were recorded that average the values on adsorption and desorption. The pore volume is recorded for pores in between 1.7 nm and 300.0 nm.

Analysis of Surface Area and Pore Analysis

The electrospinning conditions were chosen based on reproducibility and low concentration of defect structures. The solvent-addition precursors, ASB:BA and ASB:DG, produced fibers that had consistent hollow structures. At the first outgassing state of 150ºC, these fibers resulted in a S.S.A. in the range of 330 - 385 m^2/g. These values correlate to D_{AVG} within 4.6 and 5.25 nm. The small pore diameter and high specific surface area alludes to the fact that sol-gel based products retain porous networks upon drying. These micropores are formed as a result of the trapped solvents and water within the networks during gelation [23].

After firing the samples at 1200ºC, a decrease in the S.S.A. is found between 8.5-10.5

m^2/g. and ASB:BA D_{AVG} is 32.95 nm and ASB:DG is 9.75nm. This change in S.S.A. is expected due to pore collapse and also grain coarsening in the alpha phase. The change in pore diameter of the BA and DG system at 1200ºC may be due to the amount of trapped solvents in each system. The BA is comprised of a more volatile solvent, in which case, may cause larger drying stresses and pore collapse that can lead to a larger D_{AVG} upon firing. Additionally upon firing, pores often become discontinuous, leading to smaller volumes of adsorbed gas.

The mod-ASB:DG system is different because the majority of fibers produced are solid. These fibers have a lower S.S.A. of 82.87 m^2/g and D_{AVG} of 8.78 nm at 150ºC and firing at 1200ºC changes the values to 6.32 m^2/g and 52.4 nm. There is still a small initial D_{AVG} that is consistent with the usage of sol-gel precursors.

Previously mentioned in the dimensional analysis section, fired fibers were shown to have maintained the overall structures similarly found with the respective green state. Defects were observed and can also be attributed to drying stresses. During drying, the liquids move from the pore toward the outside surface, forming a meniscus and causing tension. This tension exerts pressure on the structure. Cracks are not noticeable in the green state fibers, since they are still gels; wherein gels have modest drying rates, due to the small pore size. However as the temperature increases, drying stresses are also increased, resulting in the structural defects.

Electrospinning of the alkoxide-based precursors provides fibers with pores in the range of the macroporous (4mm - 400nm) down to the microporous (< 50nm). These fibers are suitable for various applications. Although the firing reduces the S.S.A., V_{AVG}, and D_{AVG} values, these fibers maintain a great deal of potential for future applications.

Conclusions for Property Comparisons of Thermal Processing in an Electric Field

Processing effects based on alkoxide-based electrospun fibers were investigated in this chapter. Thermal processing parameters along with the electric field were investigated simultaneously.

After examining mass loss through TGA analysis, the predominant trend that electrospun samples exhibited less percent mass loss than their control counterparts. The difference in mass loss for the ASB:BA and ASB:DG is ~ 10 %. Since the mod-ASB:DG system exhibited a different trend in fiber formation and drying, it retained more solvent within the fiber and only exhibited a difference of ~ 4%.

Interestingly, the TGA-FTIR utilized Gram-Schmidt reconstructions to relate the relative amount of gas being evolved for electrospun and control samples. In doing so, the Gram-Schmidt reconstructions reaffirmed initial conclusions drawn from the TGA. Bulk analysis with the FTIR illustrated no changes in peaks for the green state of electrospun alumina material is fired. No apparent contrasts due to the electric field could be drawn with the FTIR and XRD for electrospun and control materials.

Additionally electrospun samples exhibited shrinkage, but the overall structure of the fibers were maintained. ASB:BA and ASB:DG both exhibited the least amount of shrinkage compared to mod-ASB:DG. Although the presence of cracks and some fissures were observed, it may be due to the amount of trapped organics creating drying stresses due to the use of alkoxide-based materials. It was noted that the presence of defects could be further improved in downstream processing.

Chemical analysis with FTIR allowed us to analyze changes to the fibers and control during the firing schedule. Through firing, there is a decrease in hydrophilicity, which initially

increases the amount of adsorbed hydroxyls up until a certain temperature. Bands begin to fuse and level out to illustrate structuring of the oxide network over higher temperatures.

Changes in bonding during the firing treatment leads to the presence of phase transitions. Previously it was ill conceived to most researchers of sol-gel alumina that any transition phases can be formed through cold-water hydrolysis. Since these electrospun fibers are hydrolyzed in an ambient atmosphere, cold-water hydrolysis ensues. Within this work, there is a presence of tetra-coordinated and hexa-coordinated Al alkoxides. An increasing amount of hexa-coordinated species promoted the formation of boehmite and gamma transition phases. This was supported by the use of precursors, ASB:DG and mod-ASB:DG, with an increasing amount of glycol ether promoting hexa-coordinated species. The increase in hexa-coordinated species increased the refinement of peaks and bands after firing at 300ºC and 900ºC. In addition mod-ASB:DG promoted an alpha transition at 900ºC.

Gamma phase alumina fibers can serve as potential catalytic applications. These applications require exposure to surfaces and current analysis shows initial pore sizes and specific surface areas were comparable to aerogels and xerogels, but upon firing they are reduced. The fibrous structures, hollow or solid, are still maintained throughout the firing schedule, while the pores become more discontinuous. Nonetheless the macroporous nature of these fibers can still be maintained for further applications.

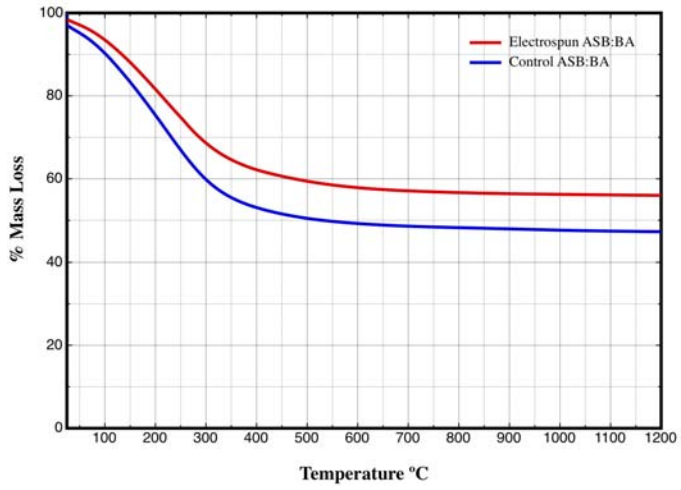

A

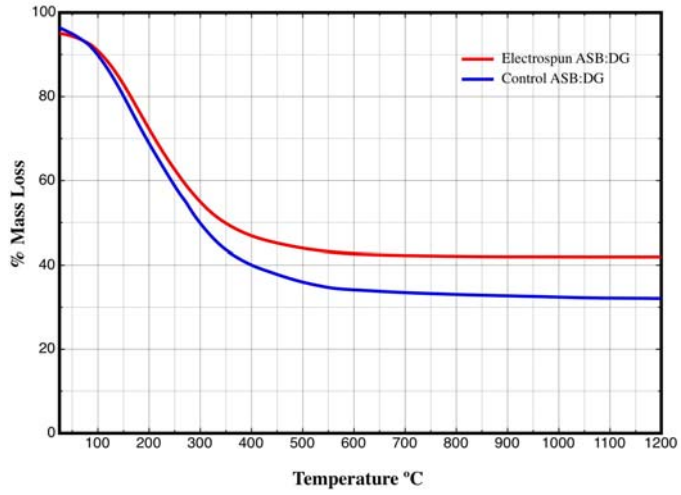

B

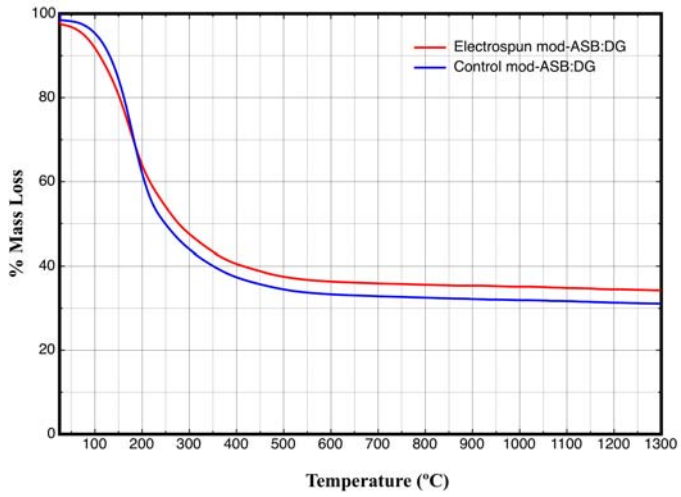

C

Figure 5-1. Thermogravimetric Analysis Comparing Electrospun And Controlled Dried Alumina At 10ºC/Min In Air, Red=Electrospun, Blue=Control: A) Plot For ASB:BA. B) Plot For ASB:DG. C. Plot For Mod-ASB:DG.

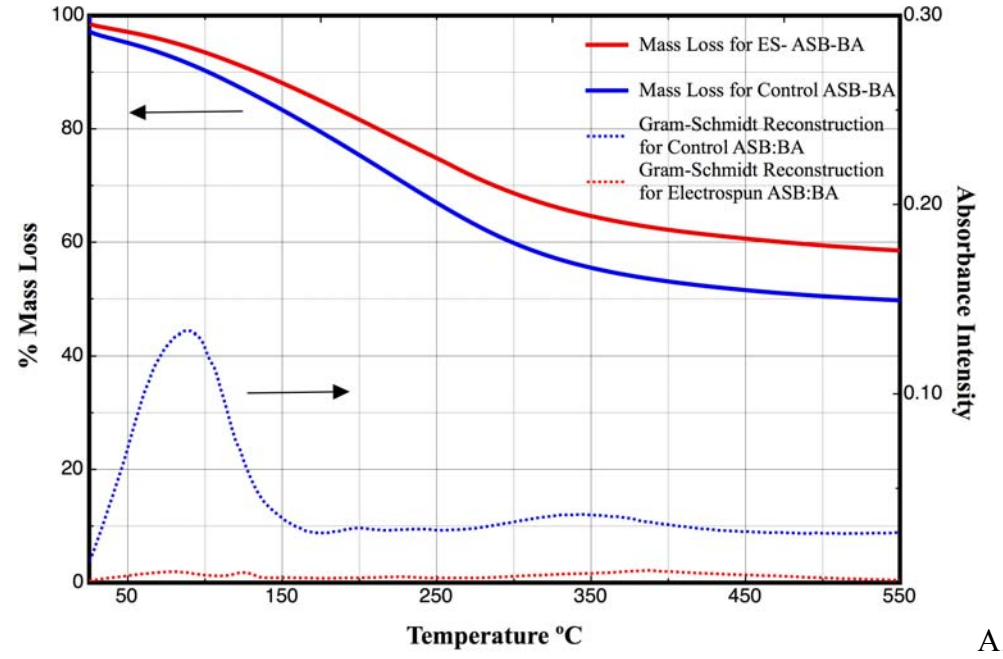

A.

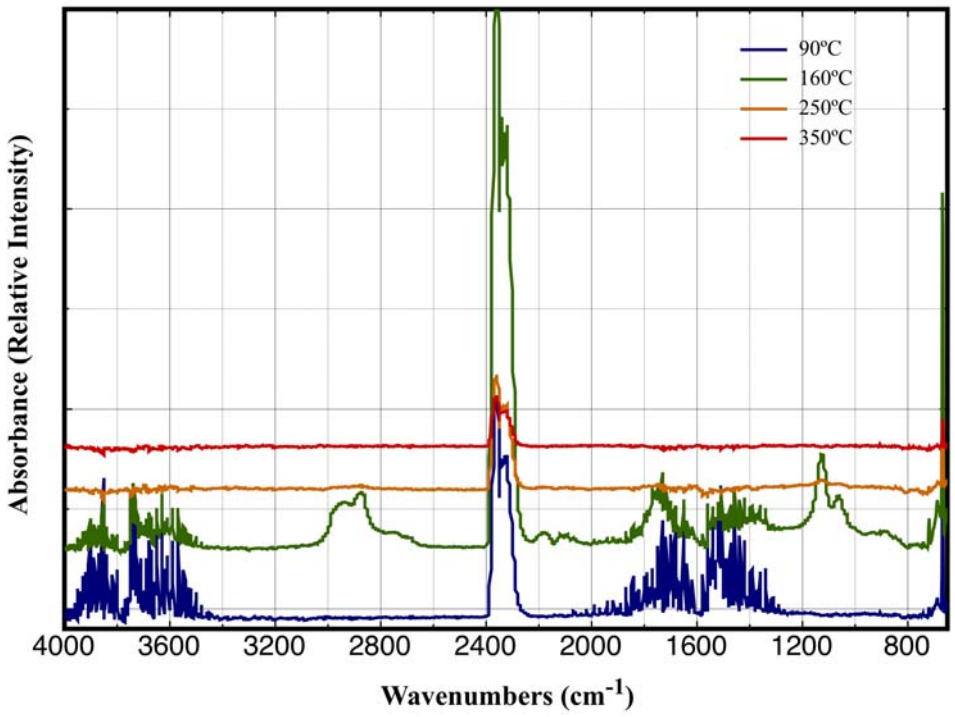

B.

Figure 5-2. TGA-FTIR For ASB:BA: A) Combined TGA And Gram-Schmidt Reconstruction For Electrospun And Control Of ASB:BA. B) Corresponding Stacked FTIR Spectra At 90ºC, 160ºC, 250ºC, And 350ºC For Control ASB:BA.

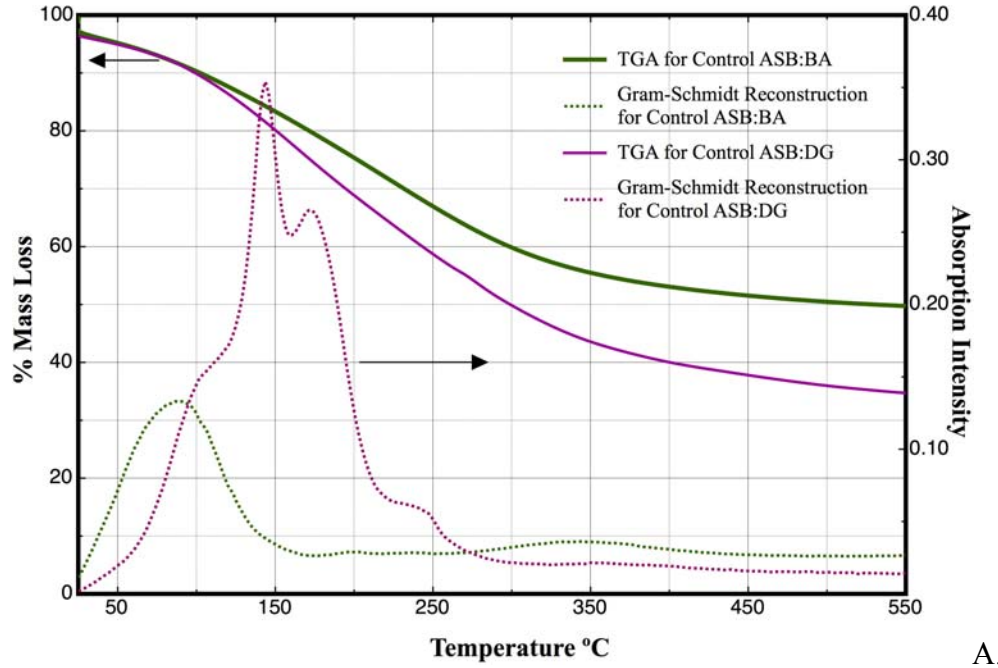

A.

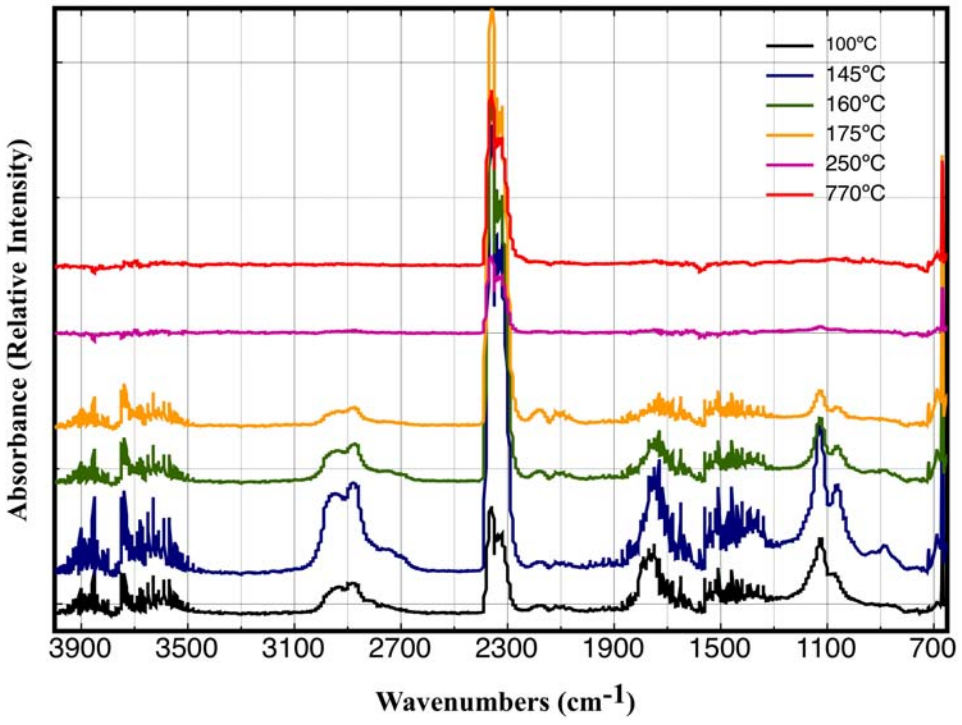

B.

Figure 5-3. TGA-FTIR For ASB:BA And ASB:DG: A) Combined TGA And Gram-Schmidt Reconstruction For Control ASB:BA And ASB:DG. B) Corresponding Stacked FTIR At 100ºC, 145ºC, 160ºC, 175ºC, 250ºC, And 770ºC For Control ASB:DG.

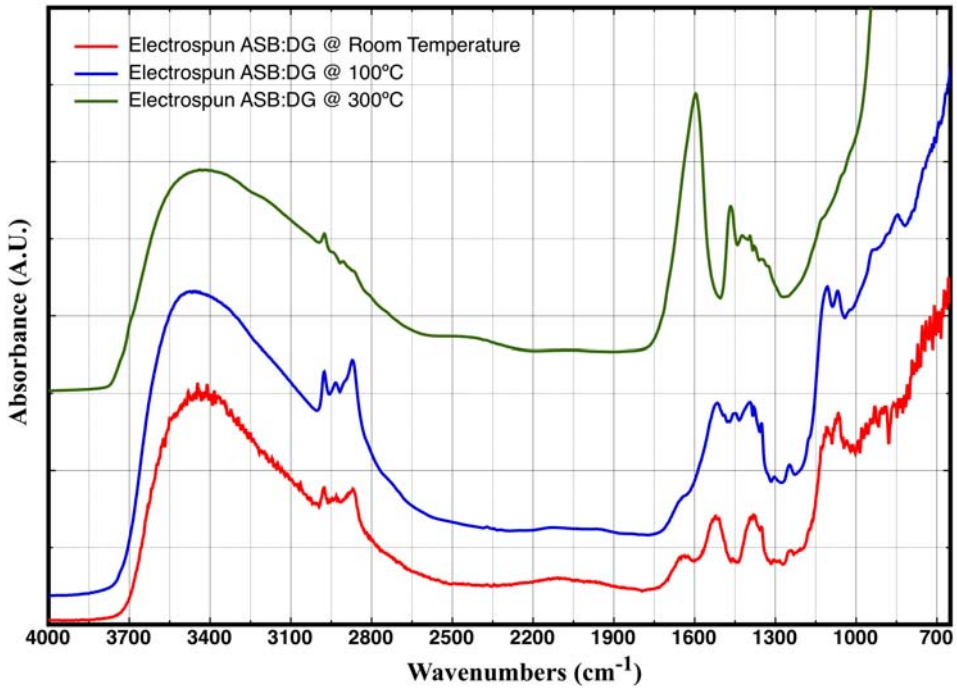

Figure 5-4. FTIR-DRIFTS Analysis Of Thermal Treatment Of Electrospun Fibers For ASB:DG At Room Temperature, 100ºC, And 300ºC.

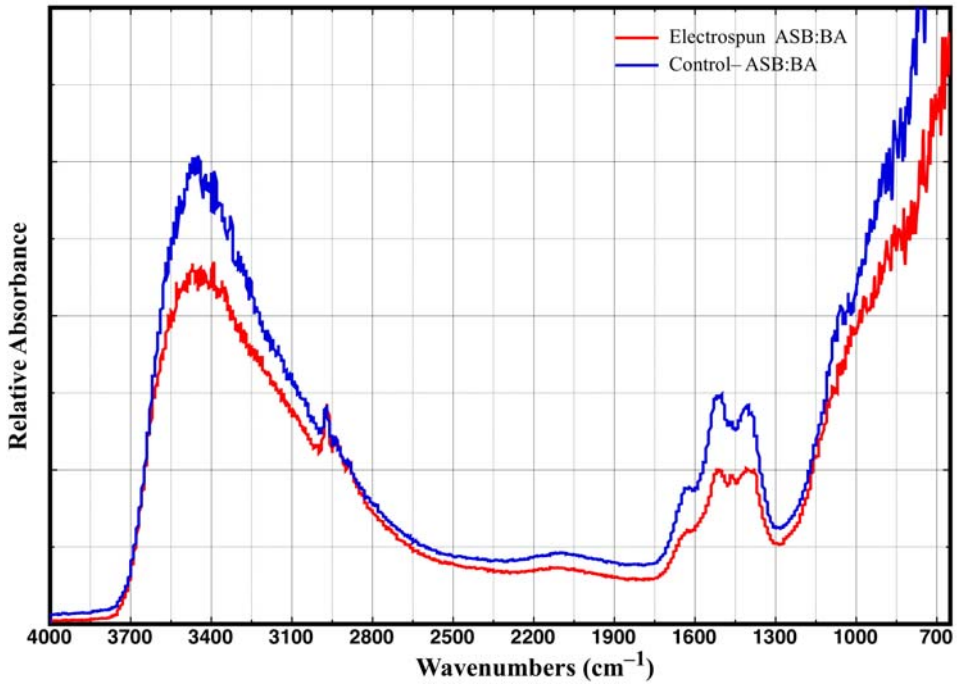

Figure 5-5. FTIR DRIFTS Spectra Of Electrospun Versus Control Of ASB:BA.

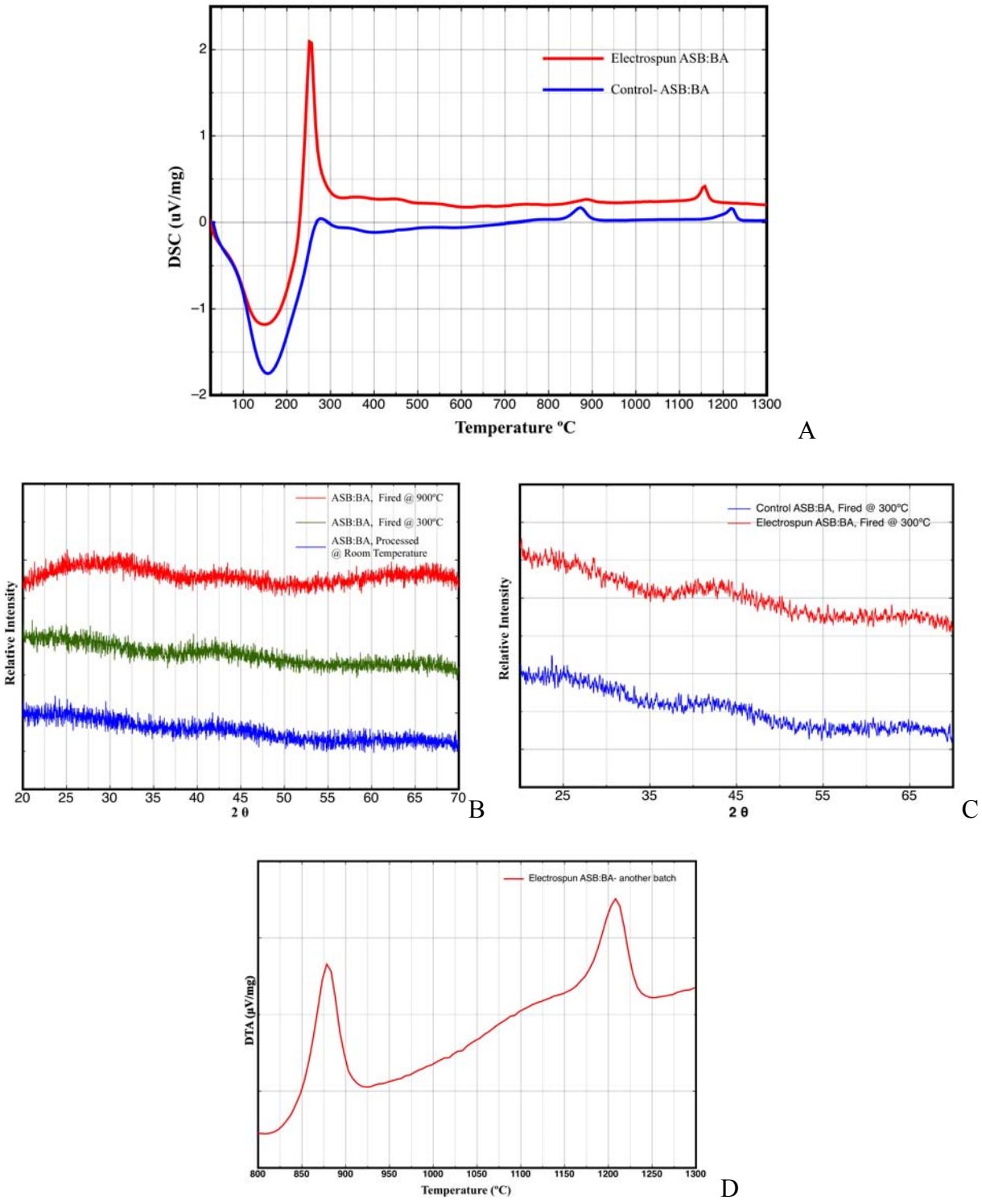

Figure 5-6. Thermal Transitions For ASB:BA: A) DTA. B) Corresponding Stacked XRD Spectra For Electrospun ASB:BA At Room Temperature, 300ºC, And 900ºC. C) XRD Of Electrospun And Control ASB:BA Fired At 300ºC. D) DTA Of Another Batch Of Electrospun ASB:BA 3-1 With Shifting Alpha Phase Transition Temperature.

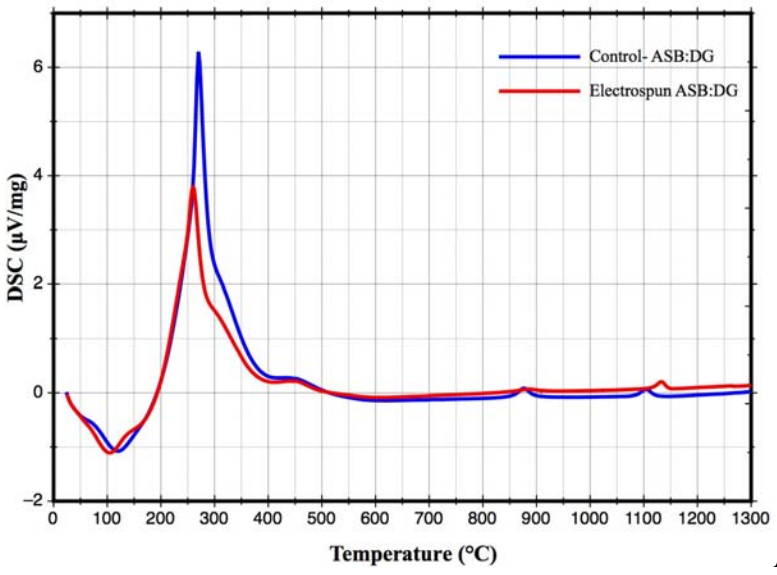

A.

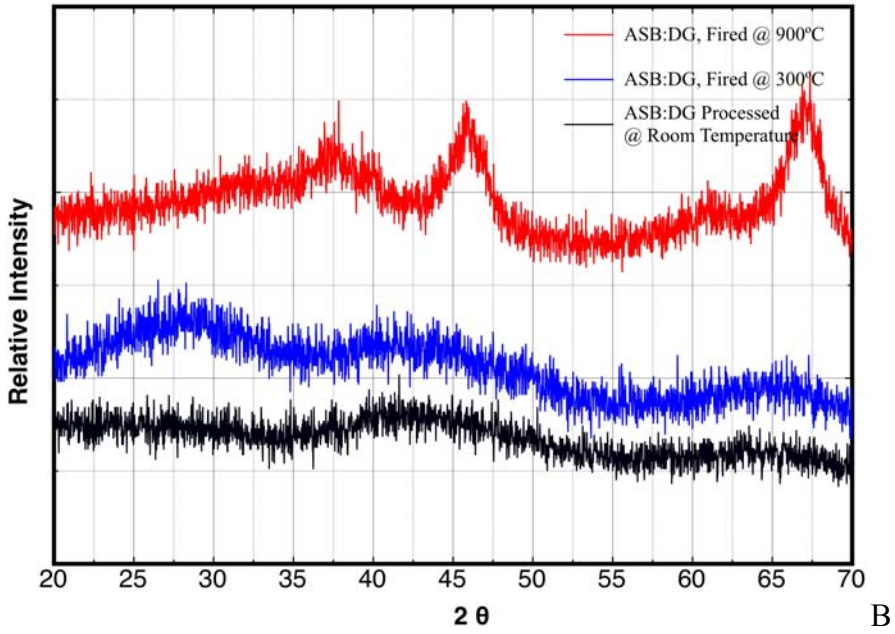

B

Figure 5-7. Thermal Transitions For ASB:DG: A) DTA. B) Corresponding Stacked XRD Spectra Of Control ASB:DG At Room Temperature, 300ºC, And 900ºC.

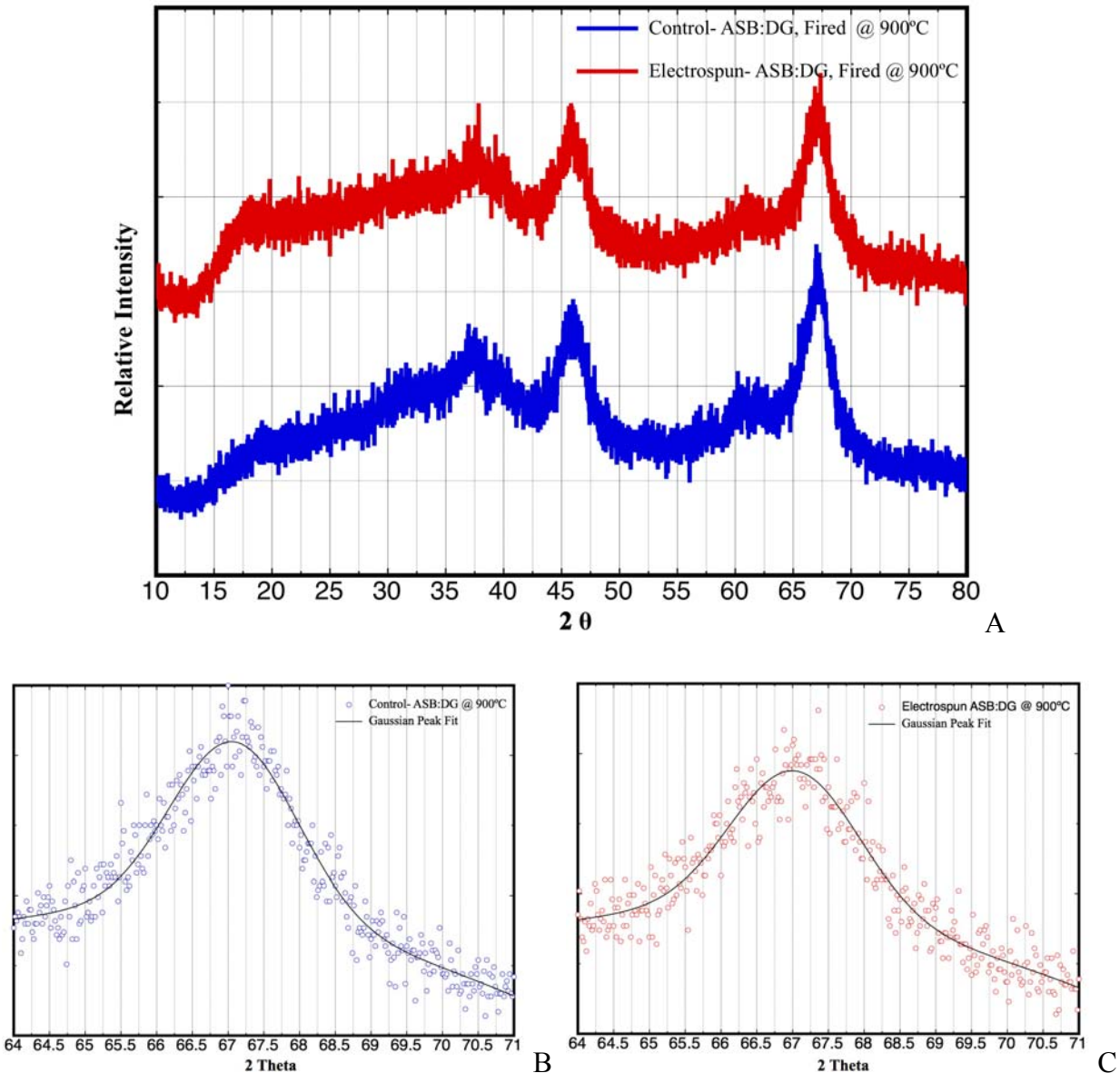

Figure 5-8. Electric Field Effect On Phase Transformations: A) XRD At 900ºC For Electrospun Vs Control For ASB:DG. B) Peak Fitting At 67.084º For Control- ASB:DG. C) Peak Fitting At 67.032º For Electrospun ASB:DG.

Sample	Expected Peak	Plane	Peak Position (2 Θ)	Peak Position (Θ)	STD of Peak Position	Peak Width (2 Θ)	STD of Peak Width	Full Width at Half Max	STD of Full Width of Half Max	Width Conversion	Scherrer Equation (nm)
Control-ASB:DG @ 900°C	67.09	[440]	67.08	33.54	0.02	0.89	0.03	2.10	0.08	0.02	8.4
Electrospun-ASB:DG @ 900°C	67.09	[440]	67.03	33.52	0.02	0.90	0.04	2.12	0.10	0.02	8.3

Figure 5-9. Values From The Comparison Of Electrospun And Control ASB:DG Of Peak Position And Calculation Of Respective Crystallite Size Through Scherrer Equation.

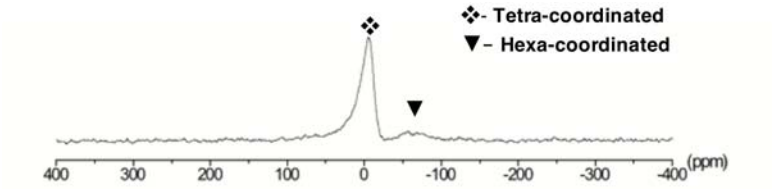

Figure 5-10. ^{27}Al MAS-NMR Of Electrospun ASB:DG: δ_{Tetra} = 10 ppm. δ_{Hexa} = - 70 ppm.

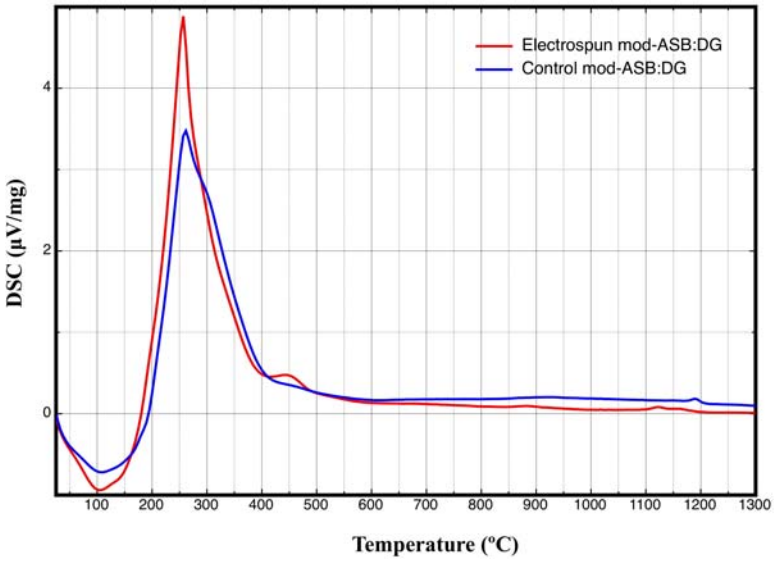

A

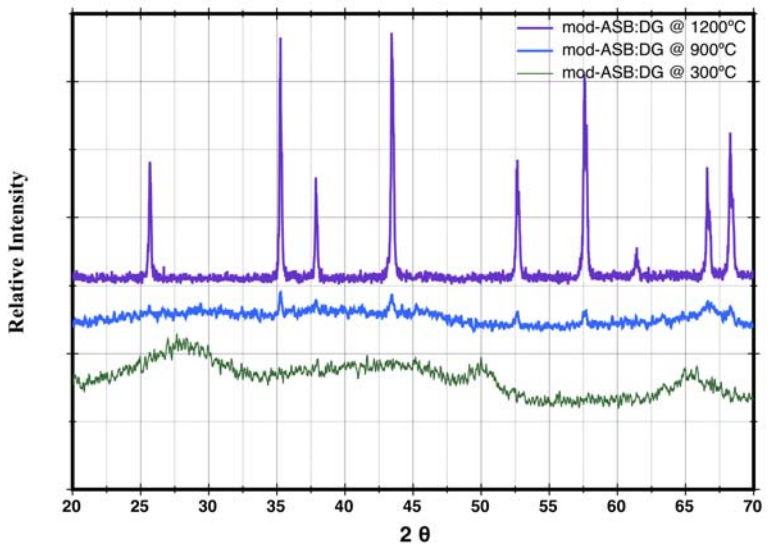

B

Figure 5-11. Firing Analysis Of mod-ASB:DG: A) DTA Of mod-ASB:DG. B) Stacked XRD Spectra Of mod-ASB:DG at 300ºC. 900ºC, and 1200ºC.

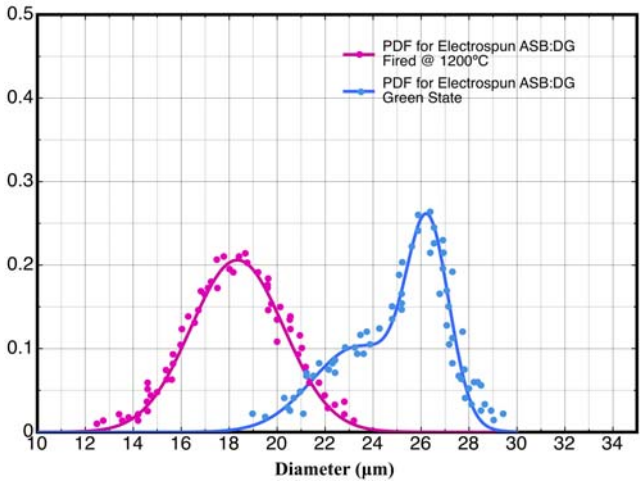

A

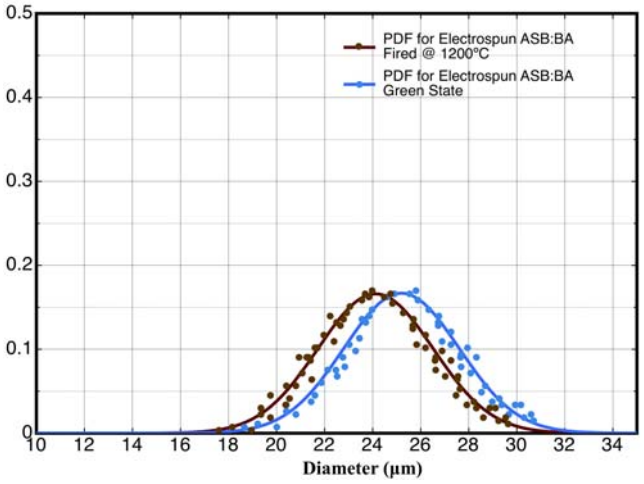

B

Figure 5-12. Probability Density Function For Dimensional Changes Due To Firing At 1200ºC Of Electrospun Fibers: A) ASB:DG System At 0.667kV/cm, 0.711mm Needle Gauge And 7.62 cc/hr. B) ASB:BA System At 1.0kV/cm, 0.711mm Needle Gauge And 8.89cc/hr.

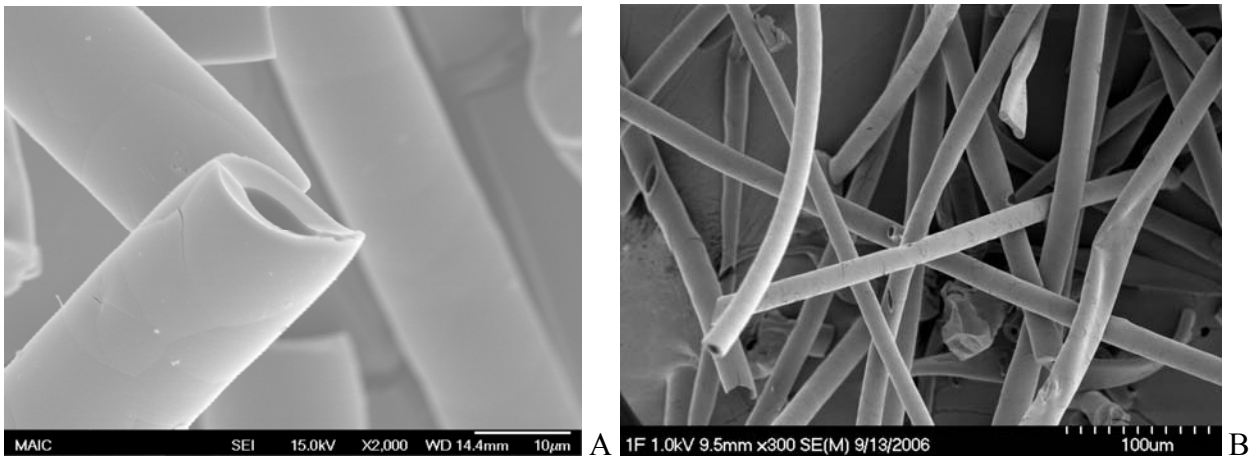

Figure 5-14. SEM Of Fired Electrospun 2-1 ASB:DG At 1200ºC: A) SEM Of Fiber Showing Crack Along Wall, Scale Bar Set = 10 μm. B) SEM Of Fiber Bundle Showing Intact Structures, Scale Bar Set = 100 μm.

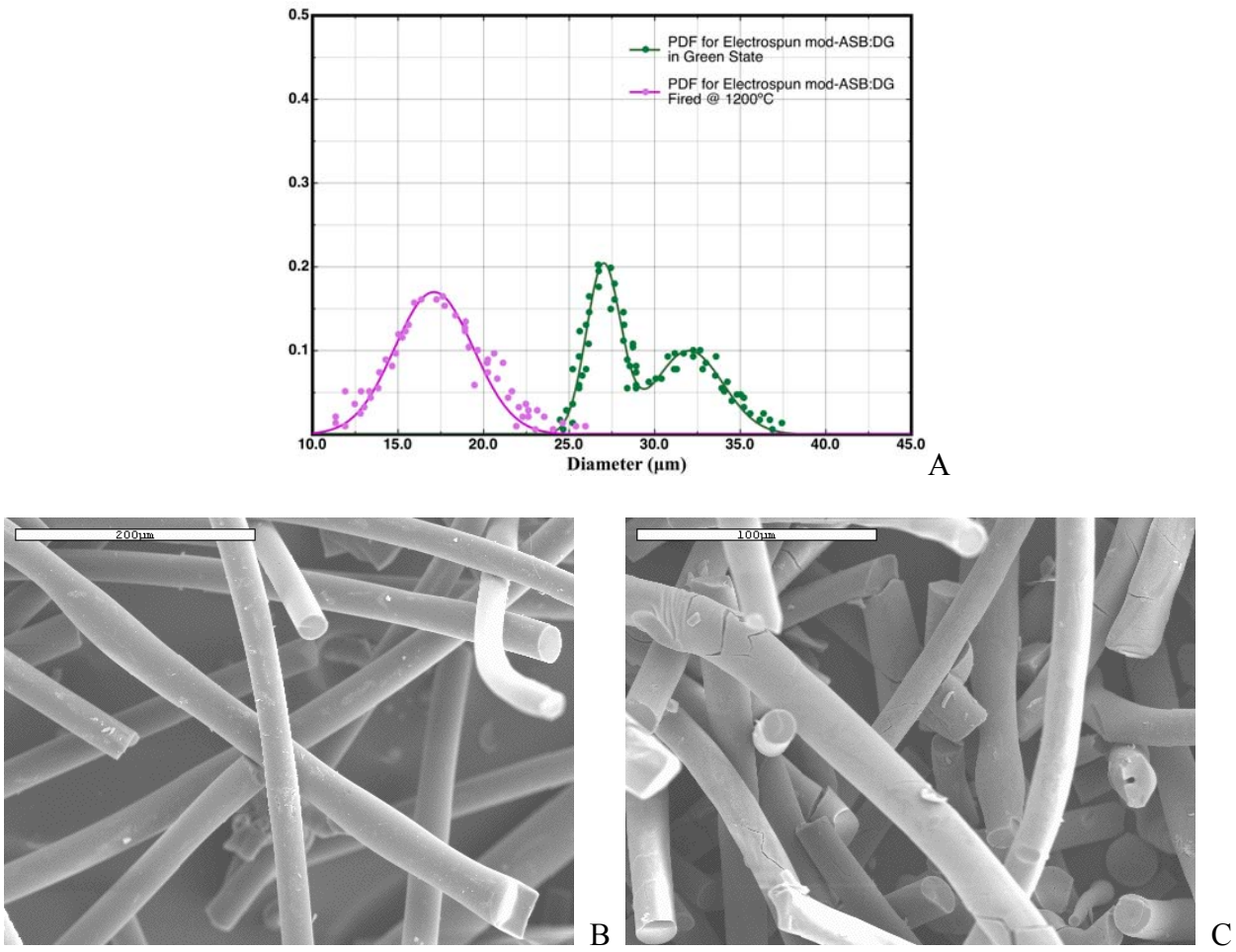

Figure 5-15. Comparison Of Green State And Fired Electrospun mod-ASB:DG: A) PDF Of Fiber Diameter Distribution Of Green And Fired @ 1200ºC. B) SEM Of Green State, Scale Bar = 200µm. C. SEM Of Fibers Fired @ 1200ºC, Scale Bar = 100µm.

Table 5-1 Table Of Values For Various Electrospun Fibers.

Samples	ρ (g/cm^3)	S.S.A. (m^2/g)	V_{AVG} (cm^3/g)	D_{AVG} (nm)
Electrospun ASB:BA- 150ºC	1.34	384.5	0.48	4.65
Electrospun ASB:DG- 150ºC	1.33	339.75	0.14	5.25
Electrospun mod-ASB:DG- 150ºC	1.68	82.87	0.2	8.78
Electrospun ASB:BA- 1200ºC	1.35	10.45	0.1	32.95
Electrospun ASB:DG- 1200ºC	1.42	8.48	0.03	9.75
Electrospun mod-ASB:DG- 1200ºC	1.74	6.32	0.01	52.4

Note: Density (ρ). BET Specific Surface Area (S.S.A.). BJH Volume (V_{AVG}). BJH Pore Diameter (D_{AVG}).

CHAPTER 6
CONCLUSIONS AND FUTURE WORK

Conclusions

The goal to redesign new precursors for direct electrospinning of alumina fibers was accomplished with reproducible alkoxide-based precursors that do not require polymer additives to increase spinnability. Three newly designed and prepared precursors can be electrospun into continuous hollow fibers, solid fibers, or hollow particles. Thus the redesign of these precursors can be applied for other electrospinning applications to produce a variety of fibers for repair of thermal insulative components, such as space suits, cryogenic fuel tanks, structural foam, tiles, and more. In addition the design and preparation of these precursors can also be used as templates to prepare other compositions for thermal, structural, photocatalytic, or biomedical applications.

Typically electrospinning of ceramics has been associated with compositional versatility but plagued with low yield, slow production times, low reproducibility, and structural issues as a result of calcination. In contrast these alkoxide-based precursors rely on atmospheric hydrolysis, also known as "cold-water" hydrolysis, which allows for a large decrease in production times. Direct electrospinning with these alkoxide-based precursors yielded an average of 1.9 g/hr of Al_2O_3, compared to literature with the highest theoretical yield calculated to be 0.68 g/hr. The quick and robust quality of electrospinning alkoxide-based precursors should be an attractive quality for use for rapid repair of ceramic fiber structures. The reliance on atmospheric hydrolysis can be factored in the design of the modular electrospinning system, which maintains a relative humidity and temperature to reproducibly fabricate fibers of certain specifications.

Electrospinning of these precursors relies on atmospheric hydrolysis and condensation of the alkoxide species. Additionally the exposure rate of the alkoxide directly relates to the flow

rate of the electrospinning system as discussed in Chapter 4. The precursors prepared relied on the addition of solvents or transesterification by vacuum distillation, which is further detailed in Chapter 3.

The difference in the volatility of the solvent and type of solvent resulted in different optimal flow rate ranges, respectively. Within optimal ranges of the appropriate precursor, continuous fibers can be produced consistently with a low concentration of defected structures.

Although this type of "cold-water" hydrolysis of aluminum alkoxides typically results in a lack of transition phases and solely an alpha transition in excess of 1200ºC, Chapter 5 proves otherwise. The addition of glycol ethers increased hexa-coordination of aluminum alkoxides, thereby resulting in transition phases and lower alpha transition temperatures found ~ 900ºC.

Electric field settings cannot take into account drying times for alkoxide-base precursors; moreover correlation studies could not be accurately drawn to changes in the electric field. Chapter 4 discusses that electric field values with high working distances produced electrospun fibers containing a distribution of diameters from 6 μm and upwards of 16 μm. Meanwhile, lower working distances lacked adequate evaporation distances, resulting in fused fibers and other defected structures.

However the notable structure-property changes as a result of processing in an electric field found that less mass is loss during firing of electrospun fibers relative to control dried powders. These differences in mass loss are found for electrospun ASB:BA and ASB:DG at ~ 10 %. This note-worthy finding is highlighted in Chapter 5 and reiterates the idea that atmospheric conditions are adequate to promote solvent evaporation and subsequent hydrolysis/condensation. Electrospinning into water and increasing the relative humidity rates

retains the overall continuous structures of the fibers. However the latter does induce some varicose instability.

Shrinkage in fiber diameters were statistically analyzed with probability density functions and compared to their green-state counterparts as discussed in Chapter 5 ASB:BA precursors with more volatile species resulted in little or no fiber diameter changes. However as the volatility of the solvent decreases and concentration increases, dimensional changes are as high as 43%.

Further applications of these ceramic fibers rely on the macroporous nature of these fibers and the BET specific surface areas were found in upwards of $330 m^2/g$ and pore diameters as low as ~ 4nm. However firing at 1200ºC decreases the specific surface area down towards ~ 9 m^2/g and increase pore diameters up to 8 times. Yet in Chapter 5, the analysis still supports the macroporous nature of the fibers to be used in a variety of applications. This is owed to the inherent stacked nature of the fibers, presence of pores due to usage of sol-gel precursors, and (with some ASB:BA and ASB:DG), the presence of hollow cores.

The milestones in this dissertation were as follows:

- Redesigned electrospinning precursors with aluminum tri sec butoxide prepared with the addition of a variety of solvents or through vacuum distillation.
- Identified optimal ranges for electrospinning flow rate values for the three prepared alkoxide-based precursors due to solvent volatility and solvent concentration.
- Produced continuous and hollow fibers with solvent-addition precursors. Production of solid fibers with modified solvent precursors.
- The electrospinning process promoted less trapped organics compared to controls. The difference in mass loss for the ASB:BA and ASB:DG is ~ 10 %.
- No phase transitions were induced due to processing in an electric field.
- Transition phases existed with “cold-hydrolyzed” aluminum alkoxides. Addition of glycol ethers induced transition phases and can lower alpha transition down to ~ 900ºC.

- The fibers exhibited little or no shrinkage with precursors prepared with volatile solvents.

Future Work

Precursors have been redesigned to rely on atmospheric hydrolysis conditions and to avoid limitations due to other noted factors. Implementation into long-term space missions is the goal. In addition, possible commercial usage of such fibers can be explored for catalytic applications and such. This section will further describe recommended research avenues to pursue to build on the framework of this dissertation.

New Compositions of Alkoxide-Based Precursors

The preparation procedures studied in this dissertation can be applied to demanded compositions such as aluminosilicates, titanates, and zirconates. Each of the latter presents a family of materials that comprise the market of advanced ceramics for thermal, electrical, and structural applications. Each of the latter can be prepared by firstly understanding the nature of the available alkoxide precursors. Material selection and ligand exchange or complexation should result in spinnable alkoxide precursors.

Aluminosilicates have previously been synthesized by mixing tetraethylorthosilicate with the ASB. Precursors were electrospun and the ratio of 4 mol% Si in the aluminosilicate compound was obtained. Additionally mixing of titanium butoxide with ASB yielded aluminotitanate fibers. These fibers yielded a 2 Al to 5 Ti molar ratio.

These preliminary studies build on the existing understanding of utilizing ASB as the main alkoxide precursor. Initially research needs to be further pursued to produce a range of aluminosilicates and aluminotitanates by optimizing miscibility ranges and electrospinning feasibility.

For direct electrospinning of solely titania or zirconia fibers, a more detailed review of literature is recommended to grasp the various precursor modification methodologies. Both

these metals have tendencies to exhibit higher coordination numbers, resulting in oligomerization of their alkoxide derivatives. This oligomerization increases the chance for these compounds to form high viscosity alkoxides. Additionally ligand modification methodologies are similar to the ones discussed in this dissertation.

Increasing Hexa-Coordination within Solvent-Addition Precursors

The aim of this potential study is to incorporate the consistency of forming continuous hollow fibers with primarily transition boehmite and gamma phases and a low-temperature forming alpha phase. The use of this high specific surface area and less dense alumina fibers may provide an advantage to catalytic applications. Additionally the use of low-firing alumina prevents high-temperature coarsening, but also can assist as sintering aids. Precursors can be altered by using a combination of the ASB:DG and mod-ASB:DG precursors. The presence of free solvents may result in similar hollow fiber formation mechanics.

Nucleation of Transition Phases by Seeding Precursors

The addition of boehmite nanoparticles may be added into existing precursors. Currently these nanoparticles can be purchased with different functionalities and can be dispersed in a variety of solvents. These boehmite nanoparticles may serve as heterogenous nucleation sites, resulting in promotion of transitional phases. Initial works on the dispersion and mixing the alkoxide should initially be performed. From these precursors, fibers can be fabricated and studied. Essentially the trend in seeding concentration and desired phase can be derived. These transition phases can assist in forming the catalytic active fibers.

Electrospinning into Water and Promoting Boehmite

Since electrospinning studies have been performed by electrospinning directly into water, it was found that the continuous hollow structures were not affected. However the combination

of electrospinning fibers into a hot water with optional catalysts can result in an increase in the boehmite phase present, thereby increasing the formation of other transition phases.

Previous studies during the course of dissertation resulted in Boehmite being induced in hot-water electrospun fibers. XRD along with Raman Spectra confirmed the distinctive boehmite peaks.

Initially it is suggested that a proper drying schedule be implemented to avoid structural issues with the hydrated fibers. Furthermore the chemical changes should be studied within the FTIR, XRD, and Raman. The effect of aging and optional catalysts can also be studied to understand the changes in the transformation energy and concentration of the boehmite phase.

Mechanical Property Investigation

The ability of these fibers to sustain commercial usage is essential for down-stream applications. Protocols established for testing commercial alumina fibers can be refined and applied to these fibers. Importantly tensile and flexure tests should be examined.

Drying Control

Additional work with the alumina fibers should be performed to reduce the presence of small cracks along side the walls during firing. Increasing ambient drying or decreasing of heating rates should be studied. Initial aging studies were performed to understand changes in mass loss. A range of samples dried in various conditions can be studied, ranging from room temperature, desiccators, ambient drying oven (~70ºC), vacuum chamber, and heating at rates below 10ºC/min can be parameters of study. Essential will the TGA data obtained and compared for the various types of aging/drying methods. Thereby reducing the organics, structural defects can be minimized.

Xerogel Fiber Production

BET S.S.A. demonstrated that electrospun fibers fired at 150ºC exhibited values ~330-350 m^2/g rivaling xerogels and some aerogels. Continous hollow fibers can be formed with porous side-walls exhibited near-net shaped dimensions after firing. However adequate aging and drying schedules should be further pursued to investigate maintenance continuous porous sidewalls and higher S.S.A values after subsequent firing. These porous fibers serve as potential for next generation insulating materials.

Producing Consistent Fiber Diameters

Although this work has pieced together the groundwork to establish the usage of alkoxide-based precursors, fibers were synthesized with a range of fiber diameters. The goal for this work should be to study factors involved to controlling consistent fiber diameters. Essentially a more in-depth study on oligomerization of ASB and stringently controlling the hydrolysis conditions should be a major variable. The production of reproducible fibers within a small fiber diameter range of 1-2 μm increases the commercial stake. Additionally understanding the factors that control fiber diameter can essentially lead to models to describe the electrospinning parameter to structure relationship. Further investigations should also be pursued to more precisely control inner hollow diameters of the continuous hollow fibers.

Overall this work brought about new and exciting changes to the field of electrospinning. This versatile direct electrospinning precursor can eventually be improved for a portable ceramic fiber production that can be used in remote locations for possible applications, such as repair of shuttle tile or spacesuit patching. However given the array of possibilities, this set of work should allow new researchers to tackle the challenges of finding predictive models and making down-stream production a possibility.

APPENDIX A
PROGRAMS FOR CREATING MOLECULAR DRAWINGS

Two types of molecular structures were created for this dissertation: the first being a 2D representation of the molecular compound and the other being a 3D representation as a ball and stick model. Therefore options A and B are provided, respectively for the explanation and replication of the desired structure (or reaction).

OPTION A: These figures or reactions are drawn with ChemBioDraw Ultra 11.0 from Cambridge Software Store. Access to the software is free through the University of Florida's Chemistry Departmental license. For more information, please see: http://www.cambridgesoft.com/software/ChemBioDraw/

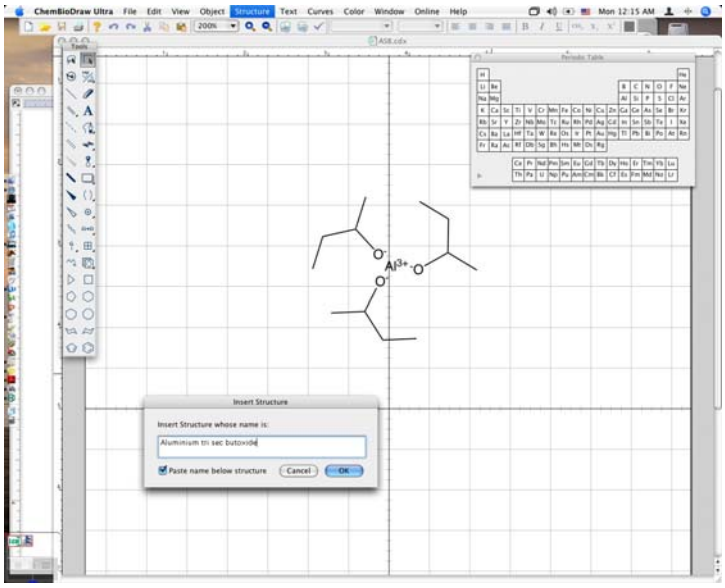

By choosing the appropriate atom and bonds, general molecular structures are rendered. Additionally the chemical's name or identification number can be entered into a query for structure rendering.

OPTION B: Creating 3D figures, such as ball and stick, required consultation of two programs.

1. Molecular Networks' CORINA allows interactive input, such that a structure in a SMILES string and/or an identifier can be submitted to generate 3D coordinates for the desired structure. This is available to everyone at:

http://www.molecular-networks.com/online_demos/corina_demo.htm

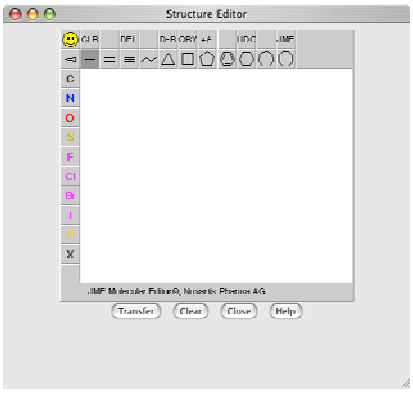

A

B

If SMILES need to be created, then a JAVA molecular editor (JME) applet can be consulted to create a general molecular structure drawing that in turn is input to produce a SMILE string (A). The SMILE string is loaded and can then be submitted (B).

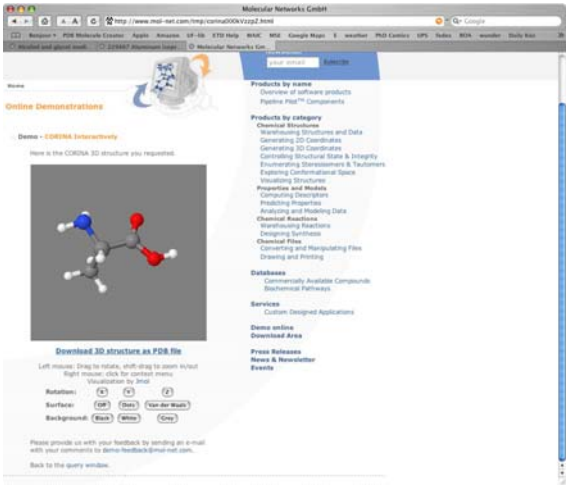

C

Once the string has been submitted CORINA's 3D structure appears and can be downloaded as a PDB file (C).

2. iMol is a MacIntosh OS X free molecular visualization software application. It supports various files of molecules and loads them in various visual arrays to allow movement and rotation, independently, or displays a molecular dynamics trajectory. For more information see, http://www.pirx.com/iMol/

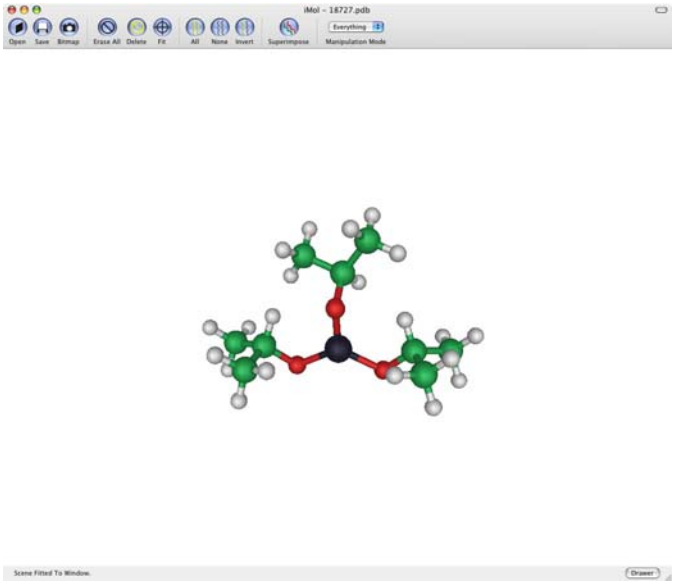

D

The iMol program opens the PDB file and displays the molecule in the desired atomic display style, such as ball and stick in this case (D). The file is then saved as a bitmap (TGA) file and then later converted to a jpg file utilizing a file mutation software.

APPENDIX B
AZEOTROPE REFERENCING AND ONLINE DATABANK

Two references were consulted to investigate azeotrope properties of desired solvents. The first is the *CRC Handbook of Chemistry and Physics*. Conferring with the handbook and to give detailed calculations is an online database created in *The Edinburgh Collection of Open Software for Simulation and Education* from Edinburgh University. The link for the latter can be found at: http://eweb.chemeng.ed.ac.uk/chem_eng/azeotrope_bank.html

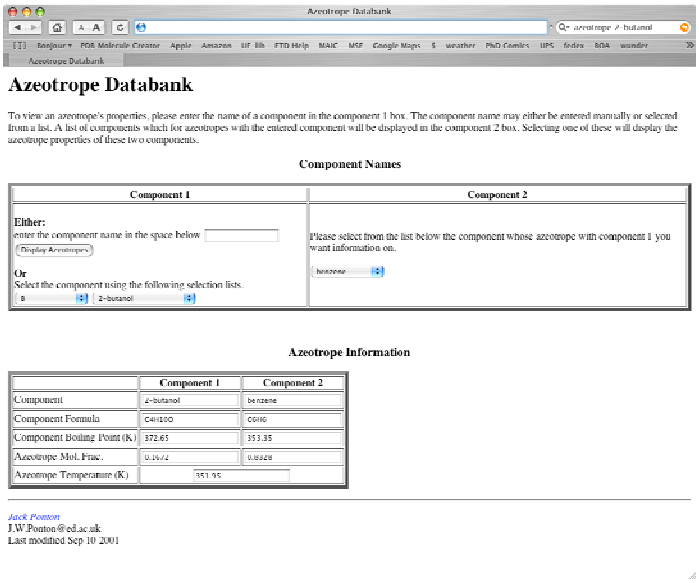

In this databank, the desired solvent can be chosen in "Component 1" and a list of possible azeotrope solvents appear in "Component 2." After selecting the interested solvent, the computed information appears in "Azeotrope Information."

LIST OF REFERENCES

[1] Y. Dzenis, Science 304 (2004) 1917-1919.

[2] D. Li, Y. N. Xia, Advanced Materials 16 (2004) 1151-1170.

[3] Formhals, A. Method and Apparatus for Spinning, United States Patent 2,160,962, 1939.

[4] A. Formhals, Method of Producing Artificial Fibers, United States Patent 2,158,415, 1937.

[5] A. Formhals, Process and Apparatus for Preparing Artificial Threads, United States Patent 1,975,504, 1934.

[6] W. Gilbert, [translated by P. F. Mottelay], De Magnete, Dover Publications, New York, 1991.

[7] R. P. A. Hartman, D. J. Brunner, D. M. A. Camelot, J. C. M. Marijnissen, B. Scarlett, Journal of Aerosol Science 30 (1999) 823-849.

[8] S. V. Fridrikh, J. H. Yu, M. P. Brenner, G. C. Rutledge, Polymeric Nanofibers 918 (2006) 36-55.

[9] S. A. Theron, E. Zussman, A. L. Yarin, Polymer 45 (2004) 2017-2030.

[10] W. Sigmund, J. Yuh, H. Park, V. Maneeratana, G. Pyrgiotakis, A. Daga, J. Taylor, J. C. Nino, Journal of the American Ceramic Society 89 (2006) 395-407.

[11] N. P. Bansal, Handbook of Ceramic Composites, Kluwer Academic Publishers, New York, 2005.

[12] A. R. Bunsell, Oxide Fibers, in: N. P. Bansal, Handbook of Ceramic Composites, Kluwer Academic Publishers, New York, 2005, pp. 3-32.

[13] T. F. Cooke, Journal of the American Ceramic Society 74 (1991) 2959-2978.

[14] T. E. Cottringer, R. H. van de Merwe, R. Bauer, W. A. Yarbrough, Alumina Sol-Gel Fiber, United States Patent 5,514,631,1996.

[15] T. Maki, S. Sakka, Journal of Non-Crystalline Solids 100 (1988) 303-308.

[16] National Materials Advisory Board, Ceramic Fibers and Coatings: Advanced Materials for The Twenty-First Century, National Academy Press, Washington D.C, USA, 1988.

[17] S. Sakka, Fibers from the Sol-Gel Process, in: L. C. Klein, Sol-Gel Technology For Thin Films, Fibers, Preforms, Electronics, and Specialty Shapes, Noyes Publications, Park Ridge, New Jersey, 1988, pp. 140-161.

[18] L. E. Seufert, Alumina Fiber, United States Patent 3,808,015, 1974.

[19] E E. Walner, B. C. Raynes, A. L. Cunningham, Liquid Polymers, Solid articles made therefrom and methods of preparing the same, United States Patent 3,180,741, 1965.

[20] R. J. Lockhart, E. Walner, Preparation of Alumina Monofilaments, United States Patent 3,271,173, 1966.

[21] S. Horikiri, K. Tsuji, Y. Abe, A. Fukui, E. Ichiki, Process for producing alumina fiber or alumina-silica fiber, United States Patent 4,101,615, 1978.

[22] C. F. Baes, Jr, R. E. Mesmer, The Hydrolysis of Cations, Robert E. Krieger Publishing Company, Inc., Malabar, Florida, 1986.

[23] C. J. Brinker, G. W. Scherer, Sol-Gel Science: The Physics and Chemistry of Sol-Gel Processing, Academic Press, Boston, 1990.

[24] . Livage, M. Henry, A Predictive Model for Inorganic Polymerization Reactions, in: J. D. Mackenzie, D. R. Ulrich, Ultrastructure Processing of Advanced Ceramics, John Wiley & Sons, New York, 1988, pp. 183-197.

[25] J. Livage, C. Sanchez, M. Henry, S. Doeuff, Solid State Ionics 32-3 (1989) 633-638.
[26] L. L. Hench, J. K. West, Chemical Reviews 90 (1990) 33-72.

[27] B. E. Yoldas, American Ceramic Society Bulletin 54 (1975) 289-290.

[28] B. E. Yoldas, American Ceramic Society Bulletin 54 (1975) 286-288.

[29] J. Livage, Catalysis Today 41 (1998) 3-19.

[30] C. Sanchez, J. Livage, M. Henry, F. Babonneau, Journal of Non-Crystalline Solids 100 (1988) 65-76.

[31] B. E. Yoldas, Journal of Materials Science 10 (1975) 1856-1860.

[32] A. Alipour, H. Jazayeri, M. M. Amini, Journal of Coordination Chemistry 51 (2000) 319-322.

[33] A. Alipour, H. Jazayeri, A. Nemati, M. M. Amini, Materials Letters 48 (2001) 15-20.

[34] M. M. Amini, M. Mirzaee, Journal of Sol-Gel Science and Technology 36 (2005) 19-23.

[35] F. Babonneau, L. Coury, J. Livage, Journal of Non-Crystalline Solids 121 (1990) 153-157.

[36] N. Bahlawane, T. Watanabe, Journal of the American Ceramic Society 83 (2000) 2324-2326.

[37] L. Bonhomme-Coury, F. Babonneau, J. Livage, Journal of Sol-Gel Science and Technology 3 (1994) 157-168.

[38] G. Buelna, Y. S. Lin, Microporous and Mesoporous Materials 30 (1999) 359-369.

[39] M. Chatterjee, D. Enkhtuvshin, B. Siladitya, D. Ganguli, Journal of Materials Science 33 (1998) 4937-4942.

[40] D. E. Clark, J. J. Lannutti, Phase Transformations in Sol-Gel Derived Aluminas, in: L. L. Hench, D. R. Ulrich, Ultrastructure Procesing of Ceramics, Glasses and Composites, John Wiley & Sons, Inc, New York, 1984, pp. 126-141.

[41] G. Fu, L. F. Nazar, a. D. Bain, Chemistry of Materials 3 (1991) 602-610.

[42] M. F. Garbauskas, J. H. Wengrovius, R. C. Going, J. S. Kasper, Acta Crystallographica Section C-Crystal Structure Communications 40 (1984) 1536-1540.

[43] M. Guglielmi, G. Carturan, Journal of Non-Crystalline Solids 100 (1988) 16-30.

[44] K. R. Han, C. S. Lim, M. J. Hong, J. W. Jang, K. S. Hong, Journal of the American Ceramic Society 83 (2000) 750-754.

[45] M. S. Hill, D. A. Atwood, Main Group Chemistry 2 (1998) 285-292.

[46] L. Ji, J. Lin, K. L. Tan, H. C. Zeng, Chemistry of Materials 12 (2000) 931-939.

[47] O. Kriz, B. Casensky, A. Lycka, J. Fusek, S. Hermanek, Journal of Magnetic Resonance 60 (1984) 375-381.

[48] S. C. Kuiry, E. Megen, S. A. Patil, S. A. Deshpande, S. Seal, Journal of Physical Chemistry B 109 (2005) 3868-3872.

[49] S. K. Lee, K. Shinozaki, N. Mizutani, Nippon Seramikkusu Kyokai Gakujutsu Ronbunshi-Journal of the Ceramic Society of Japan 100 (1992) 1140-1144.

[50] S. Rezgui, B. C. Gates, Chemistry of Materials 6 (1994) 2386-2389.

[51] S. Rezgui, B. C. Gates, S. L. Burkett, M. E. Davis, Chemistry of Materials 6 (1994) 2390-2397.

[52] T. Tsukada, H. Segawa, A. Yasumori, K. Okada, Journal of Materials Chemistry 9 (1999) 549-553.

[53] D. S. Tucker, Journal of the American Ceramic Society 68 (1985) C163-C164.

[54] W. Vedder, Vermilye, D.A., Transactions of the Faraday Society 65 (1969) 561-565.

[55] C. T. Vogelson, A. R. Barron, Journal of Non-Crystalline Solids 290 (2001) 216-223.

[56] J. H. Wengrovius, M. F. Garbauskas, E. a. Williams, R. C. Going, P. E. Donahue, J. F. Smith, Journal of the American Chemical Society 108 (1986) 982-989.

[57] R. J. Yang, F. S. Yen, S. M. Lin, C. C. Chen, Journal of Crystal Growth 299 (2007) 429-435.

[58] B. E. Yoldas, Molecular And Microstructural Effects of Condensation Reactions in Alkoxide-Based Alumina Systems, in: D. R. Ulrich, J. D. Mackenzie, Ultrastructure Processing of Advanced Ceramics, John Wiley & Sons, Inc, New York, 1988, pp. 333-354.

[59] D. Li, Y. N. Xia, Nano Letters 3 (2003) 555-560.

[60] D. Li, Y. N. Xia, Abstracts of Papers of the American Chemical Society 226 (2003) U425-U425.

[61] C. J. Li, G. J. Zhai, Z. Y. Fu, P. J. Wang, M. Chang, X. N. Li, Chinese Journal of Inorganic Chemistry 22 (2006) 2061-2064.

[62] D. Li, J. T. McCann, Y. N. Xia, Journal of the American Ceramic Society 89 (2006) 1861-1869.

[63] D. Li, Y. N. Xia, Nano Letters 4 (2004) 933-938.

[64] J. Doshi, D. H. Reneker, Journal of Electrostatics 35 (1995) 151-160.

[65] a. Theron, E. Zussman, A. L. Yarin, Abstracts of Papers of the American Chemical Society 226 (2003) U424-U425.

[66] S. A. Theron, E. Zussman, A. L. Yarin, Polymer 45 (2004) 2017-2030.

[67] L. Chun, C. Ping, Y. J. Zhang, Abstracts of Papers of the American Chemical Society 231 (2006) -.

[68] S. L. Shenoy, W. D. Bates, H. L. Frisch, G. E. Wnek, Polymer 46 (2005) 3372-3384.

[69] A. M. Azad, Materials Science and Engineering A-Structural Materials Properties Microstructure and Processing 435 (2006) 468-473.

[70] P. K. Panda, S. Ramakrishna, Journal of Materials Science 42 (2007) 2189-2193.

[71] G. Larsen, R. Velarde-Ortiz, K. Minchow, A. Barrero, I. G. Loscertales, Jounal of the American Chemical Society 125 (2003) 1154-1155.

[72] D. C. Bradley, R. C. Mehrotra, I. P. Rothwell, A. Singh, Alkoxo and Aryloxo Derivatives of Metals, Academic Press, San Diego, 2001.

[73] D. C. Bradley, R. C. Mehrotra, D. P. Gaur, The Chemistry of Metal Alkoxides, Kluwer Academics Publishers, 2002.

[74] R. C. Mehrotra, Journal of Non-Crystalline Solids 121 (1990) 1-6.

[75] L. A. O'Dell, S. L. P. Savin, A. V. Chadwick, M. E. Smith, Solid State Nuclear Magnetic Resonance 31 (2007) 169-173.

[76] N. Y. Turova, E. P. Turevskaya, V. G. Kessler, M. I. Yanovskaya, The Chemistry of Metal Alkoxides, Kluwer Academic Publishers, Norwell, 2002.

[77] C. E. Pratt, G. E. Kowalczyk, Alcohol and glycol modified aluminum tri-alkoxide complexes, United States Patent 6,953,863, 2005

[78] C. E. Pratt, G. E. Kowalczyk, Modified aluminum tri-alkoxide complexes, United States Patent 4,525,307, 2005

[79] G. C. Bye, J. G. Robinson, Colloid and Polymer Science 198 (1964) 1435-1536.

[80] J. Li, Y. Pan, C. Xiang, Q. Ge, J. Guo, Ceramics International 32 (2006) 587-591.

[81] D. T. Lundie, A. R. McInroy, R. Marshall, J. M. Winfield, P. Jones, C. C. Dudman, S. F. Parker, C. Mitchell, D. Lennon, Journal of Physical Chemistry B 109 (2005) 11592-11601.

[82] R. Nass, H. Schmidt, Journal of Non-Crystalline Solids 121 (1990) 329-333.

[83] Y. K. Park, E. H. Tadd, M. Zubris, R. Tannenbaum, Materials Research Bulletin 40 (2005) 1506-1512.

[84] T. R. Patterson, F. J. Pavlik, a. a. Baldoni, R. L. Frank, Journal of the American Chemical Society 81 (1959) 4213-4217.

[85] A. C. Pierre, D. R. Uhlmann, Journal of the American Ceramic Society 70 (1987) 28-32.

[86] A. F. Popa, S. Rossignol, C. Kappenstein, Journal of Non-Crystalline Solids 306 (2002) 169-174.

[87] S. Ramesh, E. Sominska, B. Cina, R. Chaim, A. Gedanken, Journal of the American Ceramic Society 83 (2000) 89-94.

[88] C. N. Mcmahon, L. Alemany, R. L. Callender, S. G. Bott, A. R. Barron, Chemistry of Materials 11 (1999) 3181-3188.

[89] M. A. Munoz-Hernandez, T. S. Keizer, S. Parkin, Y. H. Zhang, D. A. Atwood, Journal of Chemical Crystallography 30 (2000) 219-222.

[90] K. Tadanaga, T. Minami, Journal of the Ceramic Society of Japan 108 (2000) 420-423.

[91] R. Takahashi, S. Sato, T. Sodesawa, M. Suzuki, K. Ogura, Bulletin of the Chemical Society of Japan 73 (2000) 765-774.

[92] A. F. M. Barton, CRC Handbook of Handbook of Solubility Parameters and Other Cohesion Parameters, CRC Press, Boca Raton,1983.

[93] C. Hansen, Hansen Solubility Parameters: A user's handbook, CRC Press, Boca Raton, 2000.

[94] F. Mizukami, Y. Kiyozumi, T. Sano, S.-I. Niwa, M. Toba, S. Shin, Journal of Sol-Gel Science and Technology 13 (1998) 1027-1031.

[95] A. Pietrzykowski, T. Skrok, S. Pasynkiewicz, M. Brzoska-Mizgalski, R. Anulewicz-Ostrowska, K. Suwinska, L. Jerzykiewicz, Inroganica Chimica ACta 33 (2002) 385-394.

[96] F. E. M. Obrien, Journal of Scientific Instruments and of Physics in Industry 25 (1948) 73-76.

[97] K. M. Ganzer, L. Rebenfeld, American Laboratory 19 (1987) 40-45.

[98] I. M. Smallwood, Handbook of Organic Solvent Properties, Elsevier, 1996. Online Version available at: http://www.knovel.com/knovel2/Toc.jsp?BookID=567, , Last Accessed: September 3, 2007.

[99] J. M. Deitzel, C. Krauthauser, D. Harris, C. Pergantis, J. Kleinmeyer, Polymeric Nanofibers 918 (2006) 56-73.

[100] R. P. A. Hartman, D. J. Brunner, D. M. A. Camelot, J. C. M. Marijnissen, B. Scarlett, Journal of Aerosol Science 31 (2000) 65-95.

[101] R. P. A. Hartman, D. J. Brunner, K. B. Geerse, J. C. M. Marijnissen, B. Scarlett, Electrostatics 1999 163 (1999) 115-118.

[102] J. Macossay, A. Marruffo, R. Rincon, T. Eubanks, A. Kuang, Polymers for Advanced Technologies 18 (2007) 180-183.

[103] S. A. Theron, A. L. Yarin, E. Zussman, E. Kroll, Polymer 46 (2005) 2889-2899.

[104] A. L. Yarin, S. Koombhongse, D. H. Reneker, Journal of Applied Physics 89 (2001) 3018-3026.

[105] A. V. Bazilevsky, A. L. Yarin, C. M. Megaridis, Langmuir 23 (2007) 2311-2314.

[106] X. J. Han, Z. M. Huang, C. L. He, L. Liu, High Performance Polymers 19 (2007) 147-159.

[107] J. T. Mccann, M. Marquez, Y. N. Xia, Nano Letters 6 (2006) 2868-2872.

[108] M. Wei, B. W. Kang, C. M. Sung, J. Mead, Macromolecular Materials and Engineering 291 (2006) 1307-1314.

[109] S. V. Fridrikh, J. H. Yu, M. P. Brenner, G. C. Rutledge, Physical Review Letters 90 (2003) 144502.

[110] R. P. A. Hartman, Electrohydrodynamic Atomization in the Cone-Jet Mode: From Physical Modeling to Powder Production, Department of Chemical Engineering and Material Science, Particle Technology Group, vol doctor, Delft Univeristy of Technology, Delft, 1998, p. 177.

[111] D. Li, J. T. McCann, Y. N. Xia, Polymeric Nanofibers 918 (2006) 319-329.

[112] J. T. Mccann, J. I. L. Chen, D. Li, Z. G. Ye, Y. A. Xia, Chemical Physics Letters 424 (2006) 162-166.

[113] R. J. White, Chromatography / Fourier Transform Infrared Spectroscopy and Its Applications, Marcel Dekker, Inc., New York, 1990.

[114] J. A. de Haseth, T. L. Isenhour, Analytical Chemistry 49 (1977) 1977-1981.

[115] R. L. Frost, J. Kloprogge, S. C. Russell, J. L. Szetu, Thermochimica Acta 329 (1999) 47-56.

[116] D. A. Riesgraf, M. L. May, Applied Spectroscopy 32 (1978) 362-366.

[117] L. F. Nazar, L. C. Klein, Journal of the American Ceramic Society 71 (1988) C85-C87.

[118] W. N. Martens, R. L. Frost, J. Bartlett, J. T. Kloprogge, Journal of Materials Chemistry 11 (2001) 1681-1686.

[119] J. L. Szetu, R. L. Frost, J. T. Kloprogge, S. C. Russell, W. Martens, Thermochimica Acta 362 (2000) 37-48.

[120] M. May, J. Navarrete, M. Asomoza, R. Gomez, Journal of Porous Materials 14 (2007) 159-164.

[121] A. D. Krawitz, Introduction to diffraction in materiaos, science, and engineering, John Wiley & Sons, Inc., New York, 2001.

[122] M. Nguefack, A. F. Popa, S. Rossignol, C. Kappenstein, Physical Chemistry Chemical Physics 5 (2003) 4279-4289.

[123] G. Urretavizcaya, A. L. Cavalieri, J. M. P. Lopez, I. Sobrados, J. Sanz, Journal of Materials Synthesis and Processing 6 (1998) 1-7.

BIOGRAPHICAL SKETCH

Vasana Maneeratana is a native of Florida and proud daughter of Pornprom and Nipon Maneeratana. After the age of 8, she was raised in Gainesville, Florida and continued her higher education at the University of Florida's Department of Materials Science & Engineering with the Florida Bright Futures Scholarship was awarded her Bachelor's Degree in 2002 and Master of Science in 2005.

Although born in Tallahassee, Florida, she experienced numerous amounts of medical complications and found herself in the arms and care of Shands Hospital doctors. Realizing the need to be closer to crucial medical professionals, the Maneeratana's relocated to Gainesville, Florida and started up the Bahn Thai Restaurant, Inc and eventually converted into Gator fans.

During her enlightening doctoral studies under the supervision of her role model, Professor Wolfgang M. Sigmund, she was allowed to grow and mature with paramount support. With his full encouragement, she was urged to apply for external fellowships. In 2005, she was awarded the NASA Harriett G. Jenkins Pre-doctoral Fellowship. In addition to the latter, she received a scholarship to intern at NASA Goddard Space Flight Center through AAAS' Entrypoint Program for Persons with Disabilities. Upon returning in the Fall of 2005, she received word that she was nominated and selected to join AAAS' board-appointed Committee on Opportunities in Science with her tenure ending in Spring of 2008.

In the summer of 2006, she was awarded a mini-research award through her fellowship and an Entrypoint scholarship to continue her doctoral research at NASA Glenn Research Center. During her 5 months at GRC, she was selected to meet NASA's Deputy Director, Shana Dale and awarded a NASA GRC's First Year Scholar Award. In addition to her doctoral research at GRC alongside a good number of chemists in both the polymeric materials and environmental

and durability branches, she spearheaded an agency-wide initiative to reverse engineer Apollo-era spacesuits to establish design parameters for next generation spacesuits.

In the fall of 2006, she traveled on behalf of NASA as a Headquarters sponsored student to present her work on porous alumina fibers at the International Astronautical Congress in Valencia, Spain. To add to her conference travels, NSF sponsored her in the summer of 2006 to present her work on properties of the alkoxide-based electrospun fibers, in addition to touring around Berlin, Germany during the 10th Annual European Ceramics Society Meeting. It was during her professional travels in Germany that she met Professor Markus Antonietti at the Max-Planck Institute for Colloids where she will accept a position as a postdoctoral associate to start in early 2008 (a little after the dead of winter).

Vasana has published 7 publications- 2 of which are peer-reviewed and 4 are refereed conference proceedings. In the midst of this dissertation, Dr. Sigmund and Vasana have definite inspirations to publish a million more. She's presented 5 posters and presented 9 talks- 4 of which were invited. Along with Professor Sigmund and one of their esteemed colleagues, Professor Paolo Colombo at the University of Padova, Italy, they have a patent in final review. During her doctoral studies, Vasana has been fortunate enough to take part in course developments, various course instructing, journal reviews, report compilations, and the co-coordination of the MSETeach program in 2002-2005.

Vasana looks forward to a fabulous life experience as a world scientist. She hopes to learn and contribute to new avenues in design and fabrication of low-temperature and low-energy processing of advanced ceramic structures to bridge sustainability initiatives with materials science. One of her long-term goals is to pursue science through a faculty position, along as serving as a citizen of the world- full of integrity, curiosity, care and love for all.

Vasana is married to the wonderful Michael Funk and they have a dog with lots of attitude, named Louie. They look forward to a vast future- where anything is possible.